秋田県立大学大学院博士学位論文

Preparation and Electrical Properties of Conducting Polypyrrole Composites

Based on Different Kinds of Dopants

（異なるドーパントによる導電性ポリピロール複合材料の

創製および電気特性評価）

臧　利敏

2015 年 9 月

Abstract

Polypyrrole (PPy), as one of the most important intrinsically conducting polymers, is of great interest since its attractive merits such as high conductivity, ease of synthesis, excellent environmental stability, and appealing electrochemical behavior, which make it exhibit promising applications in energy storage, electromagnetic shielding, anticorrosion coatings, sensors, electrochemical displays and so on. However, the electrical conductivity of PPy without doping is unsatisfactory and the typical PPy suffers low processability, which hinders its potential applications. Inorganic acid with low molecular weight doped PPy may be subjected to dedoping process, which will decrease the electrical conductivity and cause the corrosion problem owing to the free acid. Moreover, the processability of PPy cannot be improved. In the present study, different kinds of dopant including aromatic multi-sulfonate dopant, solid dopant and polymeric dopant were used to dope PPy. The influence of different dopants on morphology, electrical property and other performance were investigated. Besides acting as dopant to enhance electrical conductivity of PPy, all the dopants show other effects to improve the performance of PPy.

In chapter 1, the research background, research purpose and the construction of this thesis are described.

In chapter 2, the properties of materials used in this thesis are presented. The experimental methods and characterization are also described in this chapter.

In chapter 3, PPy were prepared via chemical polymerization in the presence of aromatic multi-sulfonate acid dye (acid violet 19). Due to the unique structure of acid violet 19, it could play the role as dopant, surfactant and physical cross-linker for pyrrole polymerization, and has impact on the morphology, dispersion stability, thermal stability, electrical conductivity and electrochemical behavior of the samples. The thermal stability of the dye doped PPy is enhanced than pure PPy due to the

strong interactions between PPy and acid violet 19. The dispersion stability of the samples in water is also improved by incorporating an appropriate amount of acid violet 19. The sample with 20% of acid violet 19 shows granular morphology with the smallest diameter of ~50 nm and possesses the maximum electrical conductivity of 39.09 S/cm. The as-prepared multifunctional dye doped PPy samples are used to fabricate electrodes and exhibit a mass specific capacitance of 379-206 F/g in the current density range of 0.2-1.0 A/g. The results indicate that the multifunctional dye could improve the performances of PPy as electrode material for supercapacitors. The well dispersion stability and electrical properties also make it have the potential to prepare antistatic coatings, anticorrosion coatings and conductive ink. However, the relative higher cost (compared with polyaniline) needs to be improved.

In chapter 4, the budget spherical mesoporous silica has attracted our attention due to the unique mesoporous structure and large specific surface area. A series of PPy composites with different content of functionalized mesoporous silica, which functioned as the in-situ dopant and inorganic host, were prepared. The morphology, structure, thermal stability and electrical properties of the samples were characterized by scanning electron microscopy, Fourier transform infrared spectroscopy, X-ray diffraction, thermogravimetric analysis, cyclic voltammetry, and galvanostatic charge-discharge test. The content of functionalized mesoporous silica have been proved to have strongly impact on the morphology and electrical properties of the samples. When the value is 10%, the sample shows a bayberry-like morphology and possesses the maximum electrical conductivity of 33.33 S/cm. The sample with maximum electrical conductivity was used to fabricate electrodes and exhibited a best mass specific capacitance of 237.6 F/g. Due to the well mechanical properties of silica material, the as-prepared composites are thought to can be used as functional filler to mix with polymer matrix. The PPy layer coated on the surface of mesoporous silica is helpful to enhance the compatibility between mesoporous silica and polymer matrix. However, the micron-scale of the composite may hinder its application.

In chapter 5, polymeric dopant 一 phosphorylated polyvinyl alcohol (PPVA) were synthesized and used to prepare attapulgite/PPy nanocomposite (PPVA-ATP/PPy). The nanorod-like structure of attapulgite clay (ATP) can form network consequently improve the performance of the nanocomposite. PPVA functioned as both the dopant for PPy and the dispersant for ATP and the as-prepared nanocomposite in this work. The composites possess good dispersion stability, high electrical conductivity at room temperature, and weak temperature dependence of the conductivity. Moreover, it is found that dispersion stability in water increased with the increasing feeding ratio of PPVA. In addition, the thermal stability of conductivity PPVA-ATP/PPy composites is also enhanced by PPVA. The nanorod-like structure, improved dispersion stability and thermal stability of conductivity can broaden its potential application in antistatic coatings, anticorrosion coatings, conductive ink and filler.

In chapter 6, general conclusions of the study are made.

Content

Chapter 1 Introduction

1.1 Background

According to the electrical conductivity, materials can be classified as insulators, semiconductors, metals and superconductors. Materials with conductivity less than 10^{-9} S/cm is considered as insulators and conductivity of metals is larger than 10^2 S/cm; the semiconductors' conductivities lie in the middle ($10^{-9} \sim 10^2$ S/cm) [1, 2].
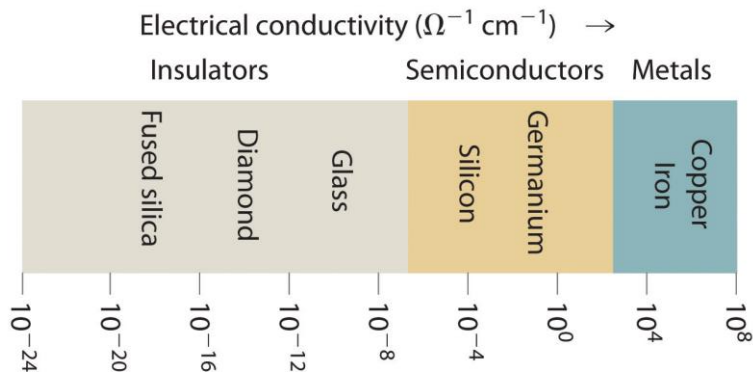
Fig. 1-1 Range of conductivities for insulators, semiconductors and metals [2].

There are a number of polymer products around our daily life, such as plastic bottles, synthetic leather, plastic bags and so on (Fig. 1-2). Polymeric materials have long been regarded as insulators and most of their applications have based on their insulating properties [4]. The discovery and development of intrinsically conducting polymers (ICPs) changed the way people think about polymeric materials that can't conduct electricity. In 1977, three scientists (Alan J. Heeger, Hideki Shirakawa and Alan G. MacDiarmid) discovered that a synthetic polymer (polyacetylene) could be conductive under certain conditions [5-8]. For the revolutionized discovery and development of conducting polymers, the Nobel Prize in Chemistry for 2000 was rewarded to the above three scientists [9-11]. Unlike traditional conducting material that disperses metal (or metal oxides) or carbon powder to insulated polymer, the structure and mechanism of

conduction of ICPs are completely different [12]. ICPs are classed as conjugated conducting polymers, charge transfer polymers and ionically conducting polymers. As the most studied ICPs, conjugated conducting polymers are discussed in more detail below.

Fig. 1-2 Household items made of various types of plastic [3].

1.1.1 Structure of conjugated conducting polymers

The molecular structures of some typical conjugated conducting polymers in their neutral form are given in Fig. 1-3. Fig. 1-4 shows the conductivity of some conjugated conducting polymers in their doped form [13]. We can see from Fig. 1-3 that alternate single-double bonds along the backbone of the polymer is a key property for conjugated conducting polymers, which differentiates them from other polymers. The "sigma" (σ) electrons that form strong covalent bonds between the carbon atoms are localized, whereas the "pi" (π) electrons can be delocalized upon certain operation. In a word, conjugation is a sine qua non for making the polymer material conductive, but not a sufficient one. The other key factor for being conductive is discussed in 1.1.2.
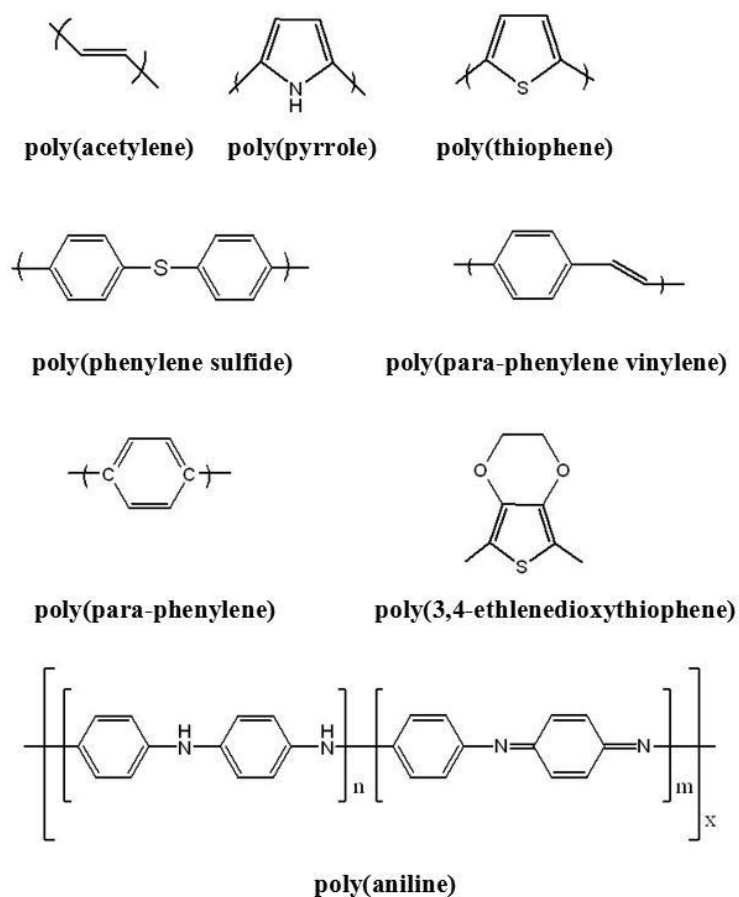
Fig. 1-3 Molecular structures of some conjugated polymers in their neutral form.
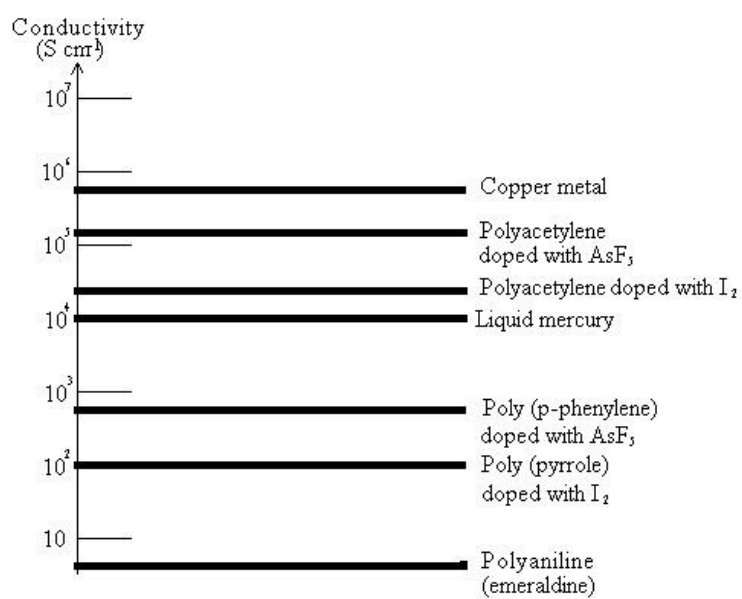
Fig. 1-4 The electrical conductivity of some doped conjugated polymers [13].

3

1.1.2 Doping in conjugated conducting polymers

Most of the conjugated polymers are poorly conductive and unstable in their neutral form. However, the conductivity of conjugated polymers can be dramatically enhanced by many orders of magnitude through doping process. The doping process that can alter the number of electrons in the polymer chain, is essentially a charge transfer reaction by oxidation or reduction. The process is generally termed as redox doping and the added simple anionic or cationic species used to generate charge carriers are known as dopants [14-18]. Redox doping can be further classed into *p*-doping and *n*-doping [19]. For *p*-doping, the polymer chain performs oxidation, meaning electrons are removed from polymer chain, whereas *n*-doping means that the polymer chain conducts reduction and electrons are injected to polymer chain (less frequently). The charge neutrality of the doped conjugated polymer is maintained by the incorporation of the counter ions [20]. The simplified processes for *p*-doping and *n*-doping are given as follows:

$$\textbf{Cp} \; \rightleftharpoons \; \textbf{Cp}^{n+}(\textbf{A}^-)_n + n\textbf{e}^- \quad (\textit{p-}\textbf{doping})$$

$$\textbf{Cp} + n\textbf{e}^- \; \rightleftharpoons \; (\textbf{C}^+)_n\textbf{Cp}^{n-} \quad (\textit{n-}\textbf{doping})$$
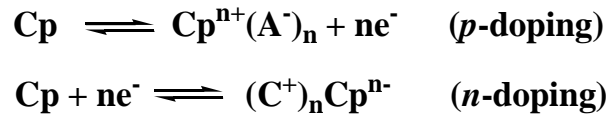
Fig. 1-5 Simplified processes for *p*-doping and *n*-doping.

Unlike inorganic semiconductors, doping in conjugated polymers is, which means doped conjugated polymers can revert to pristine state with almost no degradation upon dedoping. Doping process can be carried out by both chemical and electrochemical method. Moreover, the conductivity of conjugated polymers can be easily adjusted by altering the doping level. Fully doped (high doping level) form possesses high conductivity and undoped one is insulating or semiconducting.

1.1.3 Charge transport in conjugated conducting polymers

The conductivity (σ) of conjugated conducting polymers is proportional to carrier

concentration (n), the amount of electric charge a carrier transports (q) and the carrier mobility (μ) as shown in the following eq.:

$$\sigma = q \bullet n \bullet \mu$$

The carrier concentration of doped conjugated conducting polymer is much higher than that of undoped one, resulting in high conductivity. The mechanism of carrier transport in conjugated conducting polymer is one of the most interesting theoretical problem of this field. Among various models, delocalized band model and chemical model are generally employed to explain the mechanism. The unique conjugated structure of conjugated conducting makes charge delocalization possible. For the delocalized band model, the charges and unpaired electrons are assumed to be delocalized over a large number of monomer units [21, 22]. The chemical model supposes that the charge is localized in the polymer chain [23], or at most only some monomer units.
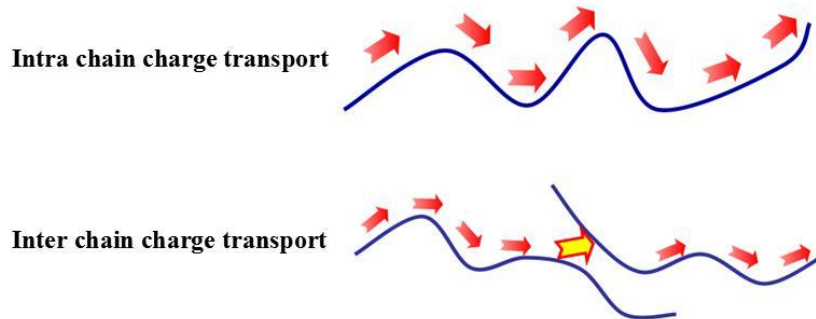
Fig. 1-6 Intra and inter chain charge transport in conjugated conducting polymers.

There are two patterns for charge transport. The transport along the polymer chain is known as intra-chain charge transport, which provides the intrinsic conductivity. Intra-chain charge transport is described in terms of band theory [24, 25]. The other transport between polymer chains is called as inter-chain charge transport, which occurs by the movement of charge carriers from the localized defect states [26-31]. Thermally activated hopping or tunneling theory is explored to explain the inter-chain charge

transport, in which the charge carriers (soliton, polaron or bipolaron) hop across or tunnel through barriers created by the presence of isolated states or domains [32-35].

1.1.4 Applications of conjugated conducting polymers

Conjugated conducting polymers have been widely applied in various fields based on their conductivity or electroactivity. Conductivity of conjugated conducting polymers can be adjusted from insulator to metal by controlling the doping level. Upon reversible doping and dedoping process, the electrical and optical properties of conjugated conducting polymers can be controlled.

Table 1-1 Applications of conjugated conducting polymers

Group 1 — Conductivity	
Antistatic materials	Conducting adhesives
Electromagnetic shielding	Printed circuit boards
Artificial nerves	Anticorrosive coating
Active electronics (diodes, transistors)	Aircraft structures
Group 2 — Electroactivity	
Molecular electronics	Electrical displays
Electrical displays	Rechargeable batteries
Drug release systems	Ion exchange membranes
Electromechanical actuators	"Smart" structures

Antistatic materials

Static electricity may be prevented by blending conducting polymers with conventional polymers or coating a very thin layer of conducting polymer on the surface of an insulator. Martins et al. prepared antistatic thermoplastic blend of polyaniline and polystyrene in a double-screw extruder using the block copolymer of styrene and

butadiene as compatibilizer [36]. Sun et al. synthesized poly(3, 4-ethylenedioxythiophene)/poly(styrenesulfonate) to prepare antistatic coating. The surface resistivity on different substrates such as polypropylene, amorphous polyethylene terephthalate and polystyrene were in the range of $10^7 - 10^8 \, \Omega$ [37].

Conductive adhesives

Conductive adhesives are used to stick conducting objects together. Polypyrrole was incorporated as a filler in an epoxy/anhydride system and its application as an isotropic conductive adhesive was studied by Mir. The results showed that they can be used as conductive adhesives in the electronics industry [38]. Kim synthesized a new nanocomposite for conductive transparent adhesives by emulsion polymerization of acrylate monomers dispersed with poly(3,4-ethylenedioxythiophene):poly(styrene sulfonate) [39].

Electromagnetic shielding

Electromagnetic radiation can be absorbed by coating a conductive surface on the inside of the plastic casing. Conducting polymers and their composites are new alternative candidates for electromagnetic shielding applications due to their lightweight, corrosion resistance, ease of processing, and tunable conductivities as compared with typical metals.

Artificial nerves

Some conducting polymers possess biocompatibility may be used as artificial nerves to transport small electrical signals through the body. Nerve growth factor-immobilized polypyrrole exhibited enhanced neurite extension [40]. Xu et al. synthesized a conducting composite nerve conduit with polypyrrole and poly(d, l-lactic acid) for peripheral nerve regeneration [41].

Active electronics

Highly conductive poly(3,4-ethylenedioxythiophene) films by vapor phase polymerization for application in efficient organic light-emitting diodes have been prepared [42]. Quantum dot/conducting polymer hybrid films are used to prepare light-emitting diodes, exhibiting a turn-on voltage of 4 V, an external quantum efficiency greater than 1.5%, and almost pure-green quantum-dot electroluminescence [43].

Electrical displays

The color of conducting polymer can be tuned by reversible doping and dedoping process because the doped and undoped states show different color. Moreover, the color can be altered by using various dopants. Polypyrrole, polythiophenes, poly(3,4-ethylenedioxythiophene):poly(styrene sulfonate), polyaniline and so on have been developed for display applications [44].

Sensors

The electrical properties of conducting polymers can be changed during reaction with diverse dopants or via their sensitivity to moisture and temperature. Such ability make them useful in sensors. By now, conducting polymers find application in chemical sensor, strain sensor, biological sensor, pH sensor, humidity sensor etc [45].

Rechargeable batteries

The polymer battery works by the oxidation and reduction of the polymer backbone. Aligned perchloricacid-doped polyaniline nanotubes prepared by a simple alumina template method exhibit better electrode performances than their commercial counterparts because they possess more active sites, higher conductivity, and relative flexibility [46]. Highly stretchable 2D buckled polypyrrole film is prepared by a simple electropolymerization method retains its electrochemical properties in Mg batteries after 2000 stretching cycles with 30% strain applied [47].

1.2 Polypyrrole

In the early 1960s, Polypyrrole (PPy) that is an intrinsically conducting polymer with excellent electrical properties was firstly discovered and reported [48]. Polypyrrole (PPy) was initially formed due to the oxidation of pyrrole in air and known as "pyrrole black". Diaz and his co-workers prepared free standing polypyrrole films by electrochemical polymerization [49, 50].

Among conducting polymers, PPy is of particular interest due to its high electrical conductivity, environmental stability, biocompatibility and ease of synthesis [51-53]. PPy exhibit a wide range of conductivities (10^{-3} S/cm $< \sigma < 10^2$ S/cm) depending on the nature of the dopant and doping level and the substitution pattern of the monomer [54]. The unique properties provide it with wide potential applications, such as rechargeable batteries [55, 56], electrochemical actuators [57-59], field effect transistor [60-62], supercapacitors [63, 64], enzyme immobilization [65-67], sensors [68, 69], separation membranes [70, 71], biomedical [72], corrosion protection [73], electromagnetic interference shielding materials [74-76] etc.

1.2.1 Mechanism of conduction

Charge carriers in PPy are produced in the following way (Fig. 1-7). When PPy backbone losses an electron, a free radical and a spinless positive charge are generated. A sequence of quinoid-like rings is supposed through the coupling of the radical and cation via local resonance of the charge and the radical. The number of quinoid-like rings is limited due to higher energy is required to create these defects than the remaining portion of the chain. Generally, it is believed that the distortion extends over four pyrrole rings. This species combines a charge site and a radical (radical cation) is called as polaron. The formation of polarons creates two energy levels that are symmetrically located about 0.5 eV from the band edges and the lower energy state being occupied by a single unpaired electron (Fig. 1-8). Further oxidation creates a new

spinless defect of the coupled cations (dication) called a bipolaron. For PPy, the bipolarons are positioned symmetrically with a band gap of 0.7 eV from the band edges (Fig. 1-8). At higher doping levels the polarons are replaced with bipolarons because creation of a bipolaron requires lower energy than the creation of two polarons. In either case, the counterions are incorporated to keep the charge neutrality of the conducting polymer. With continued oxidation, the bipolaronic energy state overlaps and forms intermediate band structures.
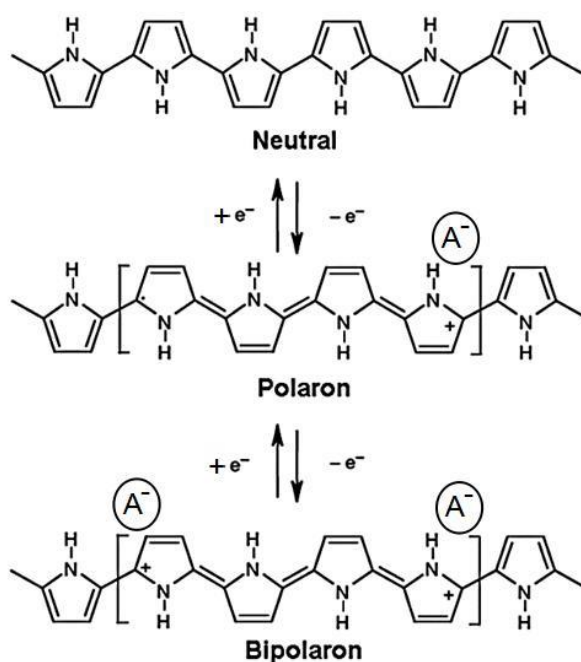
Fig. 1-7 Formation of polarons and bipolarons [77].
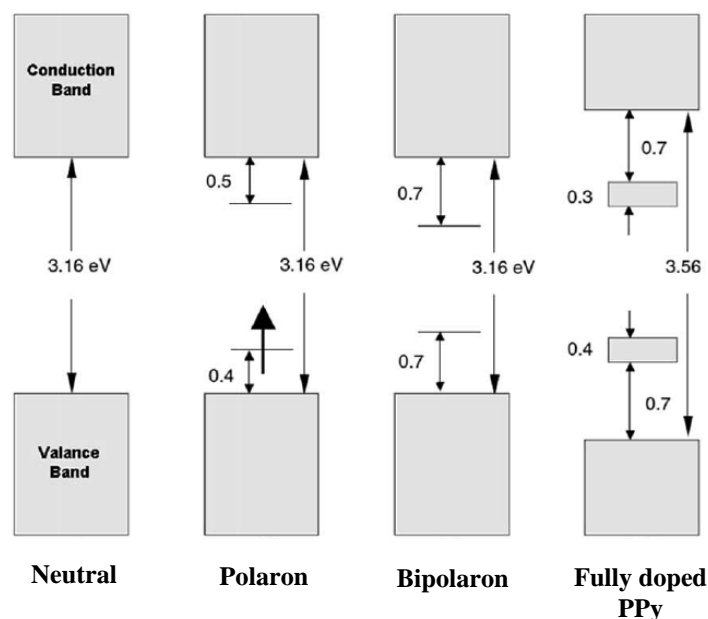
Fig. 1-8 Bands in conducting polymer [77].

1.2.2 Routes to prepare polypyrrole

PPy are prepared by the oxidation of pyrrole via chemical polymerization or electropolymerization. The former usually performs in solution using a chemical oxidant and results in an intractable powder. The latter carries out at a conductive substrate (electrode) through the application of an external potential and generates an insoluble film.

(a) Chemical polymerization

A chemical oxidant ($FeCl_3$ or $(NH_4)_2S_2O_8$) is used to conduct chemical polymerization, which simultaneously oxidizes the monomer and provides the dopant anion. The PPy powder produced by chemical oxidation polymerization shows lower conductivity than electropolymerization prepared PPy [78]. It is difficult to control over the potential within the reaction mixture, leading to overoxidation of PPy and poor doping control [79]. Chemical polymerization is beneficial to mass production and extensively used in industry. However, additional dopant is usually used to improve the

conductivity of PPy due to the small number of oxidants that can both oxidize the monomer and provide a suitable dopant.

(b) Electropolymerization

Electropolymerization is the other used approach to prepare conducting polymer, which results in a film deposited on the surface of working electrode. Potentiostatic, galvanostatic and potential cycling methods can be used to perform electropolymerization of pyrrole. The rate of polymerization and doping process can be well controlled via electropolymerization. Various dopant anions can be incorporated into the polymer to maintain electrical neutrality.

(c) Mechanism of polymerization

The mechanism of chemical polymerization is thought to be similar to electropolymerization, including the following four steps [80, 81]:

Step 1: The monomer is oxidized that forms a radical cation which exists in three pyrrole rings.

Step 2: One radical cation couples with another radical cation resulting in a dicationic dimer.

Step 3: The dicationic dimer losses two protons to form a neutral dimer.

Step 4: The neutral dimer further undergoes oxidation to form a radical cation and subsequently couples with anther radical cation. This process is known as stepwise chain growth. As polymer chain increases to a certain length, PPy becomes insoluble in the medium and precipitates.
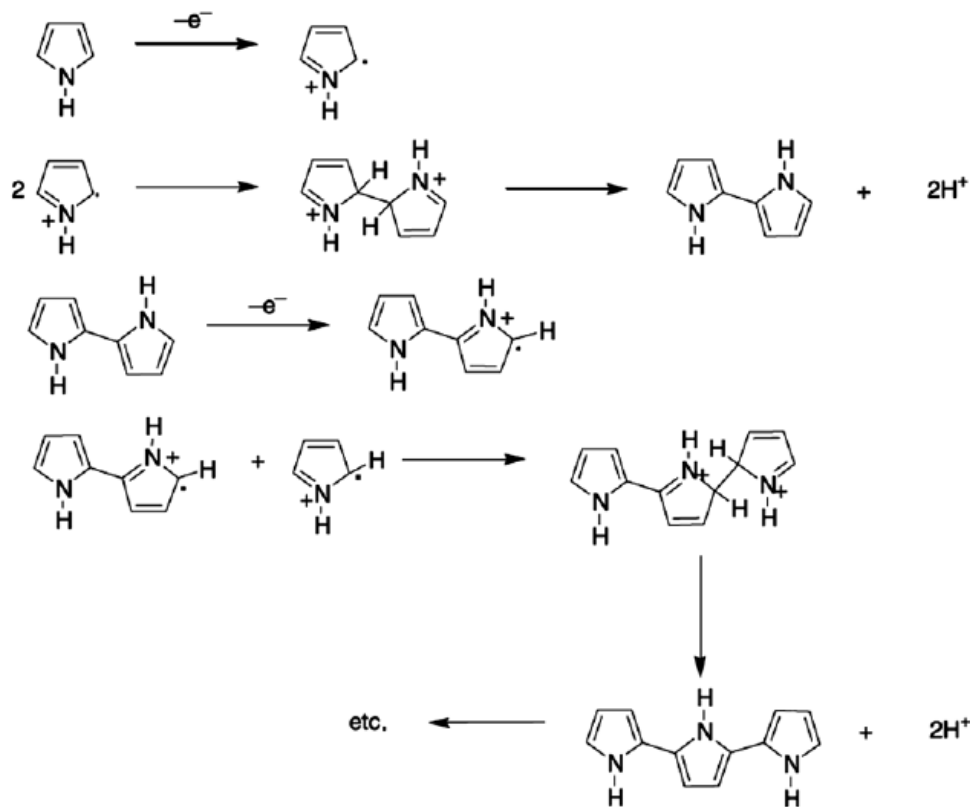
Fig. 1-9 Proposed mechanism for electropolymerization of pyrrole.

1.2.3 Properties of polypyrrole

(a) Electrical conductivity

The good electrical conductivity of PPy individuate it from other polymers and is one of the most important properties for applications. As a widely accepted view, the movement of charge carriers along polymer chains and the hopping of these carriers between chains contribute to the conductivity in PPy [31, 82]. The preparation conditions such as the species and concentration of dopant, solvent and polymerization temperature have strongly influence on the electrical conductivity of PPy. Because of hydrophobic effects, PPy prepared in water by chemical polymerization shows a cauliflower structure [83] and relative low conductivity caused by unevenness. Polymerization in alcohols can obtain PPy with higher than that prepared under the same conditions in acetonitrile, benzene, tetrahydrofuran and chloroform. Low

temperature is conducive to obtaining PPy with longer conjugation length, more regular structure and higher conductivity. Chemical polymerization of pyrrole is usually carried out between 0°C and room temperature. The dopant counterions have dramatic effects on the properties of PPy such as conductivity, morphology and solubility [84-86]. The concentration of a given dopant [87] and the molecular structure [88] would affect the conductivity of the resultant PPy. Ordinarily the electron affinity of the dopant and PPy decreases conductivity of PPy since the movement of charge carriers are limited.

(b) Electroactivity

Reduction and oxidation process in PPy are reversible meaning charge can be reversibly added to or removed from PPy. Doped PPy have positive charges and electroneutrality is balanced by dopant anions. By applying a sufficient negative potential, PPy is reduced to the neutral state (dedoping) and electroneutrality is maintained either by expelling these anions or incorporating cations. On the contrary, PPy is oxidized (doping) and counterions are incorporated to maintain electroneutrality when a sufficient positive potential is applied. If the size of dopant anions is small, both the dopant anions and electrolyte anions can be incorporated during potential sweeping. If the dopant anions have large size such as negatively charged polyelectrolytes or large surfactant anions [89, 90], it is difficult to expel the incorporated dopant anions during electrochemical reduction process and the electroneutrality is kept by the movement of the electrolyte cations into the PPy matrix. Consequently, the stability and mechanical strength of the PPy film is improved attributing to strong interactions between dopants and PPy [89].

(c) Stability

Long term stability and thermal resistance are required if the conducting polymers are to be used for successful industrial applications in future. Stability consists of intrinsically thermodynamic stability and external environmental stability. The

incorporated dopant anions in PPy make the stability become more complex than other conventional polymers. The degradation may cause by several process, consisting of the reaction of the PPy backbone with the dopant anion and the reaction of the PPy backbone with oxygen or water. The dopant itself might also suffer thermal degradation and the resulting degradation products might react with the PPy backbone.

(d) Processability

Generally, PPy powder obtained by chemical polymerization and PPy film produced by electropolymerization are infusible and insoluble in water and organic solvents due to the strong inter- and intra-molecular interactions. The poor processability hinders its applications, so preparation of processable PPy has attracted intense attention. Several methods have now been developed to improve the processability of PPy, which are discussed below.

1.2.4 Development in more processable polypyrrole

(a) Soluble PPy

The rigid structure of PPy which is attributed to the presence of strong interchain interactions results in poor solubility in water and common organic solvents. Developing soluble PPy has captured the attention of many researchers and some exciting results have been reported. By means of substituting the pyrrole ring at the 1, 3 or 4-positions for alkyl or alkoxy groups, the PPy derivatives can become soluble in tetrahydrofuran, chloroform and *o*-dichlorobenzene [91, 92] due to the large side groups reduce interactions between PPy chains. Some studies proved that using functional dopants could improve the solubility in some organic solvents. PPy incorporated of long chain dopants such as *β*-naphthalenesulfonic acid, dodecylbenzenesulfonate, dis(2-ethylhexyl) sulfosuccinate and anthraquinonesulfonic acid are then soluble in *m*-cresol, dimethylsulfoxide, *N*-methyl-2-pyrrolodinone, *N, N*-dimethylformamide and tetrahydrofuran [93-96].

(b) Dispersions

PPy dispersions in several organic media were synthesized by using polymeric ionic liquids both as steric stabilizers and as phase transfer agents [97]. Wood derivatives (polystyrene sulfonic acid, lignosulfonic acid sodium salts and carboxymethylcellulose) were used as doping/dispersing agents in the chemical polymerization to prepare PPy aqueous dispersions [98]. PPy dispersions formed by the polymerization of pyrrole in the presence of polyvinyl alcohol, poly(vinyl alcohol-co-acetate), poly(2-vinyl pyridine-co-butyl methacrylate) also have been reported [99-101].

(c) Composites

In order to expand the application of PPy, PPy composites that possess synergistic properties have been prepared by several ways. The substrate containing an appropriate oxidizing agent is exposed to pyrrole vapor and then the polymerization of PPy is induced on the substrate [102-106]. This method is modified by soaking the substrate with the pyrrole monomer and then immersing it in an oxidant solution [107]. By placing the object in a solution containing pyrrole and oxidant, PPy can be deposited directly onto/into fabrics or clay [108-111]. Especially, modification of substrate with functional groups can facilitate PPy-substrate adhesion and deposition [110, 112]. Sulphonated low density polyethylene has been used as a template for the polymerization of pyrrole, yielding PPy layers up to 80 nm thick [112].

1.3 Aim of this research

As discussed above, dopant has dramatic influences on the properties of PPy, including morphology, electrical conductivity, electrochemical property, thermal stability and so on. On the other band, the poor processability and relative high cost hinder the application of PPy materials. The overall aim of this thesis work is to improve the performances and reduce the cost of PPy production by using different kinds of dopants. Macromolecular aromatic dopant, solid dopant and polymeric dopant

were chosen in this thesis work due to the following reasons:

(1) Aromatic multi-sulfonate acid dye (acid violet 19, AV19) is attractive for being used as dopant to prepare PPy because of its unique structure. Sulfonate containing dopant is proved to be effective to improve the electrical conductivity of conjugated conducting polymer. And the multiple negative charge groups of AV19 could cause physical crosslinking of different polymer chains, which is helpful for interchain mobility of charge carriers. Moreover, the large conjugated system of AV19 would exert π–π stacking with PPy, which plays a part in improving the stabilization of AV19 within PPy. And the strong interaction between AV19 and PPy makes the resulting materials have enhanced aqueous dispersion.

(2) Mesoporous silica was functionalized with $-SO_3H$ groups and then used as solid dopant and inorganic host to prepare mesoporous silica/PPy composite. The incorporation of low cost of mesoporous silica can cut cost of PPy production. At the same time, the broad applications of mesoporous silica may broaden the application of the resulting composite. Because the $-SO_3H$ groups are anchored on the mesoporous silica, it wouldn't cause the corrosion problem owing to the release of strong inorganic acids like HCl doped conducting polymer. In addition, the relative large pore diameter as well as relative high oil absorption value of the mesoporous silica make it propitious to adsorb the pyrrole monomer to the surface and into the pore. When the mesoporous silica is used as reinforcing filler, the PPy layer coated on the surface of mesoporous silica can enhance compatibility between the mesoporous silica and polymer matrix as well as impart extra electrical and electrochemical properties to the composite.

(3) Phosphorylated polyvinyl alcohol (PPVA) was synthesized and applied as polymeric dopant. Considering the cost of PPy, cheap attapulgite clay with unique three-dimensional structure and fibrous morphology has been incorporated. PPVA contains a mass of hydroxyl groups and could improve the dispersing stability polypyrrole/attapulgite (PPy/ATP) nanocomposite. And the phosphate groups presented in PPVA could play the role as dopant so as to improve the electrical property of PPy.

The resulting composite also show a fibrous morphology owing to ATP. Such structure is in favor of formation of network, which can increase the electrical property.

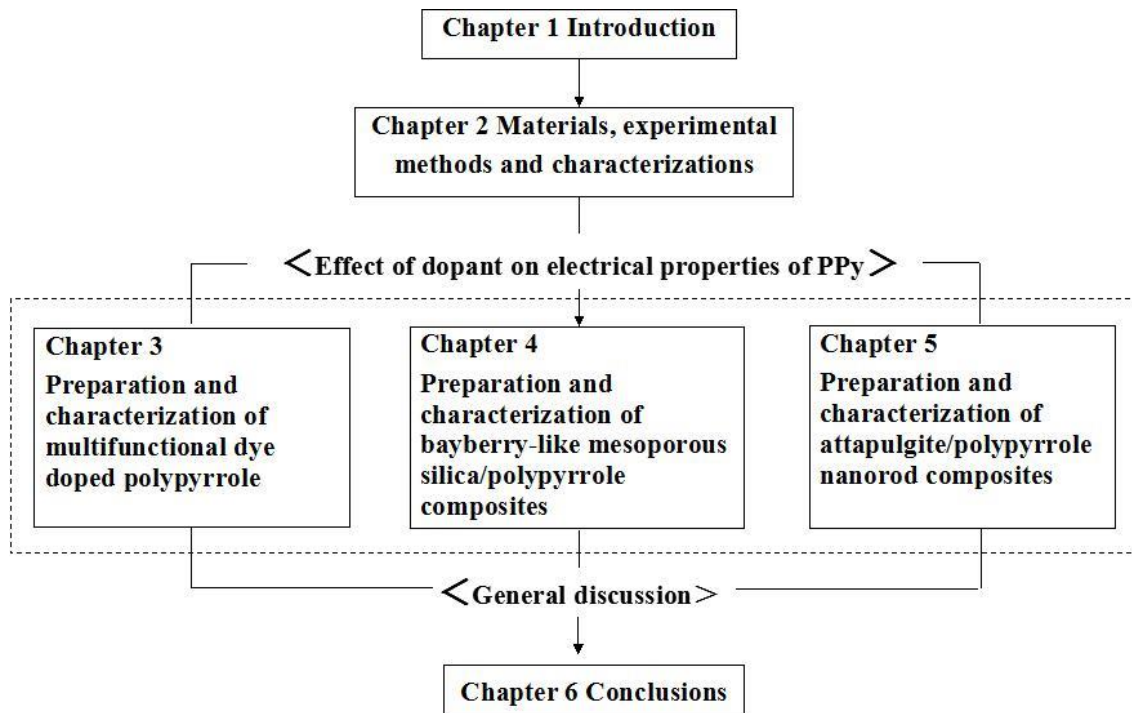The overall structure of the present study is presented in Fig. 1-10.

Fig. 1-10 The overall structure of the present study.

Reference

[1] C.M. Kachhava. Solid State Physics, Solid State Device and Electronics. New Age International Publishers. India, (2003), Part. 7.1.

[2] Bonding in Metals and Semiconductors. http://chemwiki.ucdavis.edu/Wikitexts/UC_Davis/UCD_Chem_2B/UCD_Chem_2B%3A_Larsen/Unit_II%3A_States_of_Matter/Solids/12.6%3A_Bonding_in_Metals_and_Semiconductors

[3] http://en.wikipedia.org/wiki/Plastic

[4] A.J. Epstein, J.M. Ginder, F. Zuo, R.W. Bigelow, H. Woo, D.B. Tanner, A.F. Richter, W. Huang and G.A. MacDiarmid. Insulator-to-metal Transition in Polyaniline. Synthetic Metals, 18 (1987) 303-309.

[5] H. Shirakawa, E.J. Louis, A.G. MacDiarmid, C.K. Chiang and A.J. Heeger. Synthesis of Electrically Conducting Organic Polymers: Halogen Derivatives of Polyacetylene, $(CH)_x$. Journal of the Chemical Society, Chemical Communications. (1977) 578-580.

[6] C.K. Chiang, C.R. Fincher Jr., Y.W. Park, A.J. Heeger, H. Shirakawa, E.J. Louis, S.C. Gau and A.G. MacDiarmid. Electrical Conductivity in Doped Polyacetylene. Physical Review Letter. 39 (1978) 1098-1101.

[7] C.K. Chiang, Y.W. Park, A.J. Heeger, H. Shirakawa, E.J. Louis and A.G. MacDiarmid. Conducting polymers: Halogen doped polyacetylene. The Journal of Chemical Physics. 69 (1978) 5098-5104.

[8] C.K. Chiang, M.A. Druy, S.C. Gau, A.J. Heeger, E.J. Louis, A.G. MacDiarmid, Y.W. Park and H. Shirakawa. Synthesis of Highly Conducting Films of Derivatives of Polyacetylene, $(CH)_x$. Journal of the American Chemical Society. 100 (1978) 1013-1015.

[9] A.J. Heeger. Nobel Lecture: Semiconducting and Metallic Polymers: The Fourth Generation of Polymeric Materials. Review of Modern Physics. 73 (2001) 681-700.

[10] A.G. MacDiarmid. Nobel Lecture: ''Synthetic Metals'': A Novel Role for Organic Polymers. Review of Modern Physics. 73 (2001) 701-712.

[11] H. Shirakawa. Nobel Lecture: The Discovery of Polyacetylene Film—The Dawning of An Era of Conducting Polymers. Review of Modern Physics. 73 (2001) 713-718.

[12] Y.P. Mamunya, V.V. Davydenko, P. Pissis and E.V. Lebedev. Electrical and Thermal Conductivity of Polymers Filled with Metal Powders. European Polymer Journal. 38 (2002) 1887-1897.

[13] H. Naarmann. Polymers to the Year 2000 and Beyond. John Wiley & Sons, (1993), Chapter 4.

[14] A.G. MacDiarmid, R.J. Mammone, R.B. Kaner, S.J. Porter, R. Pethig, A.J. Heeger and D.R. Rosseinsky. The Concept of 'Doping' of Conducting Polymers: The Role of Reduction Potentials [and Discussion]. Philosophical Transactions A. 314 (1985) 3-15.

[15] M.G. Kanatzidis. Polymeric Electrical Conductors. Chemical & Engineering News. 68 (1990) 36-54.

[16] P.J. Nigrey, A.G. MacDiarmid and A.J. Heeger. Electrochemistry of Polyacetylene, $(CH)_x$: Electrochemical Doping of $(CH)_x$ Films to the Metallic State. Journal of the Chemical Society, Chemical Communications. (1979) 594-595.

[17] D. MacInnes, M.A. Druy, P.J. Nigrey, D.P. Nairns, A.G. MacDiarmid and A.J. Heeger. Organic Batteries: Reversible *n-* and *p-* Type Electrochemical Doping of Polyacetylene, $(CH)_x$. Journal of the Chemical Society, Chemical Communications. (1981) 317-319.

[18] F. Genoud, M. Guglielmi, M. Nechtschein, E. Genies and M. Salmon. ESR Study of Electrochemical Doping in the Conducting Polymer Polypyrrole. Physical Review Letters. 55 (1985) 118-121.

[19] H.J. Ahonen, J. Lukkari and J. Kankare. *n-* and *p-* Doped Poly(3,4-ethylenedioxythiophene): Two Electronically Conducting States of the Polymer. Macromolecules. 33 (2000) 6787-6793.

[20] Y. Cao, P. Smith and A.J. Heeger. Counter-ion Induced Processibility of Conducting Polyaniline and of Conducting Polyblends of Polyaniline in Bulk Polymers. Synthetic Metals. 48 (1992) 91-97.

[21] A.G. MacDiarmid and A.J. Epstein. Polyanilines: A Novel Class of Conducting Polymers. Faraday Discussions of the Chemical Society. 88 (1989) 317-332.

[22] J.H. Kaufman, K. Kanazawa and G.B. Street. Gravimetric Electrochemical Voltage Spectroscopy: *In Situ* Mass Measurements during Electrochemical Doping of the Conducting Polymer Polypyrrole. Physical Review Letters. 53 (1984) 2461-2464.

[23] W.J. Albery, Z. Chen, B.R. Horrocks, A.R. Mount, P.J. Wilson, D. Bloor, A.T. Monkman and C. Elliott. Spectroscopic and Electrochemical Studies of Charge

Transfer in Modified Electrodes. Faraday Discussions of the Chemical Society. 88 (1989) 247-259.

[24] S. Kivelson and A.J. Heeger. Intrinsic Conductivity of Conducting Polymers. Synthetic Metals. 22 (1988) 371-384.

[25] H. Huang and P.G. Pickup. A Donor−Acceptor Conducting Copolymer with a Very Low Band Gap and High Intrinsic Conductivity. Chemistry of Materials. 10 (1998) 2212-2216.

[26] A.J. Heeger, S. Kivelson, J.R. Schrieffer and W.P. Su. Solitons in Conducting Polymers. Reviews of Modern Physics. 60 (1988) 781-850.

[27] J.L. Bredas, B. Themans, J.M. Andre, R.R. Chance and R. Silbey. The Role of Mobile Organic Radicals and Ions (Solitons, Polarons and Bipolarons) in the Transport Properties of Doped Conjugated Polymers. Synthetic Metals. 9 (1984) 265-274.

[28] J.L. Bredas and G.B. Street. Polarons, Bipolarons, and Solitons in Conducting Polymers. Accounts of Chemical Research. 18 (1985) 309-315.

[29] H.A. Mizes and E.M. Conwell. Stability of Polarons in Conducting Polymers. Physical Review Letters. 70 (1993) 1505-1508.

[30] J.C. Scott, P. Pfluger, M.T. Krounbi and G.B. Street. Electron-Spin-Resonance Studies of Pyrrole Polymers: Evidence for Bipolarons. Physical Review B. 28 (1983) 2140-2145.

[31] J.L. Bredas. Bipolarons in Doped Conjugated Polymers: A Critical Comparison Between Theoretical Results and Experimental Data. Molecular Crystals and Liquid Crystals. 118 (1985) 49-56.

[32] S. Kivelson. Electron Hopping in a Soliton Band: Conduction in Lightly Doped $(CH)_x$. Physical Review B. 25 (1982) 3798-3821.

[33] R.R. Chance, J.L. Brédas and R. Silbey. Bipolaron Transport in Doped Conjugated Polymers. Physical Review B. 29 (1984) 4491-4495.

[33] N.F. Mott and E.A. Davis. Electronic Processes in Non-crystalline Materials. Clarendon, Oxford, UK, (1979).

[34] L. Zuppiroli, M.N. Bussac, S. Paschen, O. Chauvet and L. Forro. Hopping in Disordered Conducting Polymers. Physical Review B. 50 (1994) 5196-5203.

[35] P. Sheng, B. Abeles and Y. Arie. Hopping Conductivity in Granular Metals. Physical Review Letters. 31 (1973) 44-47.

[36] C.R. Martins and M. De Paoli. Antistatic Thermoplastic Blend of Polyaniline and Polystyrene Prepared in a Double-Screw Extruder. European Polymer Journal. 41 (2005) 2867-2873.

[37] D.C. Sun and D.S. Sun. The Synthesis of PEDOT/PSS and Its Application in Antistatic Coating. Gaofenzi Cailiao Kexue Yu Gongcheng. 25(7) (2009) 111-113+117.

[38] I.A. Mir and D. Kumar. Development of Polypyrrole/Epoxy Composites as Isotropically Conductive Adhesives. Journal of Adhesion. 86 (2010) 447-462.

[39] B. Kim, T. Park, J. Kim and E. Kim. Waterborne Polyacrylic/PEDOT Nanocomposites for Conductive Transparent Adhesives. Journal of Nanoscience and Nanotechnology. 13 (2013) 7631-7636.

[40] N. Gomez and C.E. Schmidt. Nerve Growth Factor-Immobilized Polypyrrole: Bioactive Electrically Conducting Polymer for Enhanced Neurite Extension. Journal of Biomedical Materials Research - Part A. 81 (2007) 135-149.

[41] H. Xu, J.M. Holzwarth, Y. Yan, P. Xu, H. Zheng, Y. Yin, S. Li and P.X. Ma. Conductive PPY/PDLLA Conduit for Peripheral Nerve Regeneration. Biomaterials. 35 (2014) 225-235.

[42] P.A. Levermore, L. Chen, X. Wang, R. Das and D.D.C. Bradley. Highly Conductive Poly(3,4-ethylenedioxythiophene) Films by Vapor Phase Polymerization for Application in Efficient Organic Light-Emitting Diodes. Advanced Materials. 19 (2007) 2379-2385.

[43] J. Kwak, W.K. Bae, M. Zorn, H. Woo, H. Yoon, J. Lim, S.W. Kang, S. Weber, H.J. Butt, R. Zentel, S. Lee, K. Char and C. Lee. Characterization of Quantum Dot/Conducting Polymer Hybrid Films and Their Application in Light-Emitting Diodes. Advanced Materials. 21 (2009) 5022-5026.

[44] R.J. Mortimer, A.L. Dyer and J.R. Reynolds. Electrochromic Organic and Polymeric Materials for Display Applications. Displays. 27 (2006) 2-18.

[45] H. Yoon and J. Jang. Conducting-Polymer Nanomaterials for High-Performance Sensor Applications: Issues and Challenges. Advanced Functional Materials. 19 (2009) 1567-1576.

[46] F. Cheng, W. Tang, C. Li, J. Chen, H. Liu, P. Shen and S. Dou. Conducting Poly(aniline) Nanotubes and Nanofibers: Controlled Synthesis and Application in Lithium/Poly(aniline) Rechargeable Batteries. Chemistry-A European Journal. 12 (2006) 3082-3088.

[47] C. Wang, W. Zheng, Z. Yue, C.O. Too and G.G. Wallace. Buckled, Stretchable Polypyrrole Electrodes for Battery Applications. Advanced Materials. 23 (2011) 3580-3584.

[48] B.A. Bolto, R. McNeill and D.E. Weiss. Electronic Conduction in Polymers III: Electronic Properties of Polypyrrole. Australian Journal of Chemistry.16 (1963) 1090-1103.

[49] A.F. Diaz. Electrochemical Preparation and Characterization of Conducting Polymers. Chemica Scripta. 17 (1981) 145-148.

[50] A.F. Diaz and B. Hall. Mechanical-Properties of Electrochemically Prepared Polypyrrole Films, IBM Journal of Research and Development. 27 (1983) 342-347.

[51] G. Tourillon and F. Garnier. New Electrochemically Generated Organic Conducting Polymers. Journal of Electroanalytical Chemistry and Interfacial Electrochemistry. 135 (1982) 173-178.

[52] R. Gangopadhyay and A. De. Conducting Polymer Nanocomposites: A Brief Overview. Chemistry of Materials. 12 (2000) 608-622.

[53] K. Dutta and S.K. De. Transport and Optical properties of SiO_2–Polypyrrole Nanocomposites. Solid State Communications. 140 (2006) 167-171.

[54] A.G.B. da Cruz, J.L Wardell and A.M. Rocco. Hybrid Organic–Inorganic Materials Based on Polypyrrole and 1,3-Dithiole-2-thione-4,5-dithiolate (DMIT) Containing Dianions. Journal of Materials Science. 43 (2008) 5823-5836.

[55] J. Wang, J. Chen, K. Konstantinov, L. Zhao, S.H. Ng, G.X. Wang, Z.P. Guo and H.K. Liu. Sulphur-Polypyrrole Composite Positive Electrode Materials for Rechargeable Lithium Batteries. Electrochimica Acta. 51 (2006) 4634-4638.

[56] L. Cui, J. Shen, F. Cheng, Z. Tao and J. Chen. SnO_2 Nanoparticles@Polypyrrole Nanowires Composite as Anode Materials for Rechargeable Lithium-Ion Batteries. Journal of Power Sources. 196 (2011) 2195-2201.

[57] G. Han and G. Shi. Electrochemical Actuator Based on Single-Layer Polypyrrole Film. Sensors and Actuators, B: Chemical. 113 (2006) 259-264.

[58] J. Liu, Z. Wang, Y. Zhao, H. Cheng, C. Hu, L. Jiang and L. Qu. Three-Dimensional Graphene-Polypyrrole Hybrid Electrochemical Actuator. Nanoscale. 4 (2012) 7563-7568.

[59] A. Liu, W. Yuan and G. Shi. Electrochemical Actuator Based on Polypyrrole/Sulfonated Graphene/Graphene Tri-layer Film. Thin Solid Films. 520 (2012) 6307-6312.

[60] C.C.B. Bufon and T. Heinzel. Polypyrrole Thin-Film Field-Effect Transistor. Applied Physics Letters. 89 (2006) 012104.

[61] C.T. Kou and T.R. Liou. Characterization of Metal-Oxide-Semiconductor Field-Effect Transistor (MOSFET) for Polypyrrole and Poly(N-alkylpyrrole)s Prepared by Electrochemical Synthesis. Synthetic Metals. 82 (1996) 167-173.

[62] M.S. Lee, H.S. Kang, H.S. Kang, J. Joo, A.J. Epstein and J.Y. Lee. Flexible All-Polymer Field Effect Transistors with Optical Transparency Using Electrically Conducting Polymers. Thin Solid Film. 477 (2005) 169-173.

[63] S. Biswas and L.T. Drzal. Multilayered Nanoarchitecture of Graphene Nanosheets and Polypyrrole Nanowires for High Performance Supercapacitor Electrodes. Chemistry of Materials. 22 (2010) 5667-5671.

[64] Y. Zhao, J. Liu, Y. Hu, H. Cheng, C. Hu, C. Jiang, L. Jiang, A. Cao and L. Qu. Highly Compression-Tolerant Supercapacitor Based on Polypyrrole-Mediated Graphene Foam Electrodes. Advanced Materials. 25 (2013) 591-595.

[65] A. Rajesh, S.S. Pandey, W. Takashima and K. Kaneto. Simultaneous Co-immobilization of Enzyme and a Redox Mediator in Polypyrrole Film for the Fabrication of a Amperometric Phenol Biosensor. Current Applied Physics. 5 (2005) 184-188.

[66] A. Arslan, S. Kiralp, L. Toppare and Y. Yagci. Immobilization of Tyrosinase in Polysiloxane/Polypyrrole Copolymer Matrices. International Journal of Biological Macromolecules. 35 (2005) 163-167.

[67] M. Yousef Elahi, S.Z. Bathaie, S.H. Kazemi and M.F. Mousavi. DNA Immobilization on a Polypyrrole Nanofiber Modified Electrode and Its Interaction with Salicylic Acid/Aspirin. Analytical Biochemistry. 411 (2011) 176-184.

[68] A. Ramanavičius, A. Ramanavičiene and A. Malinauskas. Electrochemical Sensors Based on Conducting Polymer-Polypyrrole. Electrochimica Acta. 51 (2006) 6025-6037.

[69] S.A. Waghuley, S.M. Yenorkar, S.S. Yawale and S.P. Yawale. Application of Chemically Synthesized Conducting Polymer-Polypyrrole as a Carbon Dioxide Gas Sensor. Sensors and Actuators, B: Chemical. 128 (2008) 366-373.

[70] Y. Liao, X. Wang, W. Qian, Y. Li, X. Li and D.G. Yu. Bulk synthesis, Optimization, and Characterization of Highly Dispersible Polypyrrole Nanoparticles Toward Protein Separation Using Nanocomposite Membranes. Journal of Colloid and Interface Science. 386 (2012) 148-157.

[71] M. Karimi, M. Mohsen-Nia and A. Akbari. Electro-Separation of Synthetic Azo Dyes from a Simulated Wastewater Using Polypyrrole/Polyacrylonitrile Conductive Membranes. Journal of Water Process Engineering. 4 (2014) 6-11.

[72] Y. Cho and R.B. Borgens. The Preparation of Polypyrrole Surfaces in the Presence of Mesoporous Silica Nanoparticles and Their Biomedical Application. Nanotechnology. 21 (2010) 205102.

[73] E. Armelin, R. Pla, F. Liesa, X. Ramis, J.I. Iribarren and C. Alemán. Corrosion Protection with Polyaniline and Polypyrrole as Anticorrosive Additives for Epoxy Paint. Corrosion Science. 50 (2008) 721-728.

[74] E. Håkansson, A. Amiet, S. Nahavandi and A. Kaynak. Electromagnetic Interference Shielding and Radiation Absorption in Thin Polypyrrole Films. European Polymer Journal. 43 (2007) 205-213.

[75] A. Kaur, Ishpal and S.K. Dhawan. Tuning of EMI Shielding Properties of Polypyrrole Nanoparticles with Surfactant Concentration. Synthetic Metals. 162 (2012) 1471-1477.

[76] E. Håkansson, A. Amiet and A. Kaynak. Electromagnetic Shielding Properties of Polypyrrole/Polyester Composites in the 1–18 GHz Frequency Range. Synthetic Metals. 156 (2006) 917-925.

[77] P. Camurlu. Polypyrrole Derivatives for Electrochromic Applications. RSC Advances. 4 (2014) 55832-55845.

[78] T.W. Lewis and G.G. Wallace. Communicative Polymers: The Basis for Development of Intelligent Material. Journal of Chemical Education. 74 (1997) 703-708.

[79] H. Eisazadeh, G.M. Spinks and G.G. Wallace. Electrochemical Production of Polypyrrole Colloids. Polymer. 35 (1994) 3801-3803.

[80] R.J. Waltman and J. Bargon. Electrically Conducting Polymers: A Review of the Electropolymerization Reaction, of the Effects of Chemical Structure on Polymer Film properties, and of Applications Towards Technology. Canadian Journal of Chemistry. 64 (1986) 76-95.

[81] R.J. Waltman and J. Bargon. Reactivity/Structure Correlations for the Electropolymerization of Pyrrole: An INDO/CNDO Study of the Reactive Sites of Oligomeric Radical Cations. Tetrahedron. 40 (1984) 3963-3970.

[82] A.K. Meikap, A. Das, S. Chatterjee, M. Digar and S.N. Bhattacharyya. Electrical Transport in Doped Polypyrrole Films at Low Temperature. Physical Review B. 47 (1993) 1340-1345.

[83] J.M. Ribo, A. Dicko, M.A. Valles, N. Ferrer, R. Bonnett and D. Bloor. Polypyrrole with Dipyrrinone End Groups. Synthetic Metals. 33 (1989) 403-408.

[84] P. Jayamurgan, V. Ponnuswamy, S. Ashokan and T. Mahalingam. The Effect of Dopant on Structural, Thermal and Morphological Properties of DBSA-Doped Polypyrrole. Iranian Polymer Journal. 22 (2013) 219-225.

[85] C. Cassignol, P. Olivier and A. Ricard. Influence of the Dopant on the Polypyrrole Moisture Content: Effects on Conductivity and Thermal Stability. Journal of Applied Polymer Science. 70 (1998) 1567-1577.

[86] C. Ding, X. Qian, G. Yu and X. An. Dopant Effect and Characterization of Polypyrrole-Cellulose Composites Prepared by in situ Polymerization Process. Cellulose. 17 (2010) 1067-1077.

[87] N. Othman, Z.A. Talib, A. Kassim, A.H. Shaari and J.Y.C. Liew. Electrical Properties of Polypyrrole Conducting Polymer at Various Dopant Concentrations. Journal of Fundamental Sciences. 5 (2009) 29-33.

[88] A. Eftekhari, M. Kazemzad and M. Keyanpour-Rad. Significant Effect of Dopant Size on Nanoscale Fractal Structure of Polypyrrole Film. Polymer Journal. 38 (2006) 781-785.

[89] T. Shimidzu, A. Ohtani, T. Iyoda and K. Honda. Charge-Controllable Polypyrrole/Polyelectrolyte Composite Membranes: Part II. Effect of Incorporated Anion Size on the Electrochemical Oxidation-Reduction Process. Journal of Electroanalytical Chemistry. 224 (1987) 123-135.

[90] M.A. De Paoli, R.C.D. Peres, S. Panero and B. Scrosati. Properties of Electrochemically Synthesized Polymer Electrodes—X. Study of Polypyrrole/Dodecylbenzene Sulfonate. Electrochemica Acta. 37 (1992) 1173-1182.

[91] K.K. Kanazawa, A.F. Diaz, M.T. Krounbi and G.B. Street. Electrical Properties of Pyrrole and Its Copolymers. Synthetic Metals. 4 (1981) 119-130.

[92] J. Rühe, T.A. Ezquerra and G. Wegner. New Conducting Polymers from 3-Alkylpyrroles. Synthetic Metals. 28 (1989) 177-181.

[93] J.Y. Lee, D.Y. Kim and C.Y. Kim. Synthesis of Soluble Polypyrrole of the Doped State in Organic Solvents. Synthetic Metals. 74 (1995) 103-106.

[94] J.Y. Lee, K.T. Song, S.Y. Kim, Y.C. Kim, D.Y. Kim and C.Y. Kim. Synthesis and Characterization of Soluble Polypyrrole. Synthetic Metals. 84 (1997) 137-140.

[95] E.J. Oh, K.S. Jang and A.G. MacDiarmid. High Molecular Weight Soluble Polypyrrole. Synthetic Metals. 125 (2001) 267-272.

[96] Y. Shen and M. Wan. In Situ Doping Polymerization of Pyrrole with Sulfonic Acid as a Dopant. Synthetic Metals. 96 (1998) 127-132.

[97] R. Marcilla, C. Pozo-Gonzalo, J. Rodríguez, J.A. Alduncin, J.A. Pomposo and D. Mecerreyes. Use of Polymeric Ionic Liquids as Stabilizers in the Synthesis of Polypyrrole Organic Dispersions. Synthetic Metals. 156 (2006) 1133-1138.

[98] C. Sasso, M. Fenoll, O. Stephan and D. Beneventia. Use of Wood Derivatives as Doping / Dispersing Agents in the Preparation of Polypyrrole Aqueous Dispersions. BioResources. 3 (2008) 1187-1195.

[99] J. Bhadra and D. Sarkar. Polypyrrole Nanocomposite Made by Polypyrrole Dispersion in Poly (vinyl alcohol) Matrix. Indian Journal of Physics. 84 (2010) 1321-1325.

[100] S.P. Armes and M. Aldissi. Preparation and Characterization of Colloidal Dispersions of Polypyrrole Using Poly(2-vinyl pyridine)-Based Steric Stabilizers. Polymer. 31 (1990) 569-574.

[101] M.R. Simmons, P.A. Chaloner, S.P. Armes, S.J. Greaves and J.F. Watts. Synthesis and Characterization of Colloidal Polypyrrole Particles Using Reactive Polymeric Stabilizers. Langmuir. 14 (1998) 611-618.

[102] Y.F. Nicolau, S. Davied, F. Genoud, M. Nechtschein and J.P. Travers. Polyaniline, Polypyrrole, Poly(3-methylthiophene) and Polybithiophene Layer-by-Layer Deposited Thin Films. Synthetic Metals. 42 (1991) 1491-1494.

[103] C.P. De Melo, B.B. Neto, E.G. De Lima, L.F.B. De Lira and J.E.G. De Souza. Use of Conducting Polypyrrole Blends as Gas Sensors. Sensors and Actuators, B: Chemical. 109 (2005) 348-354.

[104] M. Ángeles Corres, A. Mugica, P.M. Carrasco and M. Milagros Cortázar. Effect of Crystallization on Morphology-Conductivity Relationship in Polypyrrole/Poly(ε-caprolactone) Blends. Polymer. 47 (2006) 6759-6764.

[105] P. Ludeelerd, S. Niamlang, R. Kunaruksapong and A. Sirivat. Effect of Elastomer Matrix Type on Electromechanical Response of Conductive Polypyrrole/Elastomer Blends. Journal of Physics and Chemistry of Solids. 71 (2010) 1243-1250.

[106] D.O. Kim, P.C. Lee, S.J. Kang, K. Jang, J.H. Lee, M.H. Cho and J.D. Nam. In-Situ Blends of Polypyrrole/Poly(3,4-ethylenedioxythiopene) Using Vapor Phase Polymerization Technique. Thin Solid Films. 517 (2009) 4156-4160.

[107] R.B. Bjorklund and I. Lundström. Some Properties of Polypyrrole-Paper Composites. Journal of Electronic Materials. 13 (1984) 211-230.

[108] B. Yue, C. Wang, X. Ding and G.G. Wallace. Polypyrrole Coated Nylon Lycra Fabric as Stretchable Electrode for Supercapacitor Applications. Electrochimica Acta. 68 (2012) 18-24.

[109] K. Boukerma, J.Y. Piquemal, M.M. Chehimi, M. Mravčáková, M. Omastová and P. Beaunier. Synthesis and Interfacial Properties of Montmorillonite/Polypyrrole Nanocomposites. Polymer. 47 (2006) 569-576.

[110] C. Yang, P. Liu, J. Guo and Y. Wang. Polypyrrole/Vermiculite Nanocomposites via Self-Assembling and in situ Chemical Oxidative Polymerization. Synthetic Metals. 160 (2010) 592-598.

[111] C. Yao, Y. Xu, Y. Kong, W. Liu, W. Wang, Z. Wang, Y. Wang and J. Ji. Polypyrrole/Palygorskite Nanocomposite: A New Chromate Collector. Applied Clay Science. 67-68 (2012) 32-35.

[112] M. Onoda, D. Fujita, K. Isaki and H. Nakayama. Preparation and Functions of Conductive Polymer/Insulating Polymer Composite Films Using Molecular Self-Assembly. Electrical Engineering in Japan. 128 (1999) 1-8.

Chapter 2 Materials, experimental methods and characterizations

2.1 Materials

2.1.1 Pyrrole

Pyrrole is a five-membered heterocyclic aromatic organic compound with the formula C_4H_4NH [1, 2]. It is a colorless liquid and the color will become darker when it is exposed to air. Usually, it is purified by distillation immediately prior to use. In this thesis, pyrrole was used as monomer to prepare polypyrrole by the oxidation of pyrrole. Pyrrole (analytical grade reagent) was purchased from Nacalai Tesque, Inc. (Kyoto, Japan) and freshly distilled under pressure before use.
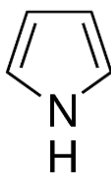

Fig. 2-1 Structure of pyrrole.

2.1.2 Ammonium persulfate

Ammonium persulfate (APS, $(NH_4)_2S_2O_8$) is an inorganic compound that is highly soluble in water. It is a strong oxidizing agent and used as initiator in polymer chemistry. In this thesis, APS that purchased from Nacalai Tesque, Inc. (Kyoto, Japan) was used as an oxidant to prepare PPy without further purification.
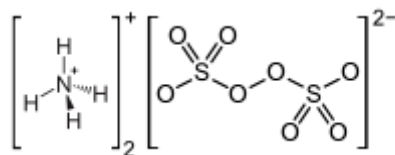

Fig. 2-2 Structure of ammonium persulfate.

2.1.3 Acid violet 19

Acid violet 19 (AV19, disodium 2-amino-5-[(Z)-(4-amino-3-sulfonatophenyl) (4-iminio-3-sulfonato-2,5-cyclohexadien-1-ylidene) methyl]-3-methylbenzenesulfonate) is an acid dye used in the Van Gieson method in conjunction with picric acid to demonstrate collagen fibers red, and in Masson's trichrome to stain smooth muscle in contrast to collagen [3]. It is also used as Andrade's indicator. It is a green crystalline powder and soluble in water. In chapter 3, AV19 was used as multi-sulfonate aromatic dopant. AV19 was purchased from Nacalai Tesque, Inc. (Kyoto, Japan) and used without further purification.
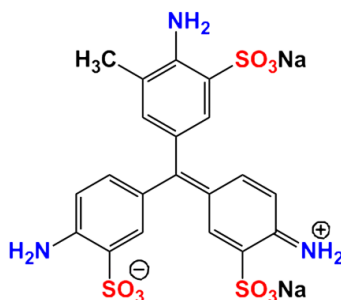

Fig. 2-3 Structure of acid violet 19.

2.1.4 Mesoporous silica

According to the pore size, porous materials can be divided into three classes: microporous, mesoporous and macroporous [4]. Microporous materials have pore diameters of less than 2 nm. Mesoporous materials have pore diameters ranging from 2 to 50 nm. Macroporous category are those that have pore diameters of greater than 50 nm. Mesoporous silica is one of the widely used mesoporous materials. Due to the large surface area and well-defined internal structure, mesoporous silica have widely applications in the fields of catalysis, adsorption, separation, sensor and drug delivery.

Mesoporous silica (MS) was purchased from AGC Si-Tech Co., Ltd and the technical

information of MS was listed in Table 2-1. MS was functionalized with –SO$_3$H groups and then used as solid dopant and inorganic host to prepare mesoporous silica/PPy composite in Chapter 4.
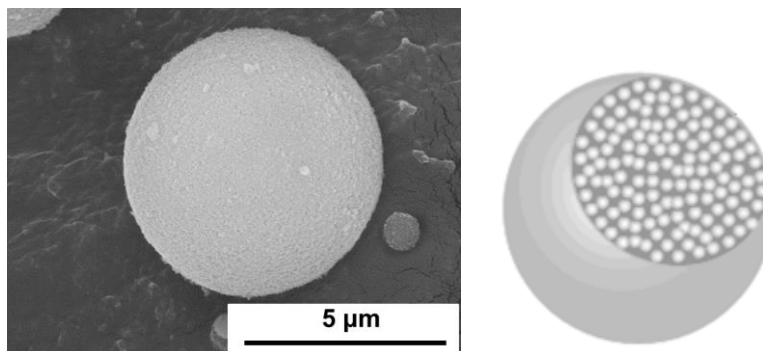

Fig. 2-4 SEM image (a) and diagrammatic sketch [5] (b) of mesoporous silica used in Chapter 4.

Table 2-1 The technical information of MS used in Chapter 4

Characteristics	Value
Mean particle size	3.2 μm
Specific surface area	719 m^2/g
Pore volume	1.8 mL/g
Pore diameter	25 nm
Oil absorption	300 mL/100g

2.1.5 Attapulgite

Attapulgite (ATP) is also called palygorskite, which is a naturally needle-like clay mineral composed of magnesium-aluminum silicate. The ideal molecular formula of ATP is (Mg, Al)$_5$Si$_8$O$_{20}$(OH)$_2$(OH$_2$)$_4$•4H$_2$O. Due to its unique three dimensional chain structure, ATP has very good colloidal and sorptive properties. It has a wide variety of applications such as: thickeners, anti-settling agent, binder, rheology modifier and catalyst carrier [6, 7].

ATP was purchased from BASF Co. Ltd. (New Jessey, USA) and the technical information of ATP was listed in Table 2-2.
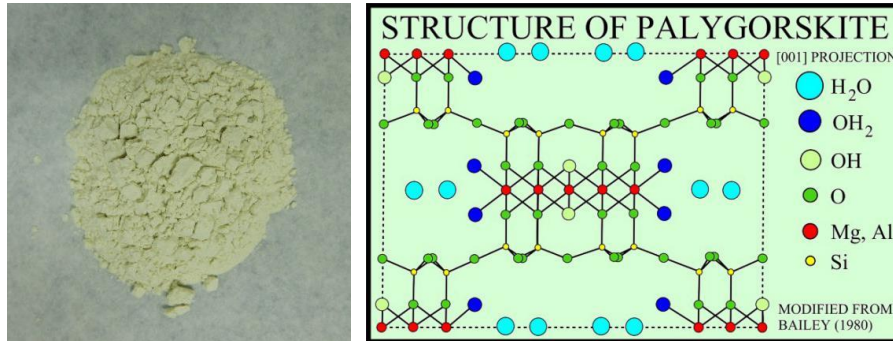

Fig. 2-5 Photograph and structure [8] of attapulgite used in Chapter 5.

Table 2-2 Composition and typical properties of ATP used in Chapter 5

Composition			
SiO_2	65.2%	Al_2O_3	12.7%
MgO	12.3%	CaO	3.9%
Fe_2O_3	3.5%	P_2O_5	1.0%
K_2O	0.8%	TiO_2	0.5%
Properties			
Specific gravity	2.4	Oil absorption	100 mL/100g
Specific surface area	150 m^2/g	Color	Light cream

2.1.6 Polyvinyl alcohol

Polyvinyl alcohol (PVA) is a water-soluble synthetic resin with an idealized formula $CH_2CH(OH)_n$ [9, 10]. PVA shows excellent film forming, barrier, emulsifying and adhesive properties. The unique properties of PVA make it have a wide variety of applications in papermaking, textiles, and coatings. The molecular structure of PVA is given below:
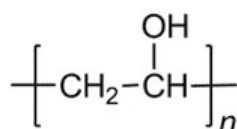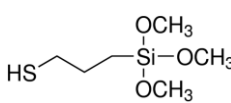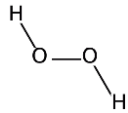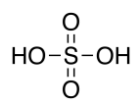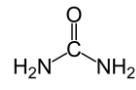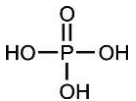
Fig. 2-6 Structure of polyvinyl alcohol.

PVA with a degree of polymerization of 1,700 in the form of 99% hydrolyzed was supplied by Sinopharm Chemical Reagent Co., Ltd., China. Then it was used to prepare phosphorylated polyvinyl alcohol (PPVA) which was served as polymeric dopant to fabricate ATP/PPy composite in Chapter 5.

2.1.7 Other materials

Table 2-3 Other materials used in this thesis work

Name	Molecular structure	Purity
γ-Mercaptopropyltrimethoxysilane (MPTMS)		96%
Hydrogen peroxide (H_2O_2)		30%
Sulfuric acid (H_2SO_4)		97%
Urea		98%
Phosphoric acid (H_3PO_4)		85%

MPTMS was provided by Shin-Etsu Chemical Co., Ltd (Tokyo, Japan) and others were purchased from Nacalai Tesque, Inc. (Kyoto, Japan) and used without further purification.

2.2 General experimental method

PPy and its composite were synthesized by chemical oxidative polymerization of pyrrole monomer using ammonium peroxidisulphate (APS) as oxidant.
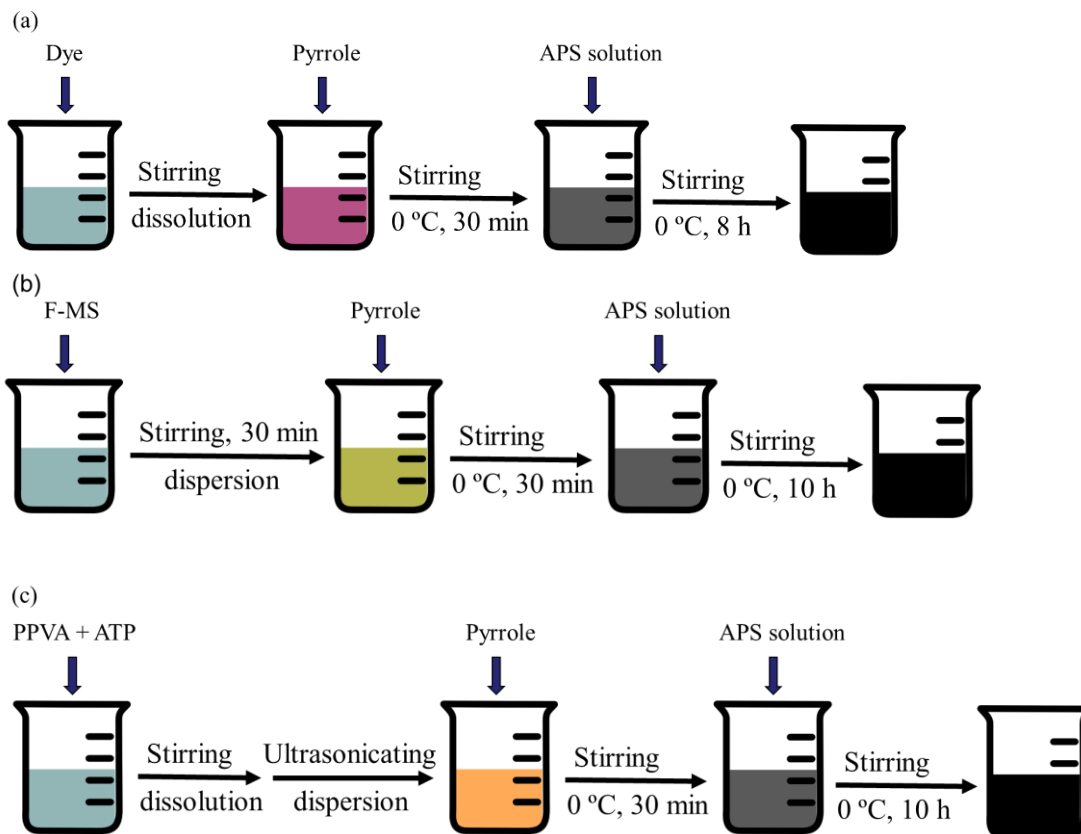
Fig. 2-7 Schematic diagram of preparation of (a) multifunctional dye doped PPy, (b) F-MS/PPy and (c) ATP/PPy composites.

For multifunctional dye doped PPy, dye was dissolved in 100 mL of double distilled water in a 250 mL round-bottom flask with stirring. Freshly distilled pyrrole (1 mL) was added to the solution with stirring for 30 min in ice-cold condition. Subsequently, 20 mL of APS aqueous solution (containing 0.9 g of APS) was added drop by drop into the above mixture to initiate the oxidative polymerization. The reaction was performed at 0 °C with vigorous stirring for 8 h under N_2 atmosphere. The resultant PPy-AV19 was

filtered, and washed with distilled water until the filtrate become colorless. The product was dried under vacuum at 60 °C for 24 h prior to further analysis.

For functionalized mesoporous silica/polypyrrole (F-MS/PPy) composites, F-MS was dispersed in 100 mL of deionized water with vigorous stirring for 30 min. The rest steps were similar to those of synthesis of multifunctional dye doped PPy.

For attapulgite/polypyrrole (ATP/PPy) composites, phosphorylated polyvinyl alcohol (PPVA) and 1.45 g of ATP were added to 100 mL of water in a 250 mL round-bottom flask and stirred until PPVA was dissolved. The mixture was then ultrasonically dispersed for 30 min. The rest steps were similar to those of synthesis of multifunctional dye doped PPy.

2.3 Characterizations

2.3.1 Electrical conductivity

The electrical conductivities of the samples were measured using SDY-4 four-point probe meter (Guangzhou Semiconductor Material Academe) at ambient temperature. The powdery samples were shaped into circular pellets with a diameter of 13 mm by subjecting the powder to a pressure of 30 MPa. The reproducibility of the result was checked by measuring the electrical conductivity three times for each pellet. The measurement principle is given in Fig. 2-8.
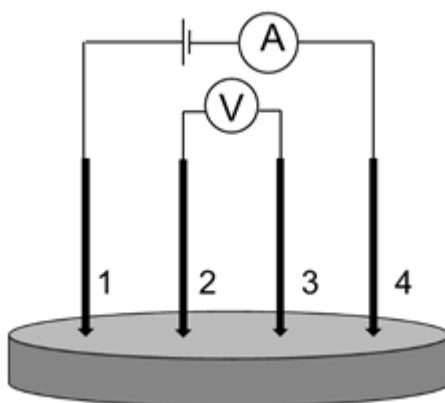

Fig. 2-8 Schematic of a four-point resistance measurement.

The electrical conductivity of the sample can be obtained according the following formula:

$$\rho = \frac{V}{I} \times F(D/S) \times F(W/S) \times W \times Fsp \quad (\Omega \cdot cm)$$

$$\sigma = 1/\rho \qquad (S/cm)$$

Where, V – the voltage between probe 2 and 3 (mV);

I – the current between probe 1 and 4 (mA);

W – the thickness of the pallets (cm);

F(D/S) – the amendatory coefficient of the diameter of the pallets;

F(W/S) – the amendatory coefficient of the thickness of the pallets;

Fsp – the amendatory coefficient of the space between the probes.

2.3.2 Cyclic voltammetry (CV) and galvanostatic charge-discharge tests

Cyclic voltammetry (CV) and galvanostatic charge-discharge tests that was performed with a CHI660A electrochemical working station in the potential window ranged from -0.6 to 0.4 V (vs. SCE). The mixture containing 80 wt.% of active materials, 15 wt.% carbon black, and 5 wt.% polytetrafluoroethylene (PTFE) was uniformly laid on a Ni foam that acted as a current collector (area was about 1 cm^2). Then the Ni foam coating PPy-based composite was pressed under 1.0 MPa for 1 min and served as the working electrode. A typical three-electrode cell, containing a working electrode, a platinum foil counter electrode, a saturated calomel reference electrode, and a 0.5 M Na$_2$SO$_4$ aqueous solution as electrolyte was utilized to evaluate the electrochemical behavior of the composites. The specific capacitance (C$_m$) can be calculated from the equation:

$$C_m = \frac{I \times \Delta t}{m \times \Delta V} \quad (F/g)$$

Where, I – the charge/discharge current (A);

Δt – the discharge time (S);

ΔV – the potential drop during discharge (V);

m – the mass of active material (g).

2.3.3 Scanning electron microscopy (SEM)

The samples covered with an ultra-thin layer of a gold/palladium alloy were analyzed by scanning electron microscope (SEM, Hitachi S-4300, Japan).

2.3.4 Transmission electron microscopy (TEM)

The morphologies of the samples were also observed using a transmission electron microscope (TEM, Hitachi H-8100, Japan). Samples for TEM analysis were firstly dispersed by ultrasonic in distilled water. A drop of the suspension solution was placed on a porous carbon film grid and then dried on filter paper.

2.3.5 Fourier transform infrared spectroscopy (FTIR)

The chemical structures of the nanoparticles were confirmed by Fourier transform infrared (FTIR, IRT-7000, Jasco, Japan) spectroscopy using KBr pellets. The FTIR spectra were recorded in the range of 4000-400 cm^{-1} at resolution 4 cm^{-1} with 30 scans.

2.3.6 UV-visible spectroscopy

The powdery samples for UV-visible Spectroscopy analysis were prepared by dispersing ultrasonically in distilled water, then the obtained suspension was analyzed using a Lambda 950 UV/Vis/NIR spectrophotometer (PerkinElmer, USA).

2.3.7 Thermogravimetric analysis (TGA)

Thermogravimetric analysis (TGA, Shimadzu DTG-60) was carried out at a heating rate of 10 °C/min from 30 to 700 °C under a nitrogen atmosphere.

2.3.8 X-ray diffraction (XRD)

The X-ray diffraction (XRD) patterns were recorded in the range of 2θ = 5–90° by step scanning with a PANalytical X'Pert Pro X-ray diffractometer with a Cu Kα

radiation source (λ=0.154 nm).

2.3.9 X-ray photoelectron spectra (XPS)

X-ray photoelectron spectra (XPS) were obtained using a PHI 5000 Series XPS instrument.

2.3.10 Temperature dependence of conductivity

The temperature dependence of conductivity was determined by WDJ-1 temperature change resistance measuring instrument (Institute of Chemistry Chinese Academy of Sciences) at a heating rate of 10 °C/min from 25 to 150 °C.

2.3.11 Thermal stability of conductivity

The thermal stability of conductivity was evaluated according to electrical conductivity retention under isothermal aging at 50, 100 and 150 °C. The electrical conductivity measurements were performed at an interval of 1 h.

Reference

[1] M.G. Loudon. "Chemistry of Naphthalene and the Aromatic Heterocycles.". Organic Chemistry (4th ed.). Oxford University Press. New York, (2002), pp.1135-1136.

[2] W.L.F. Armarego and C.L.L. Chai. Purification of Laboratory Chemicals (5th ed.). Elsevier. (2003), pp. 346.

[3] E. Gurr. Synthetic Dyes in Biology, Medicine and Chemistry. Academic Press, London, (1971).

[4] J. Rouquerol, D. Avnir, C.W. Fairbridge, D.H. Everett, J.M. Haynes, N. Pernicone, J.D.F. Ramsay, K.S.W. Sing and K.K. Unger. Recommendations for the Characterization of Porous Solids (Technical Report). Pure and Applied Chemistry. 66 (1994) 1739-1758.

[5] http://www.agc-si.com/en/technique_sunsphere01.shtml

[6] W. L. Haden Jr. Attapulgite: Properties and Uses. Clays and Clay Minerals. 10 (1961) 284-290.

[7] W. Lynwood Haden, I. Albert Schwint. Attapulgite: Its Properties and Applications. Industrial & Engineering Chemistry Research. 59 (1967) 58-69.

[8] http://pubs.usgs.gov/of/2001/of01-041/htmldocs/images/palstru.jpg

[9] M.L. Hallensleben. "Polyvinyl Compounds, Others" in Ullmann's Encyclopedia of Industrial Chemistry. Wiley-VCH. Weinheim, (2000).

[10] R.X. Yan. Water-Soluble Polymer. Chemical Industry Press. Beijing, (1998), pp.42-43.

Chapter 3 Preparation and characterization of multifunctional dye doped polypyrrole

3.1 Introduction

As mentioned in Chapter 1, PPy is of great interest since its attractive merits such as high conductivity, facile synthesis, excellent environmental stability, biocompatibility, and appealing electrochemical behavior [1-3] as one of well-known conjugated conducting polymers. However, like other conducting polymers, PPy suffers from low electrical conductivity in its native state, which couldn't come up to the level of desired performance. The poor processability of PPy also limit its application.

To improve the electrical conductivity, an additional anionic compound (dopant) that can decrease the energy band gap is typically incorporated into the polymer matrix. Recently, various organic sulfonates (anthraquinone sulfonate, p-toluenesulfonate, poly(styrene sulfonate), lignosulfonate and so on) have been widely used in the in-situ doping polymerization to afford PPy with high conductivity, enhanced specific capacitance, good solubility, and improved cycle stability [4-8]. Dyes containing sulfonate groups are attractive for preparing conjugated conducting polymers. J.J. Zhu et al. used methyl orange as reactive template and dopant to prepare PPy-based composite microtube [9]; M.A. De Paoli used indigo carmine to ensure the photoelectrochemical property [10]; E.M. Girotto reported that bromophenol blue-doped polypyrrole showed optical pH sensitive property [11].

Acid violet 19 (AV19) that has three branched sulfonate groups is widely used in histology as an acid dye [12]. The chemical structure of AV19 is shown in Fig. 2-3. Because of the multiple sulfonate groups of AV19, it was used as a dopant to improve the electrical conductivity and electrochemical performance of PPy in this chapter. The large conjugated system of AV19 would exert π–π stacking with PPy, which plays a part in improving the stabilization of AV19 within PPy [13], and the large molecular dopant

could show satisfactory stability during the charge–discharge process [14]. On the other hand, the multiple negative charge groups of AV19 and strong interaction between AV19 and PPy make the resulting materials have enhanced aqueous dispersion based on electrostatic dispersion. Moreover, some studies reported that the dopant containing multiple anions could cause physical crosslinking of different polymer chains, and the cross-linked materials with open channels could achieve fast charge carriers motion and higher capacitance [15]. The morphology, structure, and electrical properties of the resultant composites were characterized by SEM, FTIR, UV-vis, TGA, CV and galvanostatic charge-discharge test. The effects of AV19 on the morphology and electrical properties were also studied.

3.2 Experimental

Preparation of AV19 Doped PPy

A series of AV19 doped PPy (AV19/PPy) were prepared via chemical polymerization in the presence of varied concentration of AV19. The preparation method has been described in 2.2. The conditions of the polymerizations are given in Table 3-1. For comparison, pure PPy without any AV19 was synthesized in the same way.

Table 3-1 The compositions of PPy-AV19 investigated in this work

Samples	Pyrrole (mL)	AV19 (g)	Theoretic AV19 content (%)
S-1	1	0.051	5
S-2	1	0.107	10
S-3	1	0.242	20
S-4	1	0.414	30
S-5	1	0.937	50

3.3 Results and discussion

3.3.1 Morphological analysis

The particle micrographs were investigated by SEM. The SEM images of pure PPy without any AV19 are shown in Fig. 3-1. It's found that pure PPy showed a granular structure with the average diameter of ~200 nm.
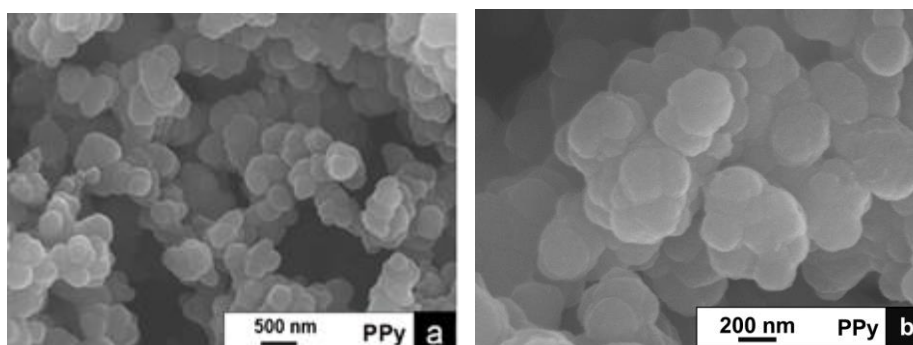

Fig. 3-1 SEM images of pure PPy nanoparticles.

For the resulting AV19/PPy nanocomposites, they showed a series of differences which was dependent on the feeding ratio of AV19 and pyrrole monomer. When AV19 was incorporated at low concentration, the sample also appeared as granular shape (S-1), but the diameter of the nanoparticles was much smaller than that of pure PPy. This is due to the AV19 with three branched sulfonate groups could also play the role as surfactant. Generally, the particle size decreased with increasing concentration of surfactant. Indeed, the diameter of the particle further decreased when the concentration of AV19 increased. When the content of AV19 increased to 20%, the sample (S-3) showed the smallest diameter of ~50 nm.
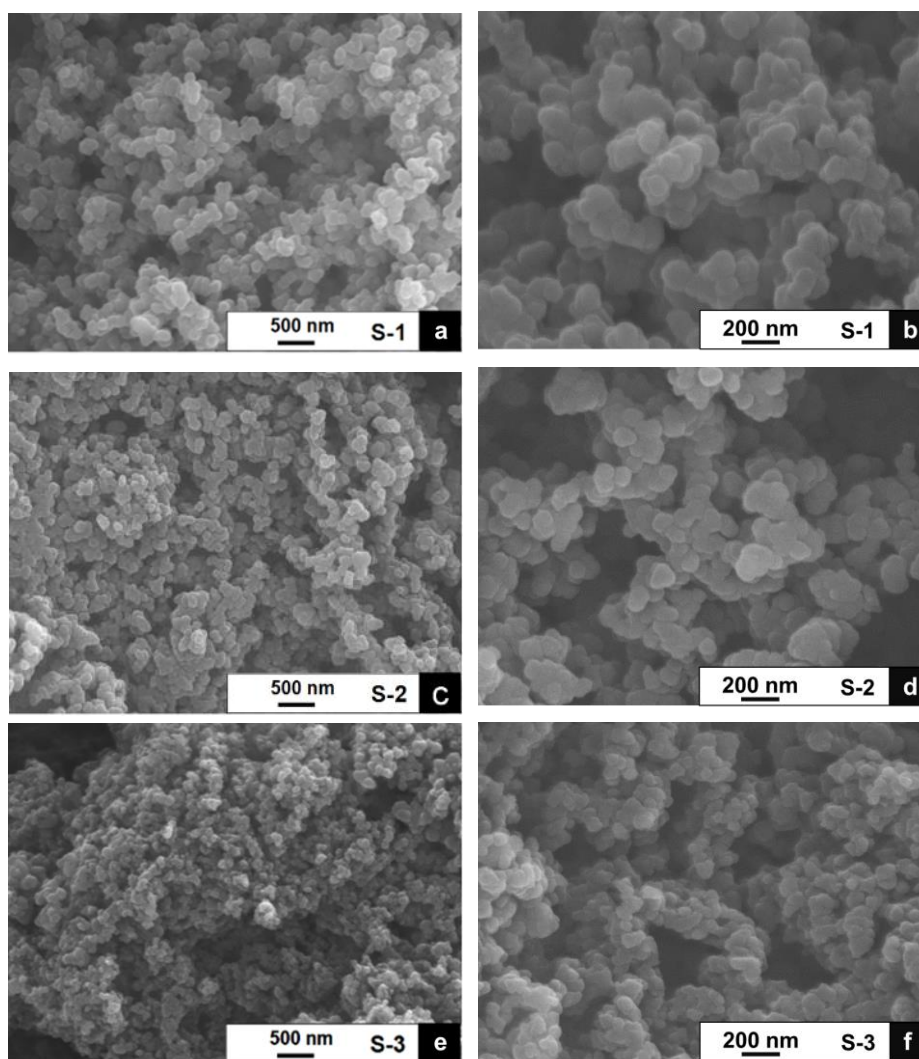
Fig. 3-2 SEM images of AV19/PPy samples with low concentration of AV19 (a, b:
S-1; c, d: S-2; e, f: S-3).

However, the sample exhibited more and more marked agglomeration with continuing increase of AV19. When the content of AV19 increased to 50% (S-5), the sample formed a block lamellar structure. This might be contributed to the strong interactions caused by three aspects: (1) The amino or imino groups presented in AV19 might form hydrogen bonds with the amino group of pyrrole, which would increase the interaction between different PPy chains. (2) The AV19 containing multiple sulfonate groups could cause physical crosslinking of PPy [15]. (3) π–π stacking interactions occurred owing to the large conjugated system of PPy and AV19. The micrographs of the PPy-AV19 nanocomposites would affect the aqueous dispersion of PPy samples.
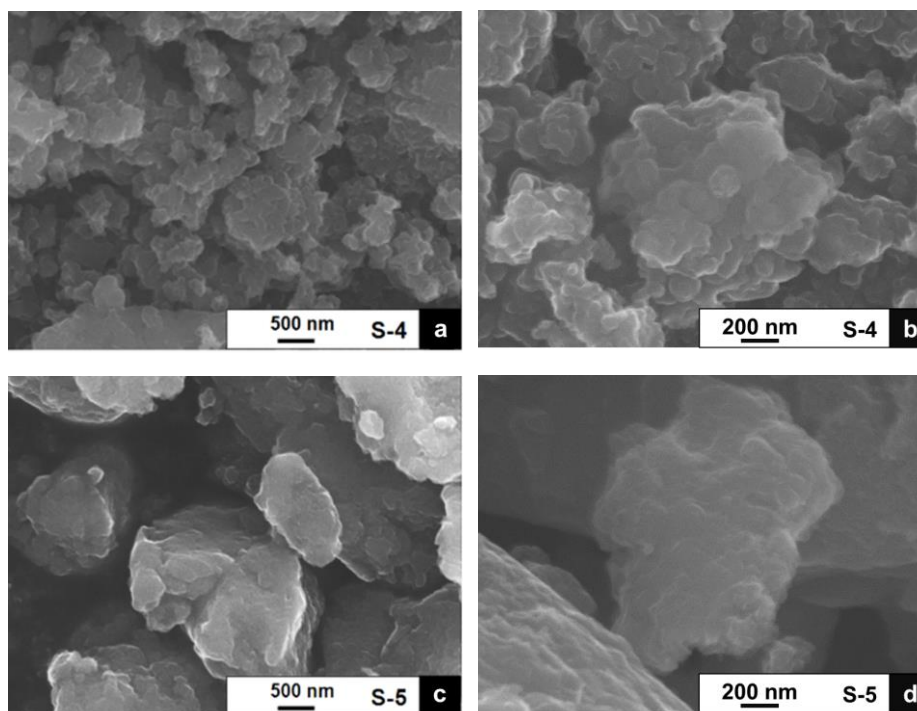
Fig. 3-3 SEM images of AV19/PPy samples with high concentration of AV19 (a, b: S-4; c, d: S-5).

3.3.2 Aqueous dispersion stability

The PPy is hard to disperse in water and the suspension of PPy shows rapid sedimentation immediately after ultrasonication due to the strong interactions between chains of PPy, which would limit its application. PPy-based materials that possess excellent dispersion stability may have more potential applications. The addition of AV19 allowed the formation of stable suspensions (Fig. 3-4a, S-1) since the multi-sulfonates of AV19 allowed electrostatic stabilization of PPy in the suspensions. S-3 exhibited the best dispersion that stabilized for more than one week in aqueous solution (Fig. 3-4b). This might be due to the relative small particle size and high content of AV19. For S-5, the excess AV19 led to PPy formation of block lamellar structure, and such agglomeration resulted in poor stability of PPy dispersion.
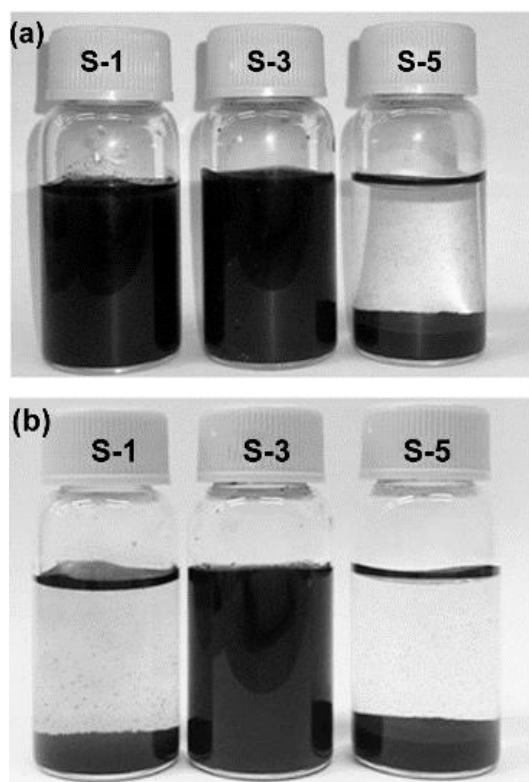
Fig. 3-4 The dispersion stability of AV19/PPy suspensions in water after (a) an hour

and (b) a week.

3.3.3 Spectral analyses

(a) FTIR analysis

The FTIR spectra of PPy, AV19/PPy and AV19 are shown in Fig. 3-5. For PPy, the peaks at 1542 and 1464 cm^{-1} are associated with the C=C and C–N stretching vibration in the pyrrole ring [16]. Additionally, the strong peaks near 872 cm^{-1} present the doping state of PPy, and the broad band at 1030 and 1300 cm^{-1} demonstrates the C–H and C–N in-plane deformation vibration and stretching vibrations respectively. Basically, the results obtained in our FTIR study are consistent with those reported by others.

For AV19/PPy samples, both of the characteristic peaks of PPy and the absorbance of S=O stretching at 1189 cm^{-1} of sulfonate appeared, which indicated that PPy was doped with AV19. As mentioned above, the content of AV19 plays a significant role in the morphology of the conducting polymer. So, it is important to inquire how PPy was

45

incorporated into PPy. We observed that the intensity for the 3400 cm^{-1} absorption band, which was attributed to the −OH, was reduced in AV19/PPy samples compared with pure PPy. And the absorption decreased with an increasing content of AV19 in AV19/PPy. It is inferred that instead of bound water, the amino or imino groups presented in AV19 would form hydrogen bonds with the secondary amine groups of PPy. And the absorption of −OH decreased when the content of AV19 was increased due to more amino and imino groups existed in the AV19/PPy nanocomposite. In addition, the C=C stretching vibration of pyrrole ring at 1542 cm^{-1} shifted to 1551 cm^{-1} after doping with AV19 (S-3), indicating the existence of the interaction between AV19 and pyrrole ring.
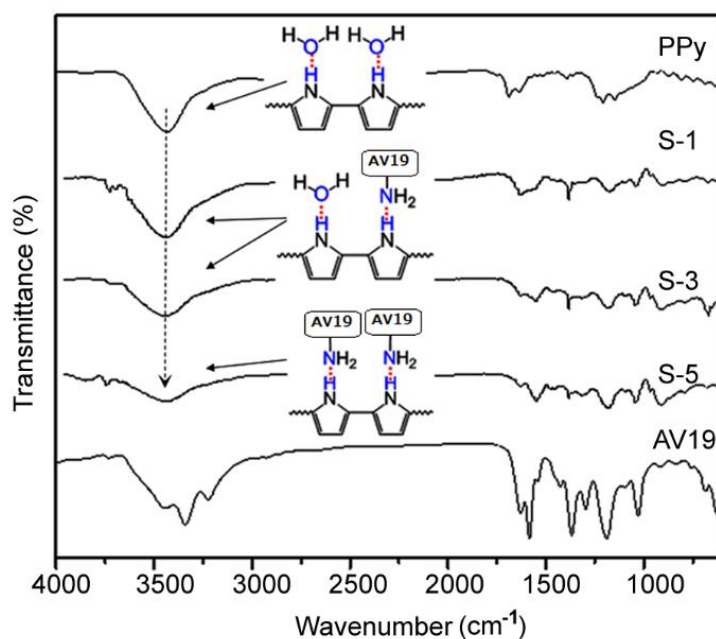
Fig. 3-5 FTIR spectra of AV19, PPy and AV19/PPy samples (S-1, S-3 and S-5).

(b) UV-vis analysis

The UV-vis spectra of aqueous solution of AV19, aqueous dispersions of PPy samples in the absence of AV19 and in the presence of AV19 were recorded and presented in Fig. 3-6. The absorption peak at around 460 nm for PPy samples in the absence of AV19 was observed, which was associated with the transition from valence band to bipolarons of

PPy [17, 18]. From the resolving of overlapping peak of AV19/PPy sample (S-3), we could observe that the absorption peak showed a red shift to 470 nm, revealing higher conjugation length conductivity [18]. Moreover, the characteristic peaks of AV19 at 494 and 545 nm also presented in the spectrum of AV19/PPy samples and shifted to higher wavelength at 521 and 566 nm, respectively. It indicates that AV19 was well incorporated with PPy and there was strong conjugation between AV19 and PPy which would be conducive to the transition of the charge carrier due to a lower energy gap [19].
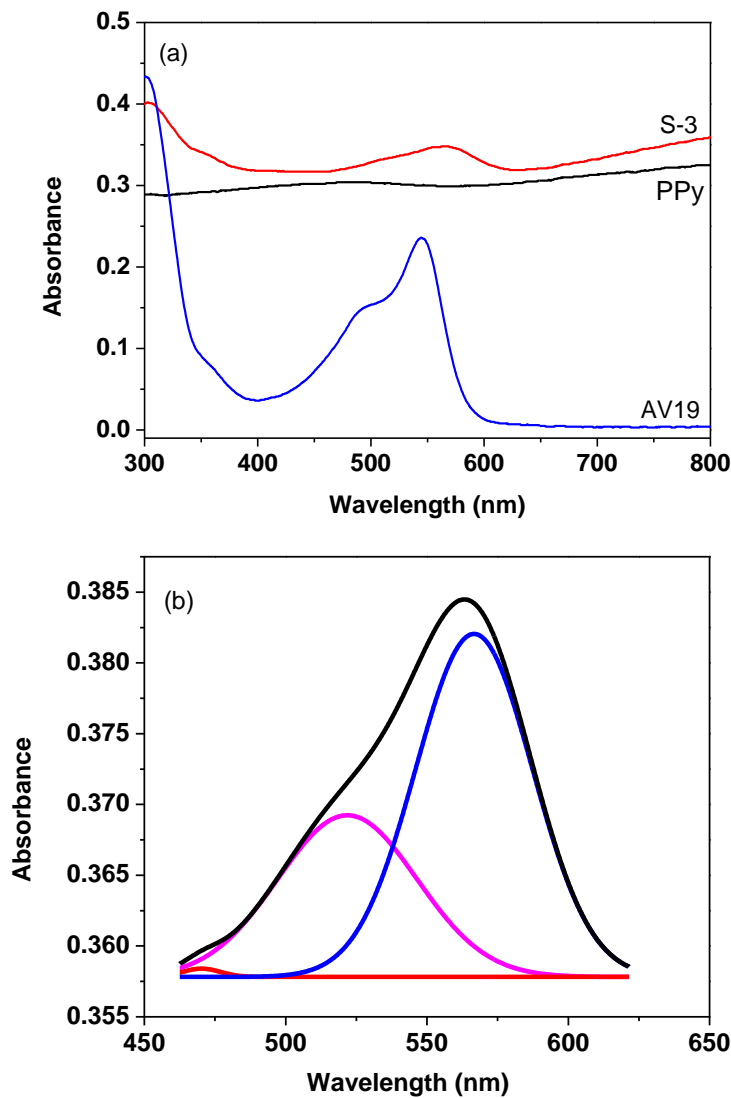

Fig. 3-6 UV-vis spectra of (a) AV19, pure PPy and AV19/PPy and (b) the resolving of overlapping peak of AV19/PPy.

(c) XPS analysis

The XPS survey spectra of the resulting AV19/PPy samples are shown in Fig. 3-7. The main peaks at 168, 285, 400 and 531 eV corresponds to S2p, C1s, N1s and O1s, respectively. Table 3-2 lists surface chemical composition of AV19/PPy samples. We can know from the table that the atomic concentration ratio of S/N increases with increasing feeding ration of AV19, indicating that more AV19 has been incorporated in the sample.
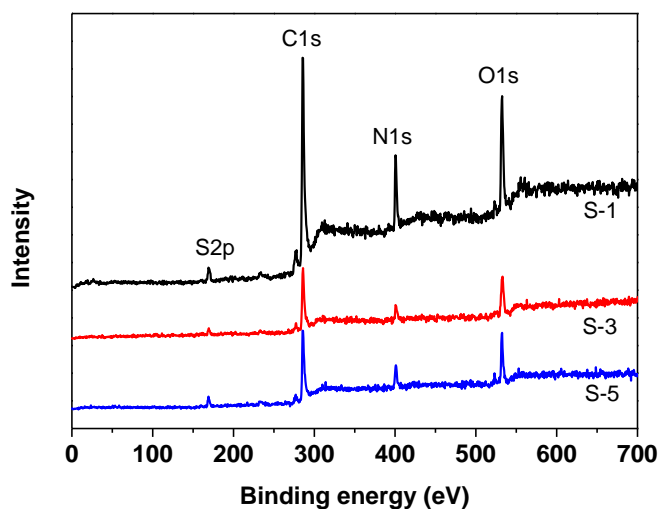
Fig. 3-7 XPS survey spectra of AV19/PPy samples (S-1, S-3 and S-5).

Table 3-2 Surface chemical composition of AV19/PPy samples determined by XPS

Sample	C (atom%)	N (atom%)	O (atom%)	S (atom%)	S/N
S-1	71.72	12.31	13.45	2.52	0.2047
S-3	71.38	9.01	16.64	2.98	0.3307
S-5	69.15	11.18	15.37	4.31	0.3855

3.3.4 Thermal analysis

The thermal properties of the AV19/PPy samples were studied by TGA as shown in Fig. 3-8. The weight loss below 120 °C was caused by the release of water molecules

owing to the hygroscopic character of the samples. The AV19/PPy samples began to decompose at about 230 °C and the weight loss above 230 °C was attributed to decomposition of PPy and AV19. The residues of the AV19/PPy samples decreased with the increasing feeding ratio of the AV19 due to the low residue of AV19.
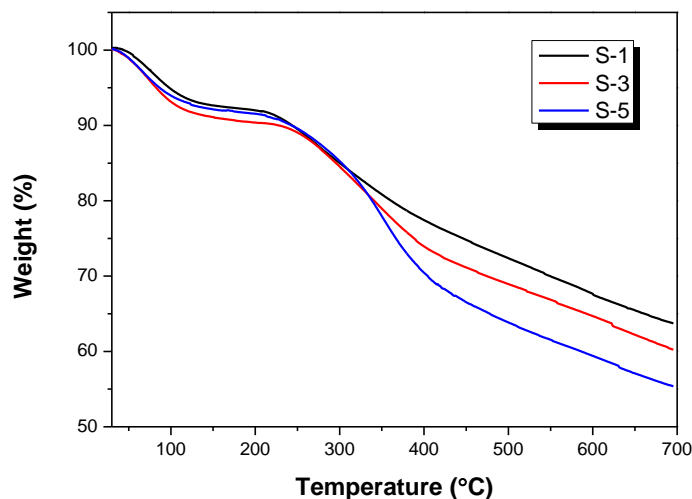
Fig. 3-8 TGA curves of AV19/PPy samples (S-1, S-3 and S-5).

In order to obtain more information about the thermal properties of AV19/PPy nanocomposites, derivative thermogravimetric (DTG) curves were analyzed. For temperatures of 230-450 °C, the DTG curve of S-1 had two peaks at 276 and 335 °C, which was attributed to decomposition of PPy and AV19, respectively. However, for S-3, a wide peak at 338 °C was observed. It indicates that AV19 has strong interaction with PPy and PPy has been well doped by AV19, resulting in enhanced thermal stability. With an increase of AV19 in AV19/PPy nanocomposite, the DTG curve of S-5 showed a strong peak at 353 °C, which indicated that the thermal stability of the AV19/PPy nanocomposite has been further improved. This is because there are more functional groups in the AV19/PPy nanocomposite that could enhance the interaction with PPy.
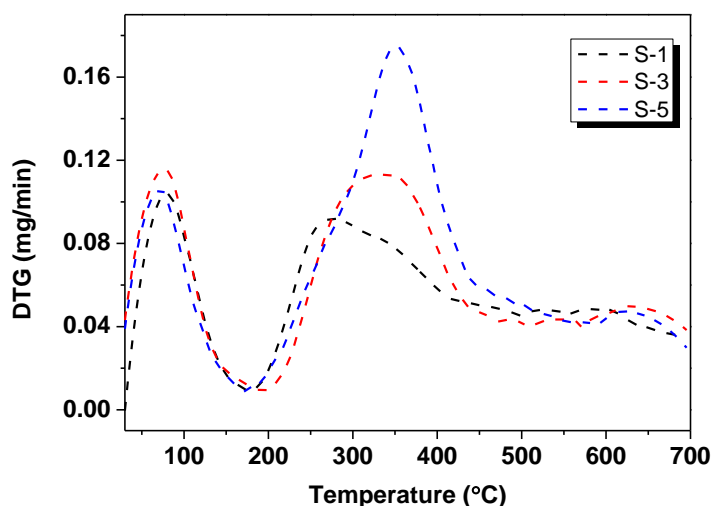
Fig. 3-9 DTG curves of AV19/PPy samples (S-1, S-3 and S-5).

3.3.5 Electrical conductivity

The dopant we used in this work has three branched sulfonate groups, which is possible to improve the conductivity of PPy. The effect of the feeding ratio of AV19 on the electrical conductivity is summarized in Fig. 3-10. S-3 sample with the AV19 feeding ratio of 20% presented granular shape with the smallest particle size ~50 nm of all samples and achieved the highest conductivity of 39.09 S/cm. This might be caused by a comprehensive effect. The doping level of the AV19/PPy nanocomposite increased and the particle size decreased with the increasing feeding ratio of AV19 at first, which were good for improving the electrical conductivity. On the other hand, with a further increase of AV19, the hydrogen bonds and π–π stacking interactions between AV19 and PPy prevented a number of AV19 from doping the PPy, and the extra AV19 molecules hindered charge carriers transmission between the conjugated chains. In addition, the block lamellar structure was harmful for forming dense conducting passage for charge carrier transfer. Based on the above reasons, with the increasing in the AV19 feeding ratio, the electrical conductivity of the AV19/PPy samples increased firstly and then decreased.
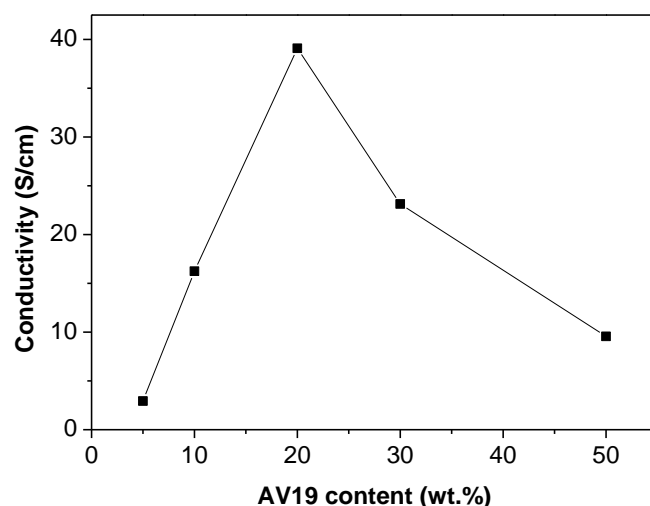
Fig. 3-10 The electrical conductivity of AV19/PPy samples.

3.3.6 Electrochemical performance

To further evaluate the applicability of the AV19/PPy in electrochemical energy storage devices, the cycling performance and the galvanostatic charge-discharge performances of the PPy-AV19 samples were investigated in three-electrode system. Fig. 3-11 shows the CV curves of the PPy-AV19 samples performed at a scan rate of 5 mV/s. The nearly box shape of the CVs indicated good capacitive behavior of PPy-AV19 nanocomposite electrodes corresponding to the redox feature of conducting polymers. The deviation from rectangle was caused by the equivalent series resistance [20]. It is inferred that the three branched sulfonate groups existing in AV19 could not only play the role as dopant but also crosslinking agent through physical crosslinking of PPy. The schematic representation of doping mechanism is illustrated in Fig. 3-12. Such structure is beneficial for the diffusivity of electrolyte so as to make the nanocomposite possess good capacitive behavior.
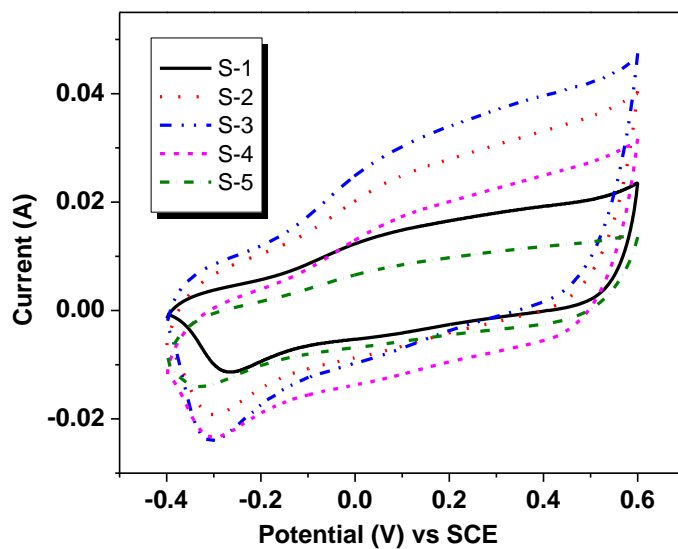
Fig. 3-11 Cyclic voltammograms of AV19/PPy nanocomposite electrodes at a scan

rate of 5 mV/s in 0.5 M Na_2SO_4 solution.
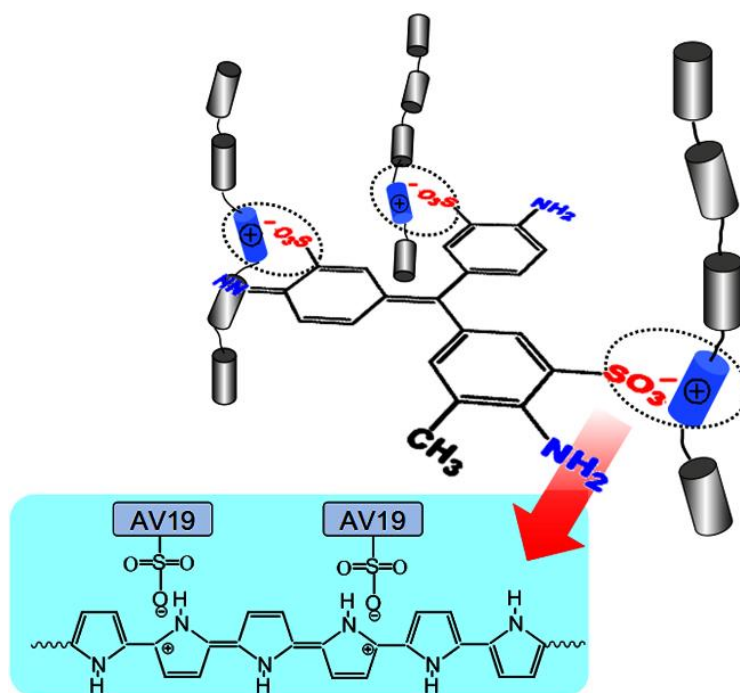
Fig. 3-12 Schematic representation for doping mechanism of PPy using AV19 as

dopant.

Galvanostatic charge-discharge curves of AV19/PPy nanocomposite electrodes with

different content of AV19 were recorded (Fig. 3-13a) at a current density of 0.2 A/g

within the potential window from -0.4 to 0.6 V. The specific capacitance (C_m) values of

S-1–S-5 calculated at a current density of 0.2 A/g is 131, 264, 379, 187, 97 F/g, respectively, which is plotted in Fig. 3-13b.
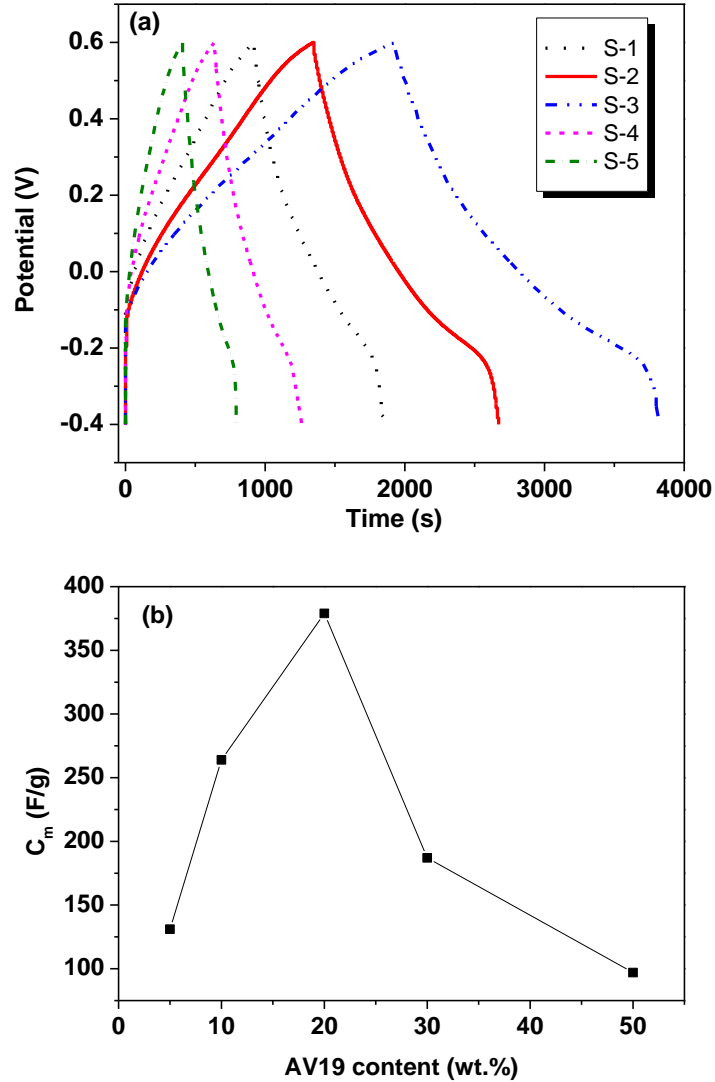
Fig. 3-13 Galvanostatic charge-discharge curves (a) and specific capacitances (b) of AV19/PPy electrodes at a current density of 0.2 A/g in 0.5 M Na_2SO_4 solution.

It is worth to note that with the increasing of AV19, the C_m increased firstly and then decreased. On the one hand, with the increasing of dopant, the doping level of the PPy and the electrical conductivity of the PPy-AV19 nanocomposite increased. And as the content of AV19 increased, the decreasing particle sizes can shorten the ion diffusion length [21, 22]. Moreover, the physical cross-linked caused by AV19 has open channels

that allow fast charge carriers motion. Based on these, the capacitance increased firstly. On the other hand, with a further increasing of AV19, the PPy-AV19 nanocomposite agglomerated to form a block lamellar structure which was detrimental to the diffusivity of electrolyte, resulting in decreasing capacitance.

Fig. 3-14 Galvanostatic charge-discharge curves (a) and specific capacitances (b) of AV19/PPy electrodes (S-3) at different current densities in 0.5 M Na_2SO_4 solution.

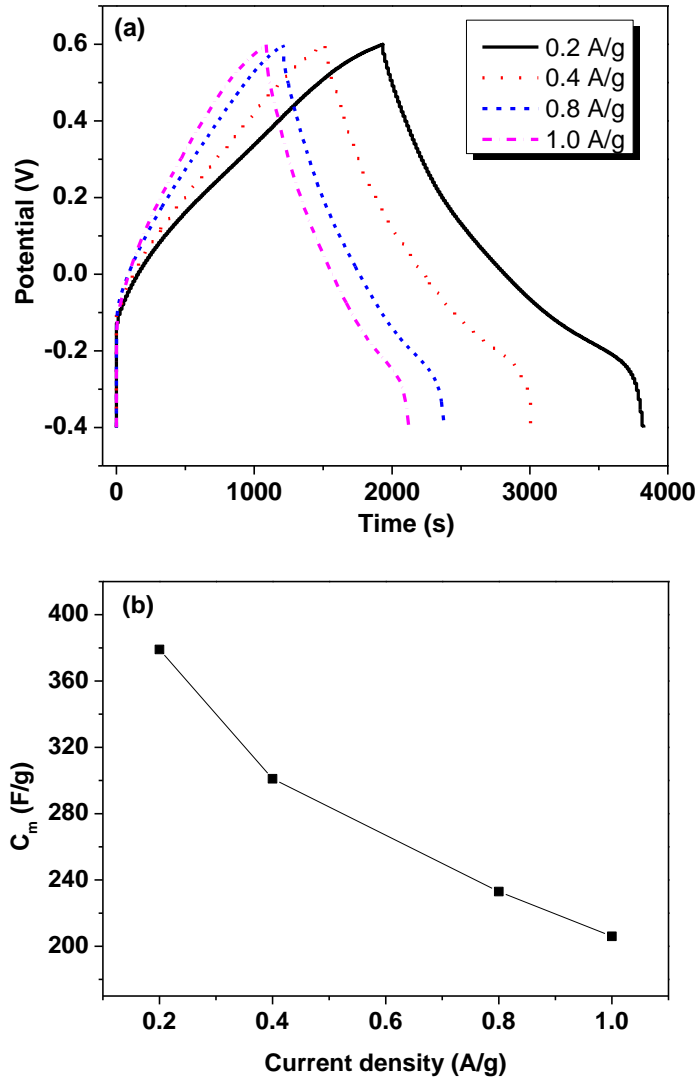The galvanostatic charge-discharge performances of S-3 at different current densities from 0.2 to 1.0 A/g were also tested and the results were shown in Fig. 3-14a. The C_m calculated at 0.2, 0.4, 0.8 and 1.0 A/g is 379, 301, 233, 206 F/g, respectively. The

reduction of C_m possibly results from the diffusional limitation at high current density [23]. However, about 54.4% of C_m was retained when the current density increased five times, indicating the electrode material has good capacitance retention.

3.4 Conclusions

In this chapter, aromatic dye AV19 containing tri-sulfonate groups was used as dopant to prepare a series of AV19/PPy nanoparticles by chemical polymerization. Besides being served as dopant, AV19 also functions as surfactant and physical cross-linker. It was found that the morphology, thermal and electrical properties were affected by the content of AV19.

(1) When the feeding ratio of AV19 was 20% (S-3), the sample composes of spherical granules showed the smallest diameter of ~50 nm.

(2) Sample S-3 had maximum electrical conductivity of 39.09 S/cm. AV19 could cause physical crosslinking and make the material open the channels, which was conducive to the diffusivity of electrolyte and improved the capacitance value. Therefore, the sample with the smallest particle size also possessed the maximum specific capacitance of 379 F/g thanks to the large area expose to electrolyte.

(3) The strong interactions between PPy and AV19 made the sample have enhanced thermal stability and dispersion stability in water.

(4) The interactions between PPy and AV19 included: hydrogen bonds forming between the amino or imino groups presented in AV19 and the amino group of pyrrole; physical crosslinking of different PPy chains; π–π stacking interactions between the large conjugated system of PPy and AV19.

Aromatic multi-sulfonate dopant is satisfying to prepare PPy nanoparticles with improved electrical properties and aqueous dispersion stability, which can broaden the applications of PPy materials in different fields. However, the cost of PPy production is unresolved.

References

[1] Y.C. Liu, H.T. Lee and S.J. Yang. Strategy for the Syntheses of Isolated Fine Silver Nanoparticles and Polypyrrole/Silver Nanocomposites on Gold Substrates. Electrochimica Acta. 51 (2006) 3441-3445.

[2] Q. Tang, X. Sun, Q. Li, J. Lin and J. Wu. Preparation and Electrical Conductivity of SiO_2/Polypyrrole Nanocomposite. Journal of Materials Science. 44 (2009) 849-854.

[3] S. Lee, M.S. Cho, J D. Nam and Y. Lee. Fabrication of Polypyrrole Nanorod Arrays for Supercapacitor: Effect of Length of Nanorods on Capacitance. Journal of Nanoscience and Nanotechnology. 8 (2008) 5036-5041.

[4] A. Rudge, I. Raistrick, S. Gottesfeld and J.P. Ferraris. A Study of the Electrochemical Properties of Conducting Polymers for Application in Electrochemical Capacitors. Electrochimica Acta. 39 (1994) 273-287.

[5] P.C. Wang, J.Y. Yu and K.H. Li. All-Organic Polymer-Dispersed Liquid Crystal Light-Valves Integrated with Electroactive Anthraquinone-2-Sulfonate-Doped Polypyrrole Thin Films as Driving Electrodes. Materials Chemistry and Physics. 130 (2011) 1346-1350.

[6] T. Raudsepp, M. Marandi, T. Tamm, V. Sammelselg, and J. Tamm. Study of the Factors Determining the Mobility of Ions in the Polypyrrole Films Doped with Aromatic Sulfonate Anions. Electrochimica Acta. 53 (2008) 3828-3835.

[7] T.M. Wu, H.L. Chang and Y.W. Lin. Synthesis and Characterization of Conductive Polypyrrole with Improved Conductivity and Processability. Polymer International. 58 (2009) 1065-1070.

[8] D.H. Nagaraju, T. Rebis, R. Gabrielsson, A. Elfwing, G. Milczarek and O. Inganäs. Charge Storage Capacity of Renewable Biopolymer/Conjugated Polymer Interpenetrating Networks Enhanced by Electroactive Dopants. Advanced Energy Materials. 4 (2014) 1300443.

[9] X. Feng, Z. Sun, W. Hou and J.J. Zhu. Synthesis of Functional Polypyrrole/Prussian Blue and Polypyrrole/Ag Composite Microtubes by Using a Reactive Template. Nanotechnology. 18 (2007) 195603.

[10] E.M. Girotto, W.A. Gazotti, C.F. Tormena and M.A. De Paoli. Photoelectronic and Transport Properties of Polypyrrole Doped with a Dianionic Dye. Electrochimica

Acta. 47 (2002) 1351-1357.

[11] J. Ferreira and E.M. Girotto. Optical pH Sensitive Material Based on Bromophenol Blue-Doped Polypyrrole. Sensors and Actuators B: Chemical. 137 (2009) 426-431.

[12] S.M. Chen and G.H. Chuang. Electropolymerization of Polymerized Fuchsin Acid Films Enhanced by Nafion® and Their Electrocatalytic Properties with Melatonin and 3,4-Dihydroxyphenylalanine. Journal of Electroanalytical Chemistry. 575 (2005) 125-137.

[13] E. Håkansson, T. Lin, H. Wang and A. Kaynak. The Effects of Dye Dopants on the Conductivity and Optical Absorption Properties of Polypyrrole. Synthetic Metals. 156 (2006) 1194-1202.

[14] Y. Yang, C. Wang, S. Ashraf and G.G. Wallace. Polypyrrole Doped with Redox-Active Poly(2-methoxyaniline-5-sulfonic acid) for Lithium Secondary Batteries. RSC Advances. 3 (2013) 5447-5452.

[15] S. Suematsu, Y. Oura, H. Tsujimoto, H. Kanno and K. Naoi. Conducting Polymer Films of Cross-Linked Structure and Their QCM Analysis. Electrochimica Acta. 45 (2000) 3813-3821.

[16] L. Li, E.T. Kang and K.G. Neoh. Preparation of Conductive Polypyrrole-Palladium Composite Nanospheres by Inverse Microemulsion Polymerization. Journal of Nanoscience and Nanotechnology. 6 (2006) 2571-2575.

[17] M.J. Antony and M. Jayakannan. Amphiphilic Azobenzenesulfonic Acid Anionic Surfactant for Water-Soluble, Ordered, and Luminescent Polypyrrole Nanospheres. The Journal of physical Chemistry B. 111 (2007) 12772-12780.

[18] V.P. Menon, J. Lei and C.R. Martin. Investigation of Molecular and Supermolecular Structure in Template-Synthesized Polypyrrole Tubules and Fibrils. Chemistry of Materials. 8 (1996) 2382-2390.

[19] K.S. Ho, T.H. Hsieh, C.W. Kuo, S.W. Lee, J.J. Lin and Y.J. Huang. Effect of Aniline Formaldehyde Resin on the Conjugation Length and Structure of Doped Polyaniline: Spectral Studies. Journal of Polymer Science Part A: Polymer Chemistry. 43 (2005) 3116-3125.

[20] S.K. Tripathi, A. Kumar and S.A. Hashmi. Electrochemical Redox Supercapacitors Using PVdF-HFP Based Gel Electrolytes and Polypyrrole as Conducting Polymer Electrode. Solid State Ionics. 177 (2006) 2979-1985.

[21] C. Yang, L. Zang, J. Qiu, E. Sakai, X. Wu and Y. Iwase. Nano-Cladding of Natural Microcrystalline Cellulose with Conducting Polymer: Preparation,

Characterization, and Application in Energy Storage. RSC Advances. 4 (2014) 40345-40351.

[22] Y.Z. Fu and A. Manthiram. Core-Shell Structured Sulfur-Polypyrrole Composite Cathodes for Lithium-Sulfur Batteries. RSC Advances. 2 (2012) 5927-5929.

[23] B.C. Kim, J.M. Ko and G.G. Wallace. A Novel Capacitor Material Based on Nafion-Doped Polypyrrole. Journal of Power Sources. 177 (2008) 665-668.

Chapter 4 Preparation and characterization of bayberry-like mesoporous silica/polypyrrole composites

4.1 Introduction

In Chapter 3, aromatic multi-sulfonate dopant has been utilized to improve the performances of PPy, including enhanced electrical conductivity, aqueous dispersion stability and thermal stability. However, the relative high cost of PPy production is still a problem. So in this chapter, we used low-price component to prepare PPy-based composite material. Composites, composing of conducting polymers and inorganic component, possess unique electrical and mechanical properties based on synergy effect, and their characteristics differ from their individual particles. So far, numerous efforts have been devoted to the preparation of inorganic/PPy nanocomposites which contain various inorganic particles, such as MnO_2, Fe_3O_4, WO_3, mullite, graphite oxide and TiO_2 [1-6]. Among inorganic particles, mesoporous silica (MS) materials are of particular interest due to the large surface area and well-defined internal structure [7, 8], which make them have widely applications in the fields of catalysis, adsorption, separation, sensing and drug delivery [9-14].

As mentioned before, the electrical conductivity of undoped PPy is unsatisfactory, so external dopants (usually HSO_4^-, BF_4^-, Cl^-, p-toluenesulfonate, anthraquinone-2-sulfonate, and dyes) are used for doping to improve the electrical conductivity [15-20]. PPy doped with external dopants has high electrical conductivity, however, the PPy may be subjected to de-doping process as a result of poor environmental stability, which will decrease the electrical conductivity or cause the corrosion problem owing to the free acid.

In this chapter, the MS with relative large pore diameter and high oil absorption value

was firstly functionalized with –SO$_3$H groups (F-MS), and then was utilized to prepare F-MS/PPy composites via *in-situ* chemical polymerization. On the one hand, the F-MS played the role as the inorganic host that can improve the thermal stability of the resultant composites. On the other hand, the –SO$_3$H groups presented on the surface of MS can make the F-MS function as the *in-situ* dopant to improve the electrical conductivity. Meanwhile, after silylation of MS, the compatibility of MS with organic polymer can be enhanced. In addition, the relative large pore diameter as well as relative high oil absorption value of the MS make it propitious to adsorb the pyrrole monomer to the surface and into the pore, and then carry out the polymerization of pyrrole to form composites. The morphology, structure, and electrical properties of the resultant composites were characterized by SEM, FTIR, XRD and TGA. The electrical conductivity of the composites were also investigated.

4.2 Experimental

4.2.1 Functionalization of mesoporous silica with –SO$_3$H groups

Functionalization of MS with –SO$_3$H groups was carried out following the reported method [21] with some modifications. Typically, 1.0 g of MS and 2.0 mL of MPTMS in 20 mL of dry toluene were refluxed for 10 h. The resulting product was filtered and then subjected to a Soxhlet apparatus to be extracted for 12 h in absolute ethanol. The obtained product was dried under vacuum at 60 °C for 24 h to obtain the thiol-functionalized MS. The thiol groups were then oxidized to –SO$_3$H groups via being treated with 30% H$_2$O$_2$ (10 mL) and methanol (5 mL) for 24 h at room temperature. After filtered and washed with ethanol, the solid was suspended in a 35 mL of 10 wt.% H$_2$SO$_4$ solution for 1 h at room temperature. The obtained particles were filtered and washed with deionized water until the pH of the wash was 7, and then dried under vacuum for 24 h at 60 °C.

4.2.2 Preparation of F-MS/PPy composites

The F-MS/PPy composites were prepared by the *in-situ* chemical oxidative polymerization method and the mass fraction of F-MS in the composites was changed by altering the feeding mass of F-MS prepared above. The schematic representation for the synthetic procedure is shown in Fig. 4-1 and the compositions of the F-MS/PPy are listed in Table 4-1. In a typical procedure, the F-MS was dispersed in 100 mL of deionized water with vigorous stirring for 30 min. Then 1.0 mL of freshly distilled pyrrole was added to the mixture with vigorous stirring for another 30 min in ice–water bath to obtain a uniform suspension. Subsequently, 20 mL of APS aqueous solution (containing 0.9 g of APS) was added drop by drop into the above mixture to initiate the oxidative polymerization. The reaction was performed at 0 °C with vigorous stirring for 10 h under N_2 atmosphere. The resulting composites were filtered and washed with distilled water and ethanol for several times, and then dried under vacuum for 24 h at 60 °C. For comparison, pure PPy was synthesized in the same way and the MS without functionalization was also used to prepare MS/PPy composites.

Table 4-1 The compositions of F-MS/PPy composites investigated in this work

Samples	Pyrrole (mL)	F-MS (g)	Feeding ratio of F-MS (wt.%)
S-1	1	0.051	5
S-2	1	0.107	10
S-3	1	0.242	20
S-4	1	0.414	30
S-5	1	0.645	40
S-6	1	0.937	50
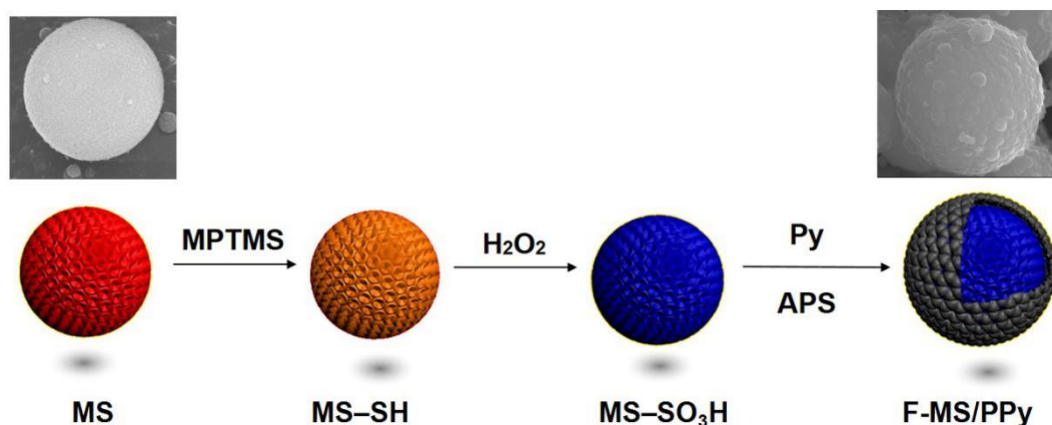
Fig. 4-1 Schematic illustration for the preparation of F-MS/PPy composites.

4.3 Results and discussion

4.3.1 Morphological analysis

The particle micrographs of MS and the F-MS/PPy composites were observed by SEM. Some reports pointed that not only the particle size but also the particle shape is influential in the characteristic properties of the composite [22, 23]. As shown in Fig. 4-2, the MS was spherical and noncohesive with a mean particle size of 3 μm. The MS used in this work has relative high oil absorption value (300 mL/100g) and relative large pore diameter (25 nm) which is favorable for adsorbing pyrrole monomer and performing polymerization to form composites. From the SEM image with high magnification, rough surface of MS was found.

Fig. 4-2 SEM images of MS particles.

The resulting F-MS/PPy composites showed different morphologies which was dependent on the feeding ratio of F-MS to pyrrole monomer.

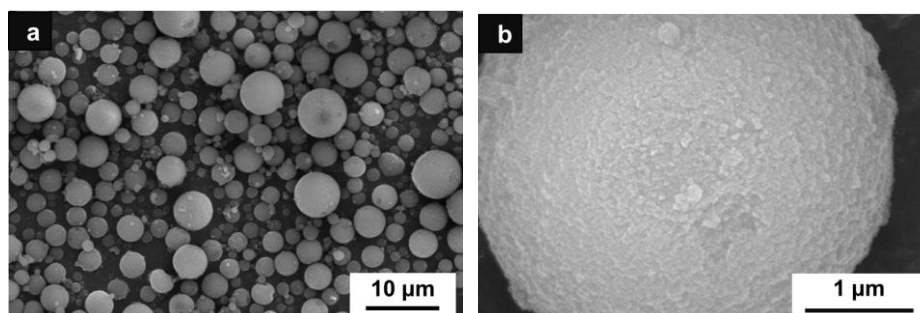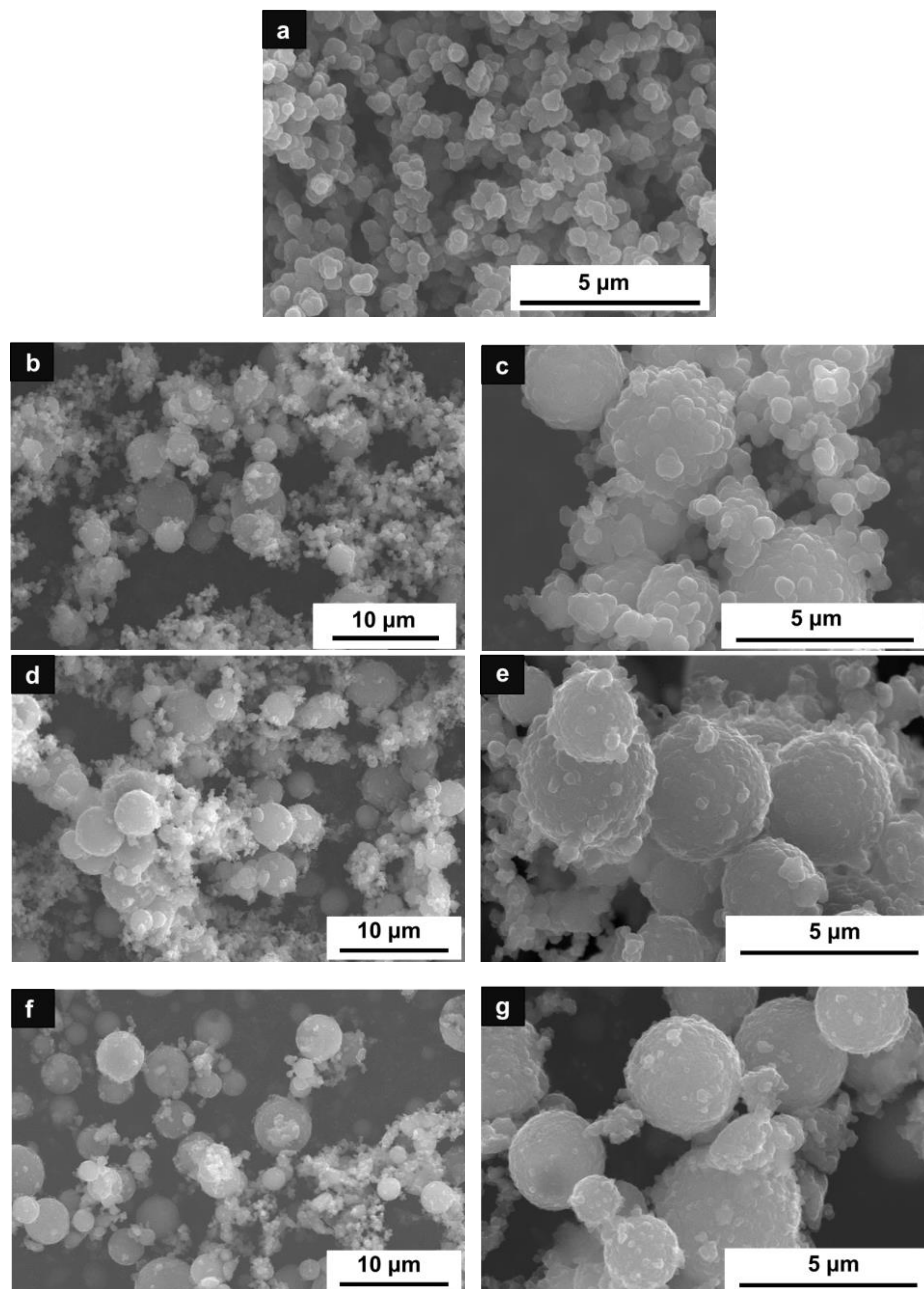Fig. 4-3 SEM images of pure PPy nanoparticles (a) and F-MS/PPy composites (b, c: S-1; d, e: S-2; f, g: S-3).

PPy prepared without any F-MS were spherical granules with nano-scale (Fig. 4-3a).

When the feeding ratio of F-MS was 5% (S-1), all of the F-MS particles were coated with a large number of PPy nanoparticles (Fig. 4-3(b, c)). Meanwhile, many free-standing PPy nanoparticles which were uniform and spherical similar to those in pure PPy sample were also obtained. When the feeding ratio of F-MS was 10% (S-2), the sample showed a unique bayberry-like morphology (Fig. 4-3(d, e)). Comparing to S-1, although all of the F-MS particles were also uniformly coated with PPy nanoparticles, the number of PPy nanoparticles coated on the F-MS and the free-standing ones were lower than that of S-1. As the feeding ratio of F-MS increased, different morphologies were observed. When the value was 20% (S-3), a thin layer of PPy was coated on the surface of F-MS and only a small quantity of free-standing PPy nanoparticles were obtained in the sample (Fig. 4-3(f, g)).

When the feeding ratio of F-MS further increased to 30% (S-4), only a part of the F-MS was coated with PPy nanoparticles (Fig. 4-4(a, b)). The tendency continues to grow with increasing feeding ratio of F-MS. Particularly, for S-6 (Fig. 4-4(e, f)), merely parts of the surface of the F-MS particles were adhered some PPy nanoparticles and many F-MS particles were as same as original. It is noteworthy that few free-standing PPy nanoparticles were observed when the content of F-MS was above 30%. It is speculated that: (1) The unique mesoporous features, large pore diameter as well as high oil absorption value of the MS make it propitious to adsorb the pyrrole monomer to the surface and into the pores to form composites. (2) There is hardly any pyrrole monomer drops in the system when the content of F-MS is higher than 30%. This speculation is in agreement with the surface polymerization theory [24-27]. The micrographs of the F-MS/PPy composites would affect the electrical conductivity which is discussed in the part of electrical conductivity analysis.
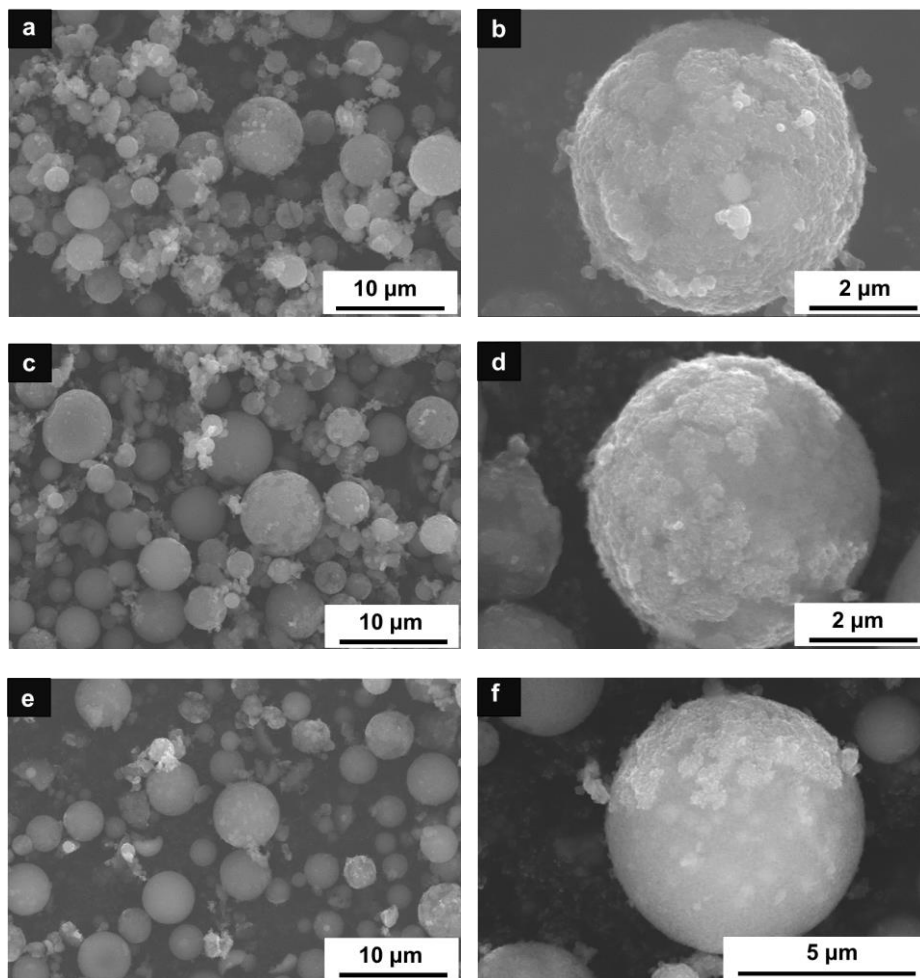
Fig. 4-4 SEM images of F-MS/PPy composites (a, b: S-4; c, d: S-5; e, f: S-6).

4.3.2 FTIR studies

The FTIR spectra of MS, F-MS, PPy and F-MS/PPy composite (S-2) are shown in Fig. 4-5. For MS, the Si–O–Si symmetrical stretching vibration at 1096 cm^{-1}, Si–O–Si asymmetrical stretching vibration at 804 cm^{-1}, and the characteristic peak at 965 cm^{-1} for Si–OH appeared. As is clearly known, silane-coupling agents are often used to modify inorganic particles to make them have functional groups or improve the compatibility with organic polymer. After silylation with MPTMS and oxidation with H$_2$O$_2$, the characteristic C–H stretching peaks at 2850 and 2925 cm^{-1}, and the S=O stretching peak at 1187 cm^{-1} arose, indicating the MS has been successfully functionalized with –SO$_3$H groups. The –SO$_3$H groups presented on the MS could play

the role as dopant to enhance the electrical properties of PPy.

For the PPy prepared without any F-MS, the sharp absorption peaks at 1540 and 1460 cm^{-1} could be assigned to the C=C stretching vibration and C–N stretching vibration of pyrrole ring, respectively [28]. The out of plane ring deformation vibration of C–H at 960 and 785 cm^{-1} also appeared. For F-MS/PPy composite (S-2), all the characteristic peaks of PPy were observed. Additionally, the new peak of S=O stretching peak at 1185 cm^{-1} appeared in the spectrum of F-MS/PPy composite, which can confirm that PPy has been doped with F-MS.
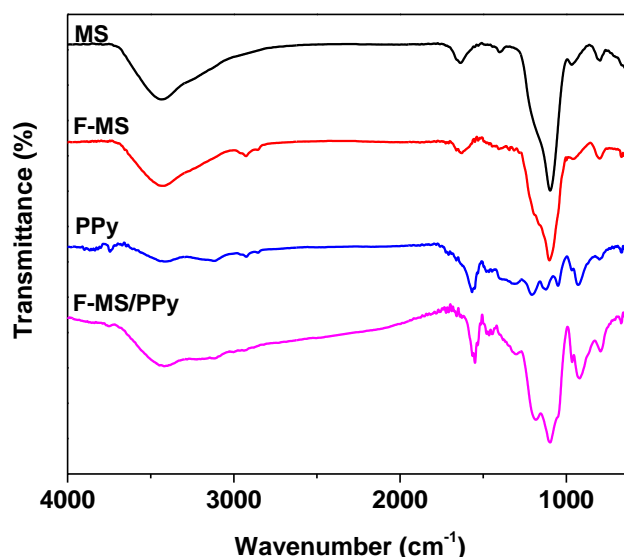
Fig. 4-5 FTIR spectra of MS, F-MS, PPy and F-MS/PPy (S-2).

4.3.3 XRD analysis

In order to investigate the structure of PPy after composed with F-MS, XRD measurements were performed. The XRD patterns of the PPy, MS and F-MS/PPy composites prepared at different contents of F-MS are shown in Fig. 4-6. The broad peak for the PPy at 2θ = 24.8° is attributed to the amorphous structure of PPy. After incorporating F-MS, the F-MS/PPy composites still keep the amorphous structure. However, the diffraction peak shifts to the low value (2θ = 22.5° for S-6) which is close

to the characteristic peak of MS with the increasing content of F-MS. This may be attributed to the high intensity of MS, and F-MS somewhat plays a part in improving the ordered structure of PPy.
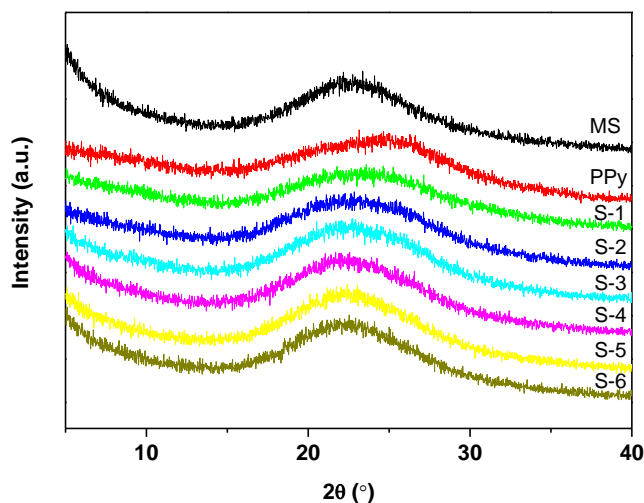
Fig. 4-6 XRD patterns of the PPy, MS and F-MS/PPy samples.

4.3.4 Thermal analysis

The thermal properties of the particles were studied by TGA. As shown in Fig. 4-7, the weight loss below 120 °C was attributed to the release of water molecules owing to the hygroscopic character of the samples. MS was thermally stable, and weight loss from 120-700 °C was 3.70%. Whereas, the weight loss for F-MS from 120-700 °C was 9.96%, which was attributed to decomposition of the alkylsulfonic acid groups [29]. It could be calculated that the content of organics covalently bound to MS was 6.26% after functionalization.
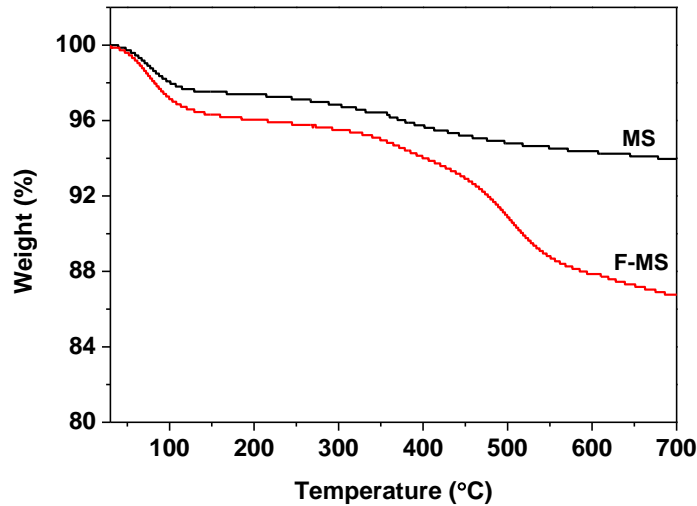
Fig. 4-7 TGA curves of MS and F-MS.

Fig. 4-8 shows the thermal property of pure PPy and F-MS/PPy composites. The pure PPy sample showed two weight loss steps over the entire testing temperature range. The first step was attribute to the elimination of moisture and the major weight loss begins at higher than 220 °C was owing to the degradation of PPy chains. For all F-MS/PPy samples, principal weight losses from 230-700 °C were observed due to the thermal decomposition of PPy chains and the alkylsulfonic acid groups presented in MS [30, 31].

Fig. 4-8 TGA curves of PPy and F-MS/PPy samples.

The onset temperature, decomposition temperature of 5%, 10% and 20%, and residue weight at 700°C are listed in Table 4-2. It's notable that the onset temperature of all the F-MS/PPy samples is higher than pure PPy and the onset temperature of the composite increases with the increasing feeding ratio of F-MS. For S-6, the onset temperature was 25 °C higher than that of pure PPy. The residues of the F-MS/PPy samples also increased with the increasing feeding ratio of the F-MS due to the excellent thermal stability of silica material. In addition, the decomposition temperature of the composite at same weight loss also increased with the increasing feeding ratio of F-MS. For example, decomposition temperature of 10% for S-6 was 403 °C, whereas the value for PPy was 243 °C. It indicates that the F-MS could improve the thermal stability of the composites due to the presence of the thermally stable MS and the well compatibility between F/MS and PPy.
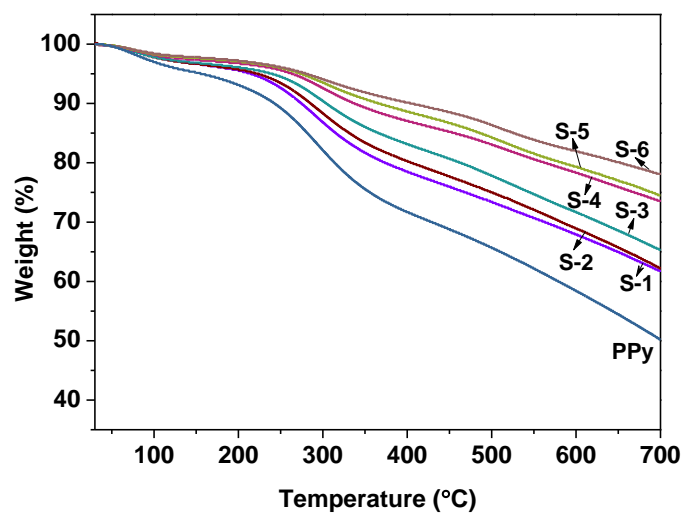
Table 4-2 The onset temperature of F-MS/PPy composites and PPy

Sample	T_{onset} (°C)	$T_{5\%}$ (°C)	$T_{10\%}$ (°C)	$T_{20\%}$ (°C)	Residue at 700°C (%)
PPy	228.9	155.1	242.9	313.6	50.20
S-1	230.5	215.4	274.2	373.6	61.61
S-2	238.9	224.1	285.8	403.8	62.13
S-3	245.4	240.7	304.2	464.4	65.32
S-4	248.9	263.2	337.8	561.9	73.41
S-5	250.9	272.7	365.0	583.5	74.52
S-6	253.9	279.2	403.3	652.3	77.96

4.3.5 Electrical conductivity

In this chapter, F-MS was used as solid dopant and inorganic host. The doping mechanism of PPy using F-MS as dopant is shown in Fig. 4-9.
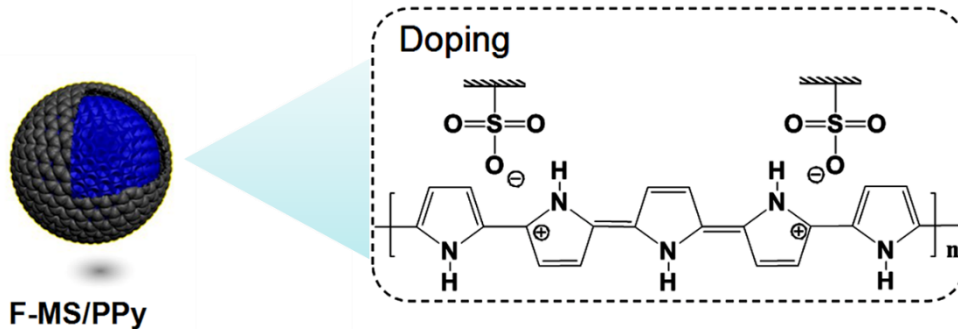
Fig. 4-9 Schematic representation for doping mechanism of PPy using F-MS as dopant.

Fig. 4-10 plots electrical conductivity of the F-MS/PPy and MS/PPy samples with different F-MS or MS contents at room temperature. The conductivity of the MS/PPy sample decreased monotonously with the increasing content of MS since the MS was insulator. The conductivity of F-MS/PPy sample was significant higher than that of the MS/PPy sample which had the same content of inorganic component. It indicates that the doping level of PPy in F-MS/PPy composite is higher than that of MS/PPy composite. This is because the $-SO_3H$ groups functionalized MS could play the role as *in-situ* dopant to improve the electrical conductivity of the composites, however, the insulating MS without functionalization just functions as the inorganic host.
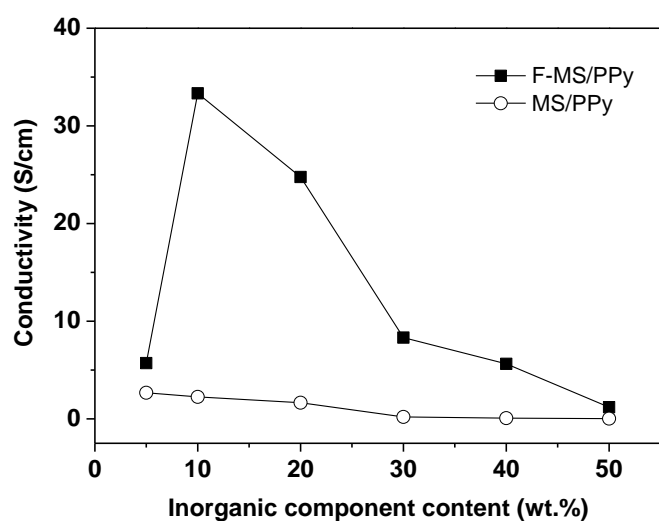
Fig. 4-10 The electrical conductivity of F-MS/PPy and MS/PPy samples.

The electrical conductivity of the F-MS/PPy samples increased firstly and then decreased with the increasing feeding ratio of F-MS. The maximum electrical conductivity was 33.33 S/cm when the feeding ratio of F-MS in the composite was 10% (S-2). This tendency is a result of comprehensive effect of several factors, including the doping level of PPy, the content of conducting component and the morphology of the composite.

The doping level of PPy in the F-MS/PPy composite has been heightened with the increasing F-MS due to more $-SO_3H$ groups in the composite, which is good for improving electrical conductivity. However, the content of conducting component PPy decreased with the increasing F-MS, which was disadvantageous to electrical conductivity. In addition, it's speculated that the morphology of the composite has strong impact on electrical conductivity. From the SEM image of S-2, we can see that PPy uniformly coated on the F-MS with suitable thickness, and a small number of free-standing PPy nanoparticles also existed. The PPy coated on the F-MS has been doped with $-SO_3H$ groups, so the conductivity is enhanced. And the free-standing PPy particles with nanoscale could serve as conducting fillers to form dense conducting passage. Furthermore, it is reported that the polymerization of pyrrole happened on both inside the pores and outside the surface owing to the unique mesoporous features of F-MS [32], which would improve the alignment of PPy chains and hence to some extent enhance the conductivity. The result agrees with XRD analysis. For S-1, there wer many free-standing PPy nanoparticles in the system, and these PPy nanoparticles without doping would decrease the conductivity of the composite. When the content of F-MS was 20% (S-3), in spite of the sample had similar morphology with S-2, the large size of the composite was prejudicial to form dense conducting network (MS used in this work are microspheres with a mean particle size of 3 μm.) and the system lacked enough free-standing PPy nanoparticles to play the role as conducting fillers. With a further increase in content of F-MS, although all of the pyrrole has been polymerized inside the pores and outside the surface of the F-MS particles, the insulating character of the F-MS

particles is the main reason for the decreasing conductivity.

4.3.6 Electrochemical studies

In order to further evaluate the electrochemical behavior of the F-MS/PPy composites, the mass specific capacitance and the cycling performance were investigated in 0.5 M Na_2SO_4 aqueous solution.
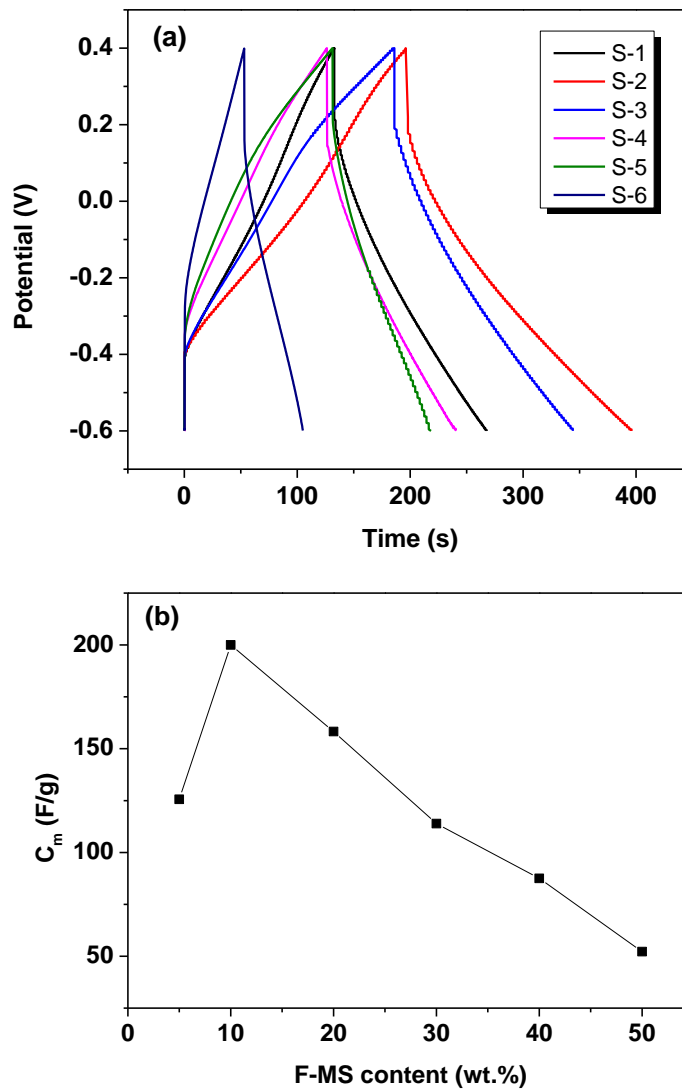
Fig. 4-11 Galvanostatic charge-discharge curves (a) and specific capacitances (b) of F-MS/PPy composite electrodes at a current density of 1.0 A/g in 0.5 M Na_2SO_4 solution.

The charge-discharge curves of F-MS/PPy composite electrodes with different content of F-MS at a current density of 1.0 A/g are shown in Fig. 4-11a. The specific capacitance (C_m) of the F-MS/PPy composite electrodes with different feeding ratio of F-MS is plotted in Fig. 4-11b. It could be found that the C_m increased with the increasing content of F-MS at first, and reached a maximum of 200.0 F/g when the content of F-MS was 10%. Then with a further increase in the content of F-MS, the C_m of the composite sharply decreased. This phenomenon is also thought to be related to the morphology of the composite as discussed in Part 4.3.5.
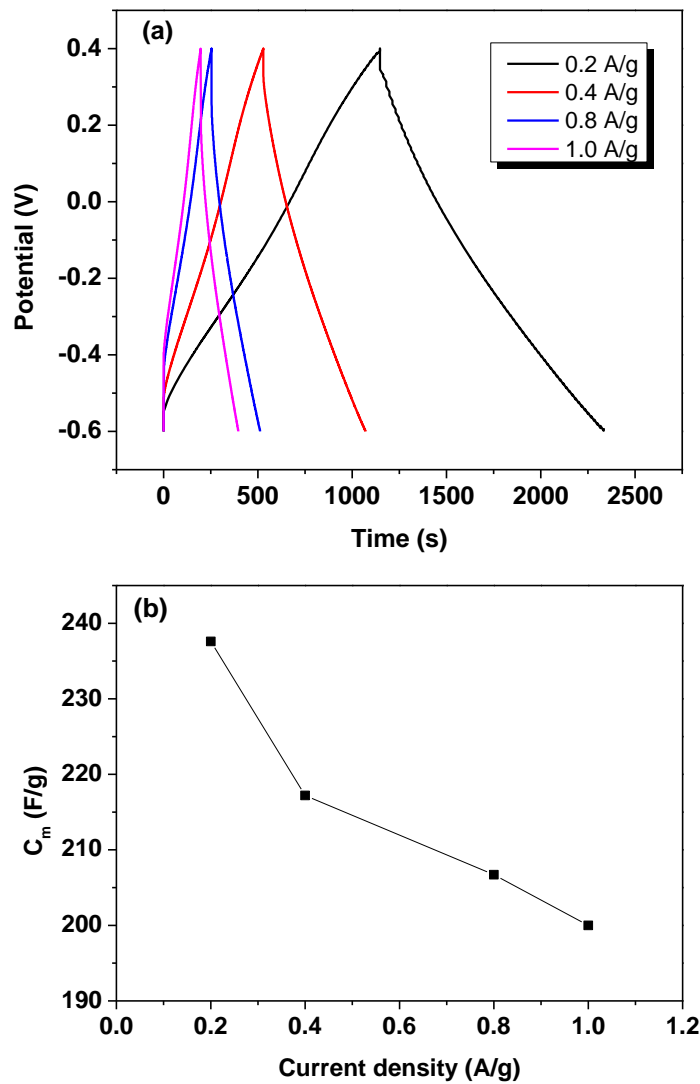
Fig. 4-12 Galvanostatic charge-discharge curves (a) and specific capacitances (b) of S-2 at different current densities in 0.5 M Na_2SO_4 solution.

For high energy and power density electrode materials, the materials should retain outstanding performance at high charge-discharge rate [33]. For this reason, the galvanostatic charge-discharge performance of the composite electrode containing 10% F-MS (S-2) at different current densities from 0.2 to 1.0 A/g were tested. The results are shown in Fig. 4-12a. The C_m calculated at corresponding current density is plotted in Fig. 4-12b. As shown in Fig. 4-12b, the C_m slightly decreased with the increase in current density, which possibly owe to the limited electronic conductivity of PPy [34-37]. The maximum C_m for S-2 was 237.6 F/g at a current density of 0.2 A/g, whereas the value at a current density of 1.0 A/g still obtained 84.2% of the maximum value. The results indicate that the F-MS/PPy composite electrodes retain satisfactory capacitance performance at high charge-discharge rate.
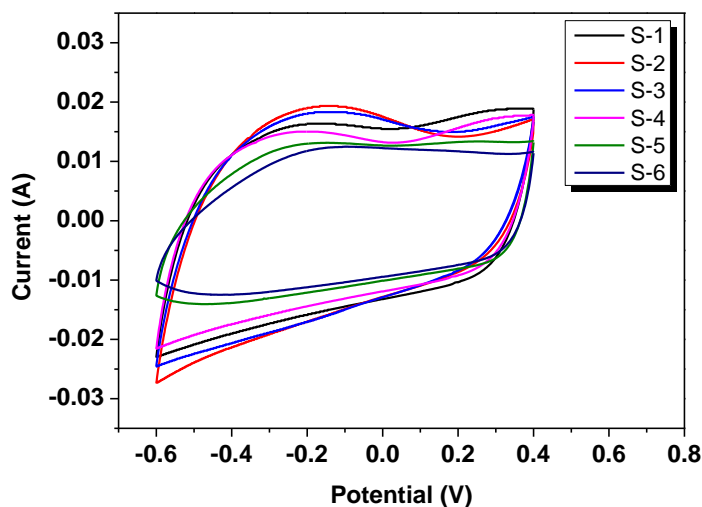
Fig. 4-13 Cyclic voltammograms of F-MS/PPy composite electrodes at a scan rate of 5 mV/s in 0.5 M Na_2SO_4 solution.

The cyclic voltammograms of F-MS/PPy composite electrodes at a scan rate of 5 mV/s between -0.6 to 0.4 V are presented in Fig. 4-13. In general, the box shape of the CV curves indicates good capacitance behavior, and the large area of CV curves indicates high capacitance [38]. The CV curves of the F-MS/PPy composite electrodes

showed a quasi-box shape, indicating that the F-MS/PPy composites were desirable as capacitor electrode material. The deviation from the box shape may cause by resistance of the electrode [39]. The area of CV curves decreased in the order of S-2 > S-3 > S-1 > S-4 > S-5 > S-6, which was consistent with the C_m that calculated by galvanostatic discharge curves.

4.4 Conclusions

In this chapter, sulfonic acid groups functionalized mesoporous silica (F-MS) was used as both the *in-situ* solid dopant and the inorganic host to prepare a series of F-MS/PPy composites by chemical polymerization. It is found that:

(1) When the feeding ratio of F-MS was 10%, the electrical conductivity of the sample reached the maximum value about 33.33 S/cm at room temperature. The maximum specific capacitance of F-MS/PPy composite electrodes was 237.6 F/g, and the composite electrodes retains satisfactory capacitance performance at high charge-discharge rate.

(2) The morphology are affected by the content of F-MS in the composites. When the feeding ratio of F-MS was below 20%, the composite showed a bayberry-like morphology accompanying unfixed number of free-standing PPy nanoparticles. When the feeding ratio of F-MS was above 30%, only a part of the F-MS was coated with PPy nanoparticles and few free-standing PPy nanoparticles were observed.

(3) We speculate that the morphology of the composite has strong influence on the electrical properties. The free-standing PPy nanoparticles play the role as conducting fillers to form dense conducting passage which is favorable for improving the conductivity.

(4) The thermal stability of the composite is significantly preferable to the pure PPy due to the outstanding thermal stability of MS as well as the well compatibility between F/MS and PPy.

(5) The appealing properties of the F-MS/PPy composite make it have potential

applications in capacitors, sensors, catalysts, sorption and separation.

The low cost of F-MS used as *in-situ* solid dopant and the inorganic host is satisfying to prepare PPy composite with improved electrical properties and reduced cost. Moreover, the composite wouldn't cause corrosion problem that often appears at hydrochloric acid doped conjugated conducting polymer, because sulfonic acid groups are covalently bonded to MS. However, the micron scale of the resulting composite and the decreased dispersity may hinder its application.

References

[1] J.G. Wang, Y. Yang, Z.H. Huang and F. Kang. Electrochemical Reactions of the Th^{4+}/Th Couple on the Tungsten, Aluminum and Bismuth Electrodes in Chloride Molten Salt. Electrochimica Acta. 130 (2014) 642-649.

[2] M.T. Ramesan. Preparation and Properties of Fe$_3$O$_4$/Polypyrrole/Poly(Pyrrole-Co-Acrylamide) Nanocomposites. International Journal of Polymeric Materials and Polymeric Biomaterials. 62 (2013) 277-283.

[3] P.G. Su and Y.T. Peng. Fabrication of a Room-Temperature H$_2$S gas Sensor Based on PPy/WO$_3$ Nanocomposite Films by *in-situ* Photopolymerization. Sensors and Actuators B: Chemical. 193 (2014) 637-643.

[4] C. Yang, H. Mo, L. Zang, J. Qiu, X. Wang and H. You. Preparation and Characterization of Coaxial Mullite/Polypyrrole Fibrous Nanocomposites via Self-Assembling and in situ Surface-Initiated Polymerization. Polymer Composites. 35 (2014) 892-899.

[5] T. Qian, C. Yu, S. Wu and J. Shen. In situ Polymerization of Highly Dispersed Polypyrrole on Reduced Graphite Oxide for Dopamine Detection. Biosensors and Bioelectronics. 50 (2013) 157-160.

[6] L. Sun, Y. Shi, B. Li, X. Li and Y. Wang. Preparation and Characterization of polypyrrole/TiO$_2$ Nanocomposites by Reverse Microemulsion Polymerization and Its Photocatalytic Activity for the Degradation of Methyl Orange under Natural Light. Polymer Composites. 34 (2013) 1076-1080.

[7] Y. Cho and R.B. Borgens. The Preparation of Polypyrrole Surfaces in the Presence of Mesoporous Silica Nanoparticles and Their Biomedical Application. Nanotechnology. 21 (2010) 205102.

[8] J. Fu, Q.Xu, J. Chen, Z. Chen, X. Huang and X. Tang. Controlled Fabrication of Uniform Hollow Core Porous Shell Carbon Spheres by the Pyrolysis of Core/Shell Polystyrene/Cross-Linked Polyphosphazene Composites. Chemical

Communications. 46 (2010) 6566-6568.

[9] Y. Klichko, M. Liong, E. Choi, S. Angelos, A.E. Nel, J.F. Stoddart, F. Tamanoi and J.I. Zink. Mesostructured Silica for Optical Functionality, Nanomachines, and Drug Delivery. Journal of the American Ceramic Society. 92 (2009) S2-S10.

[10] B.J. Melde, B.J. Johnson and P.T. Charles. Mesoporous Silicate Materials in Sensing. Sensors. 8 (2008) 5202-5228.

[11] C. Ispas, I. Sokolov and S. Andreescu. Enzyme-Functionalized Mesoporous Silica for Bioanalytical Applications. Analytical and Bioanalytical Chemistry. 393 (2009) 543-554.

[12] J.M. Thomas and R. Raja. Exploiting Nanospace for Asymmetric Catalysis: Confinement of Immobilized, Single-Site Chiral Catalysts Enhances Enantioselectivity. Accounts of Chemical Research. 41 (2008) 708-720.

[13] J.V. Ros-Lis, R. Casasus, M. Comes, C. Coll, M.D. Marcos, R. Martinez-Manez, F. Sancenon, J. Soto, P. Amoros, J. El Haskouri, N. Garro and K. Rurack. A Mesoporous 3D Hybrid Material with Dual Functionality for Hg^{2+} Detection and Adsorption. Chemistry - A European Journal. 14 (2008) 8267-8278.

[14] M. Vallet-Regi, F. Balas and D. Arcos. Mesoporous Materials for Drug Delivery. Angewandte Chemie International Edition. 46 (2007) 7548-7558.

[15] Q. Tang, X. Sun, Q. Li, J. Lin and J. Wu. Preparation and Electrical Conductivity of SiO_2/Polypyrrole Nanocomposite. Journal of Materials Science. 44 (2009) 849-854.

[16] S. Masubuchi, S. Kazama, R. Matsushita and T. Matsuyama. The Influence of Dopant Species on Transport Properties in as-Grown Polypyrrole Films Prepared by Electrochemical Method. Synthetic Metals. 69 (1995) 345-346.

[17] Y. Hu, R. Yang, D.F. Evans and J.H. Weaver. Direct Measurements of Bipolaron-Band Development in Doped Polypyrrole with Inverse Photoemission. Physical Review B. 44 (1991) 13660-13665.

[18] P.C. Wang and J.Y. Yu. Dopant-Dependent Variation in the Distribution of Polarons

and Bipolarons as Charge-Carriers in Polypyrrole thin Films Synthesized by Oxidative Chemical Polymerization. Reactive and Functional Polymers. 72 (2012) 311-316.

[19] E. Håkansson, T. Lin, H. Wang and A. Kaynak. The Effects of Dye Dopants on the Conductivity and Optical Absorption Properties of Polypyrrole. Synthetic Metals. 156 (2006) 1194-1202.

[20] J. Ferreira, M.J.L. Santos, R. Matos, O.P. Ferreira, A.F. Rubira and E.M. Girotto. Structural and Electrochromic Study of Polypyrrole Synthesized with Azo and Anthraquinone Dyes. Journal of Electroanalytical Chemistry. 591 (2006) 27-32.

[21] P. Gholamzadeh, G.M. Ziarani, A. Badiei and Z. Bahrami. Application of Sulfonic Acid Functionalized Nanoporous Silica (SBA-Pr-SO$_3$H) in the Solvent Free Synthesis of (E)-Arylidene-1,3-dihydroindole-2-ones. European Journal of Chemistry. 3 (2012) 279-282.

[22] C.P.L. Rubinger, L.C. Costa, A.C.C. Esteves, A. Barros-Timmons and J.A. Martins. Hopping Conduction on PPy/SiO$_2$ Nanocomposites Obtained via in situ Emulsion Polymerization. Journal of Materials Science. 43 (2008) 3333-3337.

[23] A. Sayari and S. Hamoudi. Periodic Mesoporous Silica-Based Organic−Inorganic Nanocomposite Materials. Chemistry of Materials. 13 (2001) 3151-3168.

[24] X. Feng, G. Yang, Y. Liu, W. Hou and J.J. Zhu. Synthesis of Polyaniline/MCM-41 Composite Through Surface Polymerization of Aniline. Journal of Applied Polymer Science. 101 (2006) 2088-2094.

[25] J. Li, L. Zhu, Y. Wu, Y. Harima, A. Zhang and H. Tang. Hybrid Composites of Conductive Polyaniline and Nanocrystalline Titanium Oxide Prepared via Self-Assembling and Graft Polymerization. Polymer. 47 (2006) 7361-7367.

[26] D.S. Sutar, N. Padma, D.K. Aswal, S.K. Deshpande, S.K. Gupta and J.V. Yakhmi. Growth of Highly Oriented Crystalline Polyaniline Films by Self-Organization. Journal of Colloid and Interface Science. 313 (2007) 353-358.

[27] X. Sun, J. Ren, L.W. Zhang, L. Chen, H. Li, R. Li and J.T. Ma. Polyaniline

Nanocomposites via Chemical Oxidative Polymerization in the Presence of Functional MCM-48 as in situ Dopant. Synthetic Metals. 160 (2010) 2244-2249.

[28] S. Cetiner, F. Kalaoglu, H. Karakas and A.S. Sarac. Dielectric, FTIR Spectroscopic and Atomic Force Microscopic Studies on Polypyrrole-Poly(acrylonitrile-co-vinyl acetate) Composites. Polymer Composites. 32 (2011) 546-557.

[29] D. Margolese, J.A. Melero, S.C. Christiansen, B.F. Chmelka and G.D. Stucky. Direct Syntheses of Ordered SBA-15 Mesoporous Silica Containing Sulfonic Acid Groups. Chemistry of Materials. 12 (2000) 2448-2459.

[30] S. Mikhailenko, D. Desplantier-Giscard, C. Danumah and S. Kaliaguine. Solid Electrolyte Properties of Sulfonic Acid Functionalized Mesostructured Porous Silica. Microporous and Mesoporous Materials. 52 (2002) 29-37.

[31] R. Marschall, I. Bannat, J. Caro and M. Wark. Proton Conductivity of Sulfonic Acid Functionalised Mesoporous Materials. Microporous and Mesoporous Materials. 99 (2007) 190-196.

[32] A. Malinauskas. Chemical Deposition of Conducting Polymers. Polymer. 42 (2001) 3957-3972.

[33] B.C. Kim, J.M. Ko and G.G. Wallace. A Novel Capacitor Material Based on Nafion-Doped Polypyrrole. Journal of Power Sources. 177 (2008) 665-668.

[34] S. Sen, J. Saraidaridis, S.Y. Kim and G.T.R. Palmore. Viologens as Charge Carriers in a Polymer-Based Battery Anode. ACS Applied Materials & Interfaces 5 (2013) 7825-7830.

[35] M. Lapkowski and G. Bidan. Electrochemical, Spectroelectrochemical and EPR Properties of Poly(pyrrole-viologens). Journal of Electroanalytical Chemistry. 362 (1993) 249-256.

[36] H. Mao and P.G. Pickup. In situ Measurement of the Conductivity of Polypyrrole and Poly[1-methyl-3-(pyrrol-1-ylmethyl)pyridinium]+ as a Function of Potential by Mediated Voltammetry. Redox Conduction or Electronic Conduction? Journal of the American Chemical Society. 112 (1990) 1776-1782.

[37] B.J. Feldman, P. Burgmayer and R.W. Murray. The Potential Dependence of Electrical Conductivity and Chemical Charge Storage of Poly(pyrrole) Films on Electrodes. Journal of the American Chemical Society. 107 (1985) 872-

[38] K. Shi and I. Zhitomirsky. Polypyrrole Nanofiber–Carbon Nanotube Electrodes for Supercapacitors with High Mass Loading Obtained Using an Organic Dye as a Co-Dispersant. Journal of Materials Chemistry A. 1 (2013) 11614-11622.

[39] C. Yang, P. Liu and Y.Q. Zhao. Preparation and Characterization of Coaxial Halloysite/Polypyrrole Tubular Nanocomposites for Electrochemical Energy Storage. Electrochimica Acta. 55 (2010) 6857-6864.

Chapter 5 Preparation and characterization of attapulgite/polypyrrole nanorod composites

5.1 Introduction

Chapter 4 proved that composing PPy with the low cost inorganic host is an effective method to induce cost of PPy production. Meanwhile, F-MS also can dope PPy to improve its electrical properties. However, the micron scale of the resulting composite may and the poor dispersion stability hinder its potential applications.

Attapulgite is of particular interest due to its unique three-dimensional structure and fibrous morphology (10~30 nm in width and ~500 nm in length). Attapulgite/polypyrrole (ATP/PPy) nanocomposite which is well-defined with nanoscale fibrous morphology has high conductivity, good thermal stability and large surface area [1-3]. However, its dispersion stability hasn't been improved. To improve its dispersion stability while retaining unique three-dimensional structure and conductivity, the method of preparing dispersible PPy powders by adding appropriate dopants is considered.

Polyvinyl alcohol (PVA) contains a mass of hydroxyl groups and could improve dispersion stability of the conducting polymers [4]. However, due to its neutral character, it cannot play the role as the dopant that can enhance the electrical conductivity of PPy [5]. On the other hand, the phosphate is usually used as the dopant, but it cannot provide the product with adequate dispersion stability in water. For this reason, phosphorylated polyvinyl alcohol (PPVA) could be taken into account [6]. Especially, there is no work reported about the high dispersible ATP/conducting polymer nanocomposite to our knowledge.

In this chapter, PPy was located on the surface of the ATP in the presence of PPVA by

the *in-situ* chemical polymerization of pyrrole. PPVA (Fig. 5-1), a polyanion with a mass of phosphate and hydroxyl groups, was used as dopant and dispersant for ATP/PPy nanocomposite. And its effects on the dispersion stability, thermal stability, electrical conductivity and temperature dependence of electrical conductivity of PPVA-ATP/PPy nanocomposites were discussed. The synthesized composites were characterized by FTIR, XRD and TGA. The electrical conductivities and temperature dependence of electrical conductivity were measured using four-point probe meter. In addition, morphological analyses were investigated by TEM.

5.2 Experimental

5.2.1 Preparation of phosphorylated polyvinyl alcohol (PPVA)

PPVA was prepared by the phosphorylation of PVA with phosphoric acid in an aqueous media according to the method of the related references [7, 8]. To a solution of dicyandiamide (10 g) and urea (15 g) in 50 mL of DMF, phosphoric acid (10 mL) was added. The solution was heated to 140 °C and PVA (6 g) was then added. The reaction solution was stirred for 80 min at 140 °C under a stream of argon. The resulting solution was dialysed against distilled water through dialysis membrane for 72 h to remove any surplus reagents. To this solution, 95 mL of aqueous HCl (6M) solution was added and the solution was dialysed against distilled water again for 1 week in order to remove water-soluble impurities. A powder of PPVA was obtained by slowly adding acetone to the dialysed PPVA aqueous solution with vigorous agitation. The precipitate was filtered, washed with acetone, and then dried at 30 °C (in vacuum) for 3 days over P_2O_5. The degree of phosphorylation (23 mol%) was determined by pH titration.
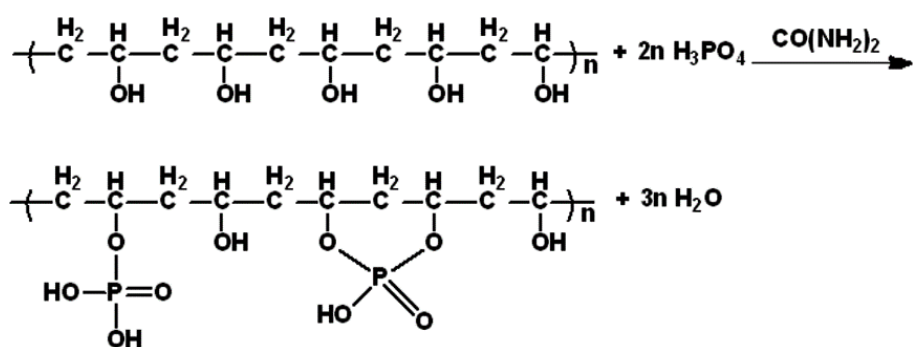
Fig. 5-1 Synthetic route for phosphorylated polyvinyl alcohol (PPVA).

5.2.2 Preparation of conducting polymer nanorod

A typical procedure for the preparation PPVA-ATP/PPy nanocomposite is given for samples. PPVA and 1.45 g of ATP were added to 100 mL of water in a 250 mL round-bottom flask and stirred until PPVA was dissolved. The mixture was then ultrasonically dispersed, and freshly distilled pyrrole (1.0 mL, 14.4 mmol) was added to the above beige white suspension. The mixture was stirred for 45 min in ice-cold condition. The conditions of the polymerizations are given in Table 5-1. APS (3.3 g, 14.4 mmol) dissolved in 20 mL of double distilled water was added drop by drop to the above suspension, and stirring was continued for 10 h under ice-cold condition. The resulting product was purified by being filtered and washed with distilled water and ethanol until the filtrate became colorless. The black powder samples were dried under vacuum (0.1 mm of Hg) at 60 °C for 24 h prior to further analysis.

Table 5-1 The conditions of the polymerizations investigated in this work.

Sample	Pyrrole (mL)	PPVA (g)	PPVA Feeding Ratio (%)	ATP (g)
S-1	1.0	0.13	5	1.45
S-2	1.0	0.27	10	1.45
S-3	1.0	0.43	15	1.45
S-4	1.0	0.61	20	1.45
S-5	1.0	1.04	30	1.45

5.3 Results and discussion

5.3.1 Morphological analysis

To characterize the size and shape of the presented PPVA-ATP/PPy nanocomposites, TEM was conducted. It is seen from the micrographs (Fig. 5-2) that the ATP showed rod-like structure. The width was ~20 nm and the length was ~500 nm. It is observed that the feeding ratio of PPVA has considerable influence on the morphology of the nanocomposites. For the PPVA-ATP/PPy nanocomposites with low PPVA feeding ratio, the serious aggregation of ATP and PPy particles were observed. However, with the increasing feeding ratio of PPVA, the dispersibility of the PPVA-ATP/PPy sample increased (Fig. 5-2 (c, d)), and the smaller PPy nanoparticles were uniformly coated on the surface of ATP forming a coaxial nanorod morphology.
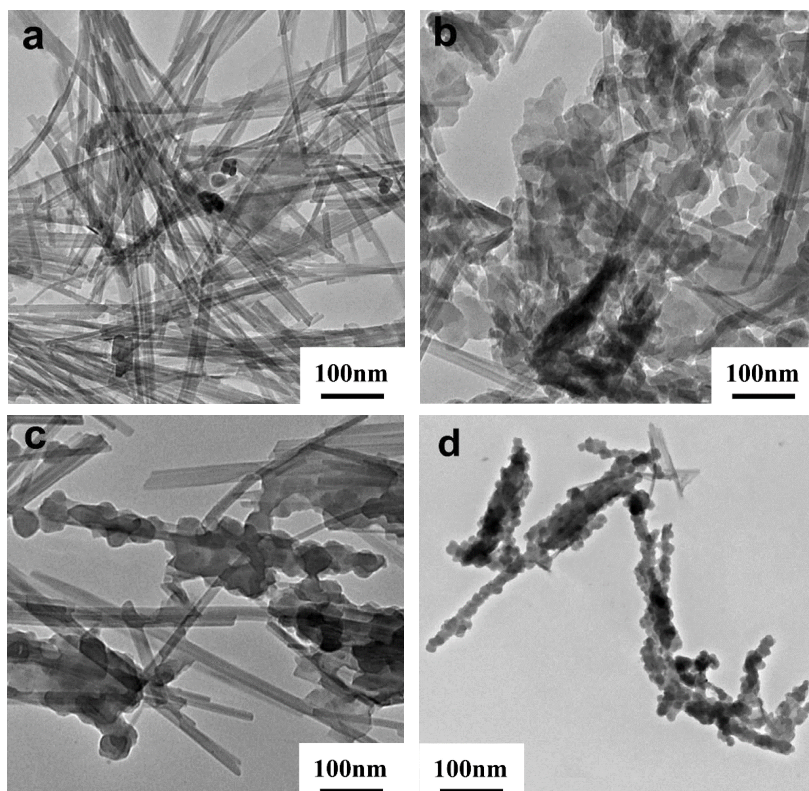

Fig. 5-2 TEM images of raw-ATP (a) and PPVA-ATP/PPy nanocomposites ((b) S-1, (c) S-3, and (d) S-5).

The fabrication process of PPVA-ATP/PPy nanocomposites with different feeding ratio of PPVA is illustrated in Fig. 5-3. PPVA is anionic polymer with a number of phosphate groups, which could play the role as dispersant of ATP due to steric and electrostatic repulsion. When the feeding ratio of PPVA is low, ATP could not be dispersed well and masses of ATP connect each other by amorphous aggregate PPy particles to become one big mass, as shown in Fig. 5-2b. In contrast, high feeding ratio is beneficial for dispersing ATP. In addition, the smaller PPy particles were produced in high PPVA feeding ratio. The subsequent of experiment, which focused on the aqueous dispersion stability PPVA-ATP/PPy nanocomposites, has similar results.
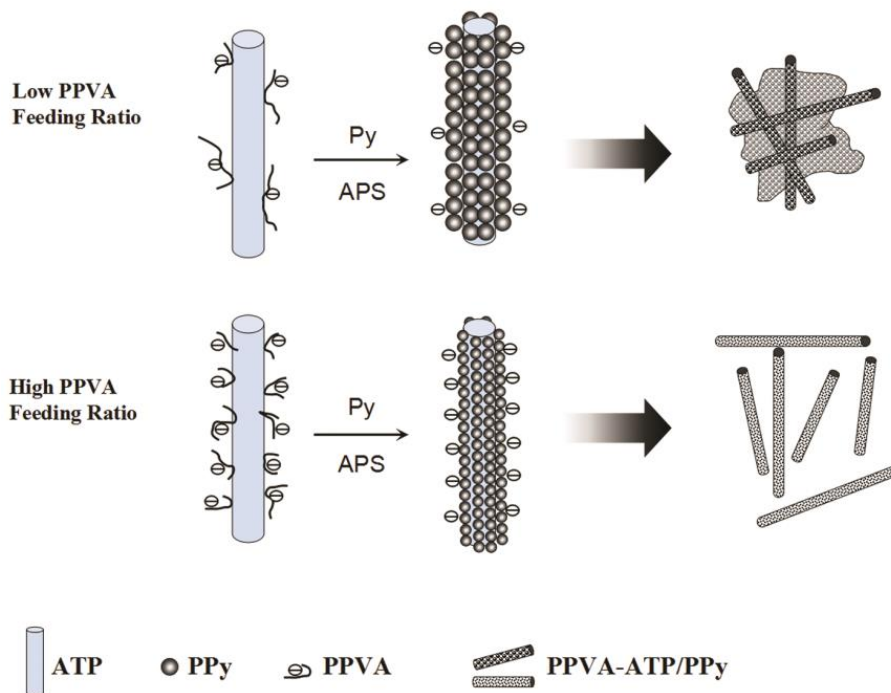

Fig. 5-3 Illustration of the PPVA-ATP/PPy nanocomposites fabrication process with different feeding ratios of PPVA.

5.3.2 FTIR analysis

FTIR spectra of PVA, PPVA, ATP and PPVA-ATP/PPy nanocomposite (S-3) are displayed in Fig. 5-4. The spectrum of PVA showed the typical peaks which were

attributed to the –OH stretching vibrations at 3200-3400 cm^{-1}, alkyl stretching vibrations at 2850-2900 cm^{-1}, –CH$_2$ bending absorptions at 1424 cm^{-1}, and –C–O–H stretching at 1097 cm^{-1} position [7]. Teeny peak at 1730 cm^{-1} appeared due to residual vinyl acetate groups. For the PPVA, the new peaks could be distinctly identified at 1286, 994 and 853 cm^{-1} assigned to introduction of P=O, P–O and P–OH groups in the polymer [8]. In addition, –OH stretching region was broadened compared to PVA, due to more number of –OH groups in PPVA and increased hydrogen bonds.
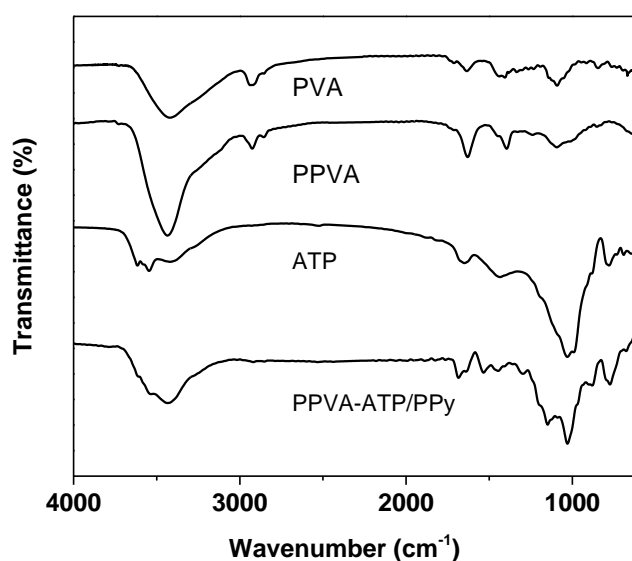
Fig. 5-4 FTIR spectra of the PVA, PPVA, ATP and PPVA-ATP/PPy (S-3).

For the PPVA-ATP/PPy samples, the band at 1542 cm^{-1} was assigned to the pyrrole ring, i.e., the combination of C=C and C–C stretching vibrations and the peak at 1468 cm^{-1} was associated with the C–N stretching vibration [9]. The peaks at 1294 and 1179 cm^{-1} were attributed to the in-plain vibrations of C–H. The 1114 cm^{-1} was assigned to the overlap peaks of the Si–O–Si symmetric stretching mode and the C–H in-plane bending. The band at 817 cm^{-1} was assigned to the overlap peaks of Si–O and C–H out of plane bending. The band associated to Si–O bending vibration was located at 467 cm^{-1}. All results demonstrated almost the same peak positions of the main IR bands,

which were associated with the structure of the PPy [10]. The absorbance of P=O, P–O stretching at 1286 and 853 cm^{-1} of phosphate, indicated that PPy has been doped with PPVA.

5.3.3 XRD analysis

Fig. 5-5 shows the XRD patterns of the PPy and PPVA-ATP/PPy nanocomposites prepared at different feeding ratios of PPVA. For the XRD patterns of the PPVA-ATP/PPy nanocomposites, the broad peak for the PPy at 25° which belonged to the characteristic amorphous structure of PPy appeared. The peaks at 8.4°, 13.8°, 19.8° and 26.6° corresponded to the primary diffraction of the (110), (200), (040) and (400) planes of ATP, respectively [11, 12]. The main peaks for the nanocomposites were similar to the ones of ATP, which revealed that the crystal structure of ATP was well maintained after incorporating of PPVA and PPy.
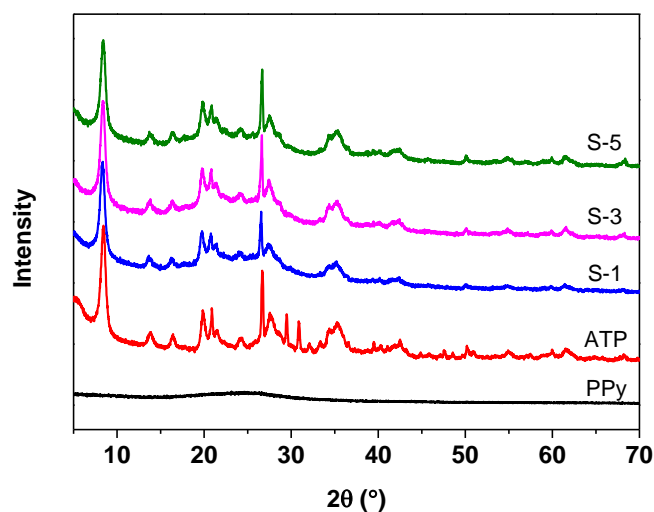

Fig. 5-5 XRD patterns of PPy, ATP and the PPVA-ATP/PPy samples.

5.3.4 Aqueous dispersion stability

The PPVA-ATP/PPy samples were dispersed in vial containing distilled water in ultrasonic bath for 30 min. Then, the dispersion and stability were characterized by

standing observation. The dispersion stability of the PPVA-ATP/PPy samples in water was also found to be improved with the increasing feeding ratio of PPVA. The sedimentation was found in S-1, S-2, and S-3 in less than an hour. However, as shown in Fig. 4-6a, S-4 had been well-dispersed for more than 1 week. Especially for S-5, the suspension has been stable for more than 6 weeks. Obviously, the dispersion stability of the PPVA-ATP/PPy samples prepared in higher PPVA feeding ratios was improved. It is due to electrostatic repulsive force and stereo-hindrance effect of linear PPVA which contains a large number of phosphate and hydroxyl groups. The results also indicate that PPVA is an effective polymeric dispersant for the nanocomposite.
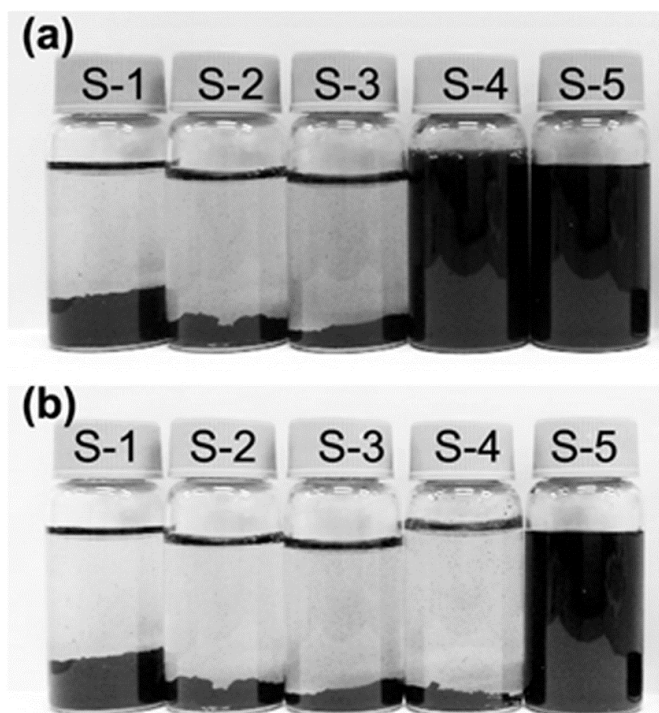

Fig. 5-6 Stability of the PPVA-ATP/PPy nanocomposites in water for (a) a week and (b) 6 weeks.

5.3.5 Thermal analysis

Fig. 5-7 illustrates the results of the TGA curves of PPVA and the PPVA-ATP/PPy

nanocomposites. For the PPVA sample, the weight loss over the entire testing temperature range was caused mainly by three steps. The first step was attributed to the release of adsorbed water. The second step at about 236 °C was owing to the degradation of side chain of PVA, whereas the third step at about 437 °C was due to the breakage of the main chain [13].

For the nanocomposites, the TG curves showed the same tendency. The initial weight loss below 120 °C was mainly caused by the hygroscopic character of the samples. The sharp weight loss from 230 °C was attributed to the thermal decomposition of polymer chains. The residues of the samples were higher than the feeding ratio of ATP because PPy and PPVA could not completely decompose in nitrogen and were carbonized to form graphitic structures [14].
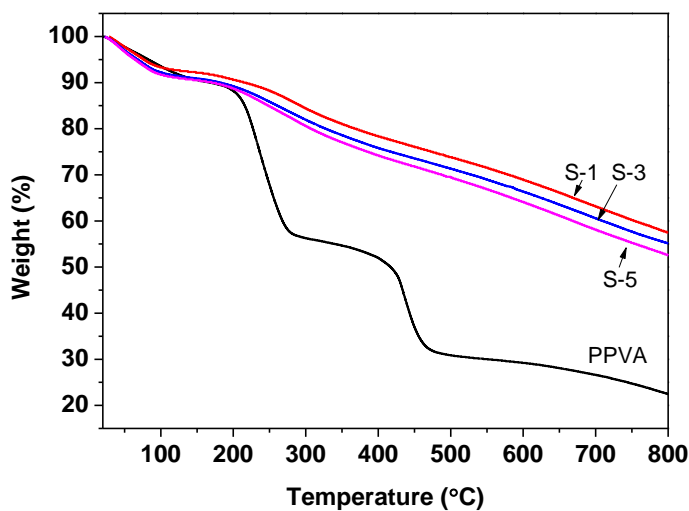
Fig. 5-7 TGA curves of PPVA and PPVA-ATP/PPy samples.

In order to obtain more information about the thermal properties of PPVA-ATP/PPy nanocomposites, the corresponding differential thermogravimetric (DTG) curves were analyzed (Fig. 5-8). For S-1, the DTG curve in the temperature range of 150~400 °C, a weak peak at about 190 °C and a strong peak at about 285 °C were observed. The former was attributed to the release of water that formed hydrogen bonds with the secondary amine groups of PPy, and the latter was caused by the decomposition of PPy

and PPVA. However, for S-3, the weak peak at about 190 °C disappeared and only a wide peak at about 270 °C was observed. It indicates that PPy could be well doped by PPVA, and instead of water, the large number of phosphate and hydroxyl groups in PPVA formed hydrogen bonds with PPy. With an increase of PPVA, the DTG curve of S-5 showed two peaks at 238 and 280 °C, which was ascribed to decomposition of PPVA and PPy, respectively. This is because the excessive PPVA could not play the part of dopant and it interacted with PPy through the formation of hydrogen bonds.
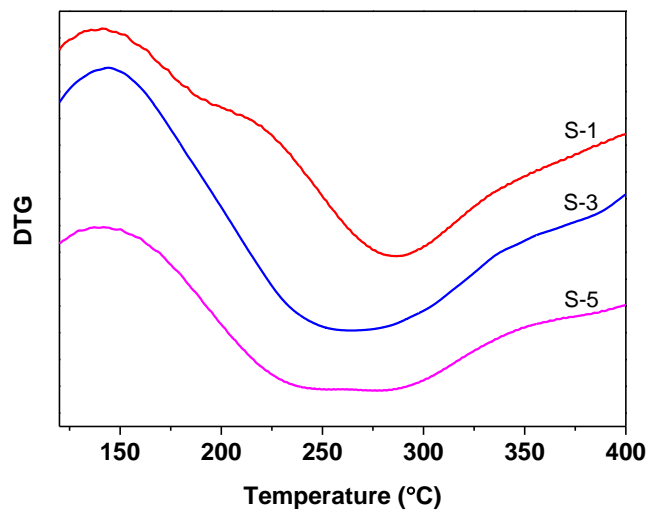
Fig. 5-8 DTG curves of PPVA-ATP/PPy samples.

5.3.6 Electrical conductivity

The effect of feeding ratio of PPVA on the electrical conductivity of PPVA-ATP/PPy nanocomposites is plotted in Fig. 5-9. The electrical conductivities of the samples at room temperature clearly depend on the feeding ratio of PPVA. In the present study, the conductivity slightly increased to a maximum of 28.57 S/cm when the feeding ratio of PPVA was 15%. Generally, the factors that influence the electrical conductivity include two aspects as follows: (1) microscopic conductivity, which depends upon the doping level, conjugation length, chain length, etc. and (2) macroscopic conductivity, which is

determined by external factors such as the compactness of the samples. The increase in the PPVA content caused two contrary effects on the conductivity of PPVA-ATP/PPy nanocomposite. On the one hand, the doping level of PPy and the compactness of the samples increased with the increasing feeding ratio of PPVA, which were beneficial to improve the electrical conductivity. On the other hand, the content of PPy in the nanocomposite decreased with the increasing feeding ratio of PPVA, which was responsible for the decreasing electrical conductivity. Based on the above reasons, the conductivity firstly increased and then decreased with the increase in the feeding ratio of PPVA.
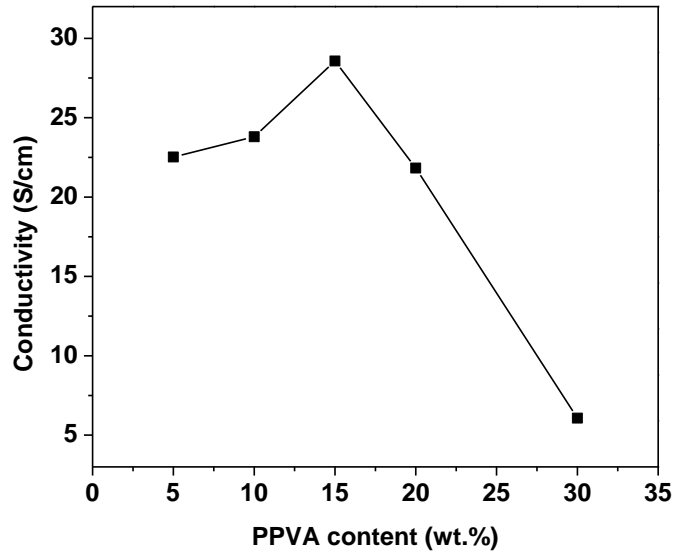
Fig. 5-9 The electrical conductivity of PPVA-ATP/PPy samples at room temperature.

The temperature dependence of the electrical conductivity for the samples is also studied and shown in Fig. 5-10. For a better comparison of temperature dependence of conductivity, we chose temperature coefficient of resistance (TCR) rather than the absolute value of the conductivity (σ) [15]. The TCR could be calculated according to the equation as follows:

$$\text{TCR} = \frac{\frac{R_2 - R_1}{R_1}}{T_2 - T_1}$$

Where R is the resistance at corresponding temperature T. In this work, T_1 and T_2 was 298 and 423 K, respectively. As the temperature increased from 298 to 423 K, all of the TCR were negative numbers, meaning that conductivity increased with the increasing temperature. It's worth noting that absolute value of TCR decreased with an increase in PPVA content, indicating that it was not sensitive to temperature. It is thought that the increasing PPVA was beneficial to the movement of charge carriers along PPy chains but would hindered the hopping of these carriers between PPy chains. When the PPVA content was low, the movement of charge carriers along PPy chains was the dominant factor for the relative high value of TCR, whereas the hopping of these carriers between PPy chains was the dominant factor for the relative low value of TCR when the PPVA content was high.
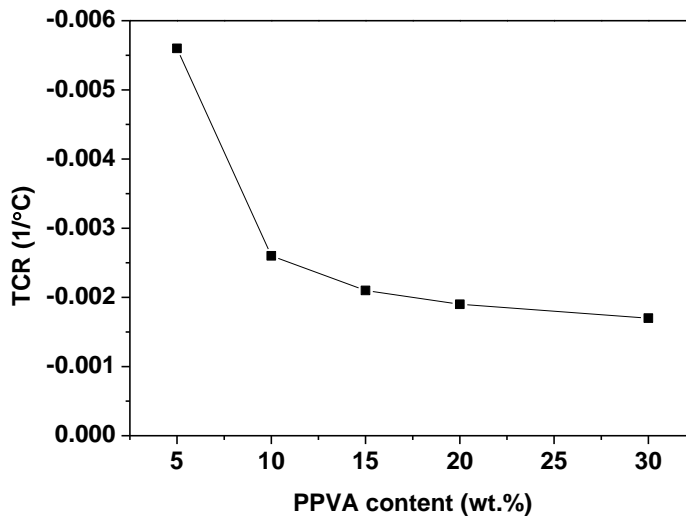
Fig. 5-10 Temperature dependence of electrical conductivity of PPVA-ATP/PPy samples

Fig. 5-11 shows the thermal stability of electrical conductivity for PPVA-ATP/PPy samples during 5 h isothermal ageing test at 50, 100 and 150 °C. The electrical conductivity was measured at an interval of 1 h in the isothermal ageing experiments. All the samples showed stable electrical conductivity at 50 °C over the entire testing time range. As the isothermal ageing temperature increased to 100 °C, the electrical

conductivity decreased with ageing time. However, the sample prepared with higher feeding ratio of PPVA exhibited lower conductivity decrement rate. After isothermal ageing at 100 °C for 5 h, the electrical conductivity retention of S-5 was about 47.2%, whereas, S-1 kept only 33%. The electrical conductivity of all the samples sharply decreased at 150 °C with testing time. However, the sample with the highest content of PPVA (S-5) showed maximum stability. It indicated that the presence of PPVA had a vital effect on the thermal stability of electrical conductivity. In this chapter, polymeric PPVA was employed as dopant and it had strong interactions with PPy chains. When it well-incorporated into PPy, the polymer chain structure was conducive to preventing deprotonation and improving electrical stability at isothermal ageing [16].
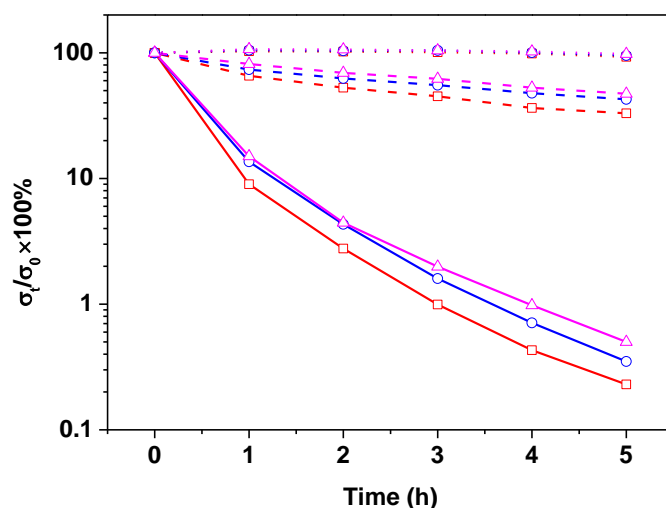
Fig. 5-11 Thermal stability of electrical conductivity of S-1 (squares), S-3 (circles) and S-5 (triangles) in air at 50 (dot lines), 100 (dash lines) and 150 °C (solid lines).

5.4 Conclusions

In this chapter, phosphorylated polyvinyl alcohol (PPVA) was served as polymeric dopant and dispersant to prepare PPy/inorganic nanocomposite. ATP clay that possessed unique fibrous morphology and properties were chosen as inorganic host. The main results in this chapter include:

(1) Owing to the unique structure of ATP, the resulting PPVA-ATP/PPy nanocomposites also had rod-like structures.

(2) The crystal structure of ATP in the composite was well-maintained, which was confirmed by XRD.

(3) The feeding ratio of PPVA had strong influence on the electrical conductivity of the resulting composite. The conductivity firstly increased and then decreased with the increase in the feeding ratio of PPVA, and the maximum value was 28.57 S/cm at room temperature when the feeding ratio of PPVA was15 %.

(4) The incorporation of PPVA could improve the thermal stability of conductivity, which was attributed to the strong interaction between PPVA and PPy.

(5) The electrostatic repulsive force and stereo-hindrance effect of linear PPVA impart excellent dispersion stability to the PPVA-ATP/PPy nanocomposite. The sample with the highest feeding ratio of PPVA showed the best aqueous dispersion stability for more than 6 weeks.

The cost can be considerably reduced by incorporating cheap ATP clay. The PPVA-ATP/PPy nanocomposite with good dispersion stability and electrical conductivity has broad potential applications in antistatic coatings, anticorrosion coatings, catalysts, sorption, etc. Moreover, the nanorod morphology and appealing mechanical property of ATP make it can be used as conducting reinforcing filler like carbon nanotube.

References

[1] C. Yang and P. Liu. Core-Shell Attapulgite@Polypyrrole Composite with Well-Defined Corn Cob-Like Morphology via Self-Assembling and in situ Oxidative Polymerization. Synthetic Metals. 159 (2009) 2056-2062.

[2] C. Yao, Y. Xu, Y. Kong, W. Liu, W. Wang, Z. Wang, Y. Wang and J. Ji. Polypyrrole/Palygorskite Nanocomposite: A New Chromate Collector. Applied Clay Science. 67-68 (2012) 32-35.

[3] Y. Chen, H. Xu, S. Wang and L. Kang. Removal of Cr(vi) from Water Using Polypyrrole/Attapulgite Core-Shell Nanocomposites: Equilibrium, Thermodynamics and Kinetics. RSC Advances. 4 (2014) 17805-17811.

[4] R. Gangopadhyay and M.R. Molla. Polypyrrole-Polyvinyl Alcohol Stable Nanodispersion: A Prospective Conducting Black Ink. Journal of Polymer Science, Part B: Polymer Physics. 49 (2011) 792-800.

[5] N.V. Blinova, J. Stejskal, M. Trchová, J. Prokeš and M. Omastová. Polyaniline and Polypyrrole: A Comparative Study of the Preparation. European Polymer Journal. 43 (2007) 2331-2341.

[6] R. Gangopadhyay and A. De. An Electrochemically Synthesized Conducting Semi-IPN from Polypyrrole and Poly(vinyl alcohol). Journal of Materials Chemistry. 12 (2002) 3591-3598.

[7] M. Suzuki, T. Yoshida, T. Koyama, S. Kobayashi, M. Kimura, K. Hanabusa and H. Shirai. Ionic Conduction in Partially Phosphorylated Poly(vinyl alcohol) as Polymer Electrolytes. Polymer. 41 (2000) 4531-4536.

[8] Y. An, T. Koyama, K. Hanabusa, H. Shirai, J. Ikeda, H. Yoneno and T. Itoh. Preparation and Properties of Highly Phosphorylated Poly(vinyl alcohol) Hydrogels Chemically Crosslinked by Glutaraldehyde. Polymer. 36 (1995) 2297-2301.

[7] S. Ahmad, N. PK and U. Riaz. Effect of Microwave Processing on the Spectral,

Mechanical, Thermal, and Morphological Characteristics of Sustainable Resource Based Castor Oil Epoxy/PVA Blends. Advances in Polymer Technology. 30 (2011) 96-109.

[8] J.H. Liu, Y.A. Zheng, W.B. Wang and A.Q. Wang. Preparation and Swelling Properties of Semi-IPN Hydrogels Based on Chitosan-g-Poly(acrylic acid) and Phosphorylated Polyvinyl alcohol. Journal of Applied Polymer Science. 114 (2009) 643-652.

[9] P. Jayamurgan, V. Ponnuswamy, S. Ashokan and T. Mahalingam. The Effect of Dopant on Structural, Thermal and Morphological Properties of DBSA-Doped Polypyrrole. Iranian Polymer Journal. 22 (2013) 219-225.

[10] H. Liu and S. Wang. Preparation of the Cotton Fabric with Ultraviolet Resistance and Antibacterial Activity Using Nano Attapulgite Colloidal Particles. Fibers and Polymers. 13 (2012) 1272-1279.

[11] D.M. Araújo Melo, J.A.C. Ruiz, M.A.F Melo, E.V Sobrinho and A.E Martinelli. Preparation and Characterization of Lanthanum Palygorskite Clays as Acid Catalysts. Journal of Alloys and Compounds. 344 (2002) 352-355.

[12] B. Gu, H. Zhong, L. Zhang, Z. Cheng, Y. Wang, X. Li, J. Xu and C. Yao. Attapulgite Clay Combined with Tris(2,2'bipyridyl)ruthenium(II) for the Enhancement of the Electrogenerated Chemiluminescence Sensing. International Journal of Electrochemical Science. 7 (2012) 6202-6213.

[13] M.S. Peresin, Y. Habibi, J.O. Zoppe, J.J. Pawlak and O.J. Rojas. Nanofiber Composites of Polyvinyl Alcohol and Cellulose Nanocrystals: Manufacture and Characterization. Biomacromolecules. 11 (2010) 674-681.

[14] J. Jang and H. Yoon. Novel Fabrication of Size-Tunable Silica Nanotubes Using a Reverse-Microemulsion-Mediated Sol–Gel Method. Advanced Materials. 16 (2004) 799-802.

[15] T.N. Ng, W.R. Silveira and J.A. Marohn. Dependence of Charge Injection on Temperature, Electric Field, and Energetic Disorder in an Organic Semiconductor.

Physical Review Letters. 98 (2007) 066101.

[16] J. Stejskal, M. Omastová, S. Fedorova, J. Prokeš and M. Trchová. Polyaniline and Polypyrrole Prepared in the Presence of Surfactants: A Comparative Conductivity Study. Polymer. 44 (2003) 1353-1358.

Chapter 6 Conclusions

Polypyrrole (PPy) is a promising intrinsically conducting polymer because of its attractive merits such as high conductivity, ease of synthesis, excellent environmental stability and appealing electrochemical behavior. However, the poor processability and relative high cost of PPy limit its potential applications. To overcome these problems while retaining the excellent electrical properties, different kinds of dopants were used to dope PPy in this thesis. The dopants have strong influences on morphology, electrical property and other performance of the conducting PPy composites.

In chapter 1, the research background and the construction of this thesis are described. The objectives of the research are to study the influences of different kinds of dopants on the properties of PPy composite, and improve the processability as well as reduce the cost.

In chapter 2, the properties of materials used in this thesis, experimental methods and characterization are presented.

In chapter 3, aromatic dye AV19 containing tri-sulfonate groups was used as dopant to prepare a series of AV19/PPy nanoparticles by chemical polymerization. AV19 functions as dopant, surfactant and physical cross-linker. The AV19/PPy nanoparticles are spherical granules with the smallest diameter of ~50 nm when the feeding ration of AV19 is 20%. This sample also has maximum electrical conductivity and specific capacitance of 39.09 S/cm and 379 F/g, respectively. AV19 has strong interactions with PPy, including hydrogen bonds forming between the amino or imino groups presented in AV19 and the amino group of pyrrole; physical crosslinking of different PPy chains; π–π stacking interactions between the large conjugated system of PPy and AV19. The strong interactions between PPy and AV19 make the sample have enhanced electrical properties, thermal stability and aqueous dispersion stability. Thus aromatic multi-sulfonate dopant is satisfying to prepare PPy nanoparticles with improved electrical properties and processability, which can broaden the applications of PPy

materials in different fields.

In chapter 4, the budget spherical mesoporous silica was functionalized with –SO₃H groups and used as *in-situ* solid dopant and the inorganic host to prepare a series of F-MS/PPy composites by chemical polymerization. The feeding ratio of functionalized mesoporous silica has strongly impact on the morphology and electrical properties of the samples. When the value is 10%, the sample shows a bayberry-like morphology accompanying a number of free-standing PPy nanoparticles. This sample possesses the maximum electrical conductivity and specific capacitance of 33.33 S/cm and 237.6 F/g, respectively. The composite electrodes retains satisfactory capacitance performance at high charge-discharge rate. The morphology of the composite has strong influence on the electrical properties. The PPy coated on the F-MS are well doped and the free-standing PPy nanoparticles play the role as conducting fillers to form dense conducting passage which is favorable for improving the conductivity. The thermal stability of the composite is also enhanced due to the outstanding thermal stability of MS as well as the well compatibility between F/MS and PPy. Since the –SO₃H groups are covalently bonded to MS, the problems that caused by release of micromolecular acid such as corrosion and poor cycle stability would be abated. The unique properties of MS and PPy make the composite have potential applications in capacitors, sensors, catalysts, sorption and separation based on synergy effect. The cost can be reduced by incorporating MS.

In chapter 5, phosphorylated polyvinyl alcohol (PPVA) were synthesized and used as polymeric dopant and dispersant to prepare attapulgite/PPy nanocomposite (PPVA-ATP/PPy). The nanorod-like structure of attapulgite clay (ATP) can form network consequently improve the performance of the nanocomposite. The conductivity firstly increases and then decreases with the increase in the feeding ratio of PPVA, and the maximum value is 28.57 S/cm at room temperature when the feeding ratio of PPVA is 15%. PPVA can impart excellent dispersion stability to the PPVA-ATP/PPy nanocomposite due to the electrostatic repulsive force and stereo-hindrance effect. The

sample with the highest feeding ratio of PPVA (30%) shows the best aqueous dispersion stability for more than 6 weeks. The thermal stability of conductivity is also improved by incorporating PPVA. The PPVA-ATP/PPy nanocomposite with good dispersion stability and electrical conductivity has broad potential applications in antistatic coatings, anticorrosion coatings, catalysts, sorption, etc. Moreover, the nanorod morphology and appealing mechanical property of ATP make it can be used as conducting reinforcing filler like carbon nanotube. And the PPy layer coated on the surface of ATP can enhance the compatibility between ATP and polymer matrix. The cost also can be considerably reduced by incorporating cheap ATP clay.

Publications

Ⅰ. Periodical papers

(1). <u>Limin Zang</u>, Jianhui Qiu, Chao Yang, Eiichi Sakai

Preparation and Characterization of Bayberry-Like Polypyrrole Composites Using Functionalized Mesoporous Silica as In Situ Dopant

International Journal of Polymeric Materials and Polymeric Biomaterials, Vol.64, (2015), pp.489-495.

(2). <u>Limin Zang</u>, Jianhui Qiu, Eiichi Sakai, Chao Yang

In Situ Preparation of Polypyrrole Nanorod Composite in the Presence of Phosphorylated Polyvinyl Alcohol

Advances in Polymer Technology, DOI: 10.1002/adv.21497

(3). <u>Limin Zang</u>, Jianhui Qiu, Chao Yang, Eiichi Sakai

Enhanced Conductivity and Electrochemical Performance of Electrode Material Based on Multifunctional Dye Doped Polypyrrole

Journal of Nanoscience and Nanotechnology, DOI:10.1166/jnn.2015.10759

(4). <u>Limin Zang</u>, Jianhui Qiu, Chao Yang, Eiichi Sakai

Preparation and Characterization of Conducting Polymer Microspheres

Applied Mechanics and Materials, Vol.543-547, (2014), pp.3874-3877.

(5). <u>Limin Zang</u>, Jianhui Qiu, Xueli Wu, Wenjuan Zhang, Eiichi Sakai, Yi Wei

Preparation of Magnetic Chitosan Nanoparticles as Support for Cellulase Immobilization

Industrial & Engineering Chemistry Research, Vol.53, (2014), pp.3448-3454.

(6). Chao Yang, <u>Limin Zang</u>, Jianhui Qiu, Eiichi Sakai, Xueli Wu, Yuki Iwase

Nano-cladding of natural microcrystalline cellulose with conducting polymer: preparation, characterization, and application in energy storage

RSC Advances, Vol.4, (2014), pp.40345-40351.

(7). Chao Yang, Haodao Mo, <u>Limin Zang</u>, Jianhui Qiu, Xue Wang, Hui You

Preparation and characterization of coaxial mullite/polypyrrole fibrous

nanocomposites via self-assembling and in situ surface-initiated polymerization

Polymer Composites, Vol.35, (2014), pp.892-899.

(8). Chao Yang, Haodao Mo, <u>Limin Zang</u>, Jianhui Qiu, Hui You, Xue Wang

Structural investigation of anionic functional poly(vinyl alcohol) doped polypyrrole

nanospheres

Fibers and Polymers, Vol.15, (2014), pp.2019-2025.

(9). Chao Yang, Haodao Mo, <u>Limin Zang</u>, Jianhui Qiu, Eiichi Sakai, Xueli Wu

A facile method to synthesize polypyrrole nanoparticles in the presence of natural

organic phosphate

Physica B, Vol.449, (2014), pp.181-185.

(10). Jianhui Qiu, <u>Limin Zang</u>, Chao Yang, Kengo Uchiya, Eiichi Sakai, Lijun Wang

Preparation and Volume Resistivity of CNT/Polycarbonate Nanocomposites with

Different Injection Molding Temperatures

Applied Mechanics and Materials, Vol.543-547, (2014), pp.3878-3881.

(11). Wenjuan Zhang, Jianhui Qiu, <u>Limin Zang</u>, Eiichi Sakai

Preparation of functionalized magnetic silica nanospheres for the cellulase

immobilization

Nano, Vol.10, (2015), 1550013 (9 pages)

(12). Wenjuan Zhang, Jianhui Qiu, Huixia Feng, <u>Limin Zang</u>, Eiichi Sakai

Increase in stability of cellulase immobilized on functionalized magnetic

nanospheres

Journal of Magnetism and Magnetic Materials, Vol.375, (2015), pp.117-123.

(13). Wenjuan Zhang, Jianhui Qiu, Huixia Feng, Xueli Wu, <u>Limin Zang</u>, Eiichi Sakai

Synthesis and characterization of functionalized magnetic silica nanospheres for

the acremonium cellulase immobilization

Journal of Nanoscience and Nanotechnology, in Press

(14). Xueli Wu, Jianhui Qiu, Wenjuan Zhang, <u>Limin Zang</u>, Eiichi Sakai, Peng Liu

Synthesizing multi-walled carbon nanotube-polymethyl methacrylate conductive

composites and poly(lactic acid) based composites

Polymer Composites, in Press,

(15). Wenjuan Zhang, Jianhui Qiu, Huixia Feng, Xueli Wu, <u>Limin Zang</u>, Yi Wei, Eiichi

Sakai

Preparation and characterization of functionalized magnetic silica nanospheres

with the immobilized cellulase

Applied Mechanics and Materials, Vol.543-547, (2014), pp.3892-3895.

Ⅱ. International conference paper

(1). <u>Limin Zang</u>, Jianhui Qiu, Chao Yang, Eiichi Sakai

Preparation and Characterization of Conducting Polymer Microspheres

2014 2nd International Conference on Materials and Manufacturing Research,

Guilin, Guangxi, China, March 29-30, (2014).

(2). Jianhui Qiu, <u>Limin Zang</u>, Kengo Uchiya, Eiichi Sakai, Lijun Wang

Preparation and Volume Resistivity of CNT/Polycarbonate Nanocomposites with

Different Injection Molding Temperatures

2014 2nd International Conference on Materials and Manufacturing Research,

Guilin, Guangxi, China, March 29-30, (2014).

(3). Wenjuan Zhang, Jianhui Qiu, Huixia Feng, Xueli Wu, <u>Limin Zang</u>, Wei Yi, Eiichi

Sakai

Preparation and characterization of functionalized magnetic silica nanospheres

with the immobilized cellulase

2014 2nd International Conference on Materials and Manufacturing Research,

Guilin, Guangxi, China, March 29-30, (2014).

Ⅲ. Domestic conference paper

(1). <u>Limin Zang</u>, Jianhui Qiu, Chao Yang, Eiichi Sakai

Preparation of Polypyrrole Nanoparticles in the Presence of Phytic Acid via

Chemical Oxidative Polymerization

Proceedings of the 39th Symposium on Composite Materials, pp.213-214, Akita,

Japan, September 18-19, (2014).

(2). Chao Yang, <u>Limin Zang</u>, Jianhui Qiu, Eiichi Sakai

Preparation and Characterization of Electrically Conductive Composite Based on

Mullite Fibers and Polypyrrole

Proceedings of the 39th Symposium on Composite Materials, pp.15-16, Akita,

Japan, September 18-19, (2014)

(3). <u>Limin Zang</u>, Jianhui Qiu, Eiichi Sakai

Immobilization of Cellulase on Fe_3O_4–Chitosan Nanoparticles and Determination

of Its Activity

Proceedings of 49th Autumn Meeting of the Japan Society of Mechanical

Engineers Tohoku Branch, pp.45-46, Morioka, Japan, September 20, (2013).

Acknowledgements

I would firstly like to acknowledge the guidance and support of my supervisor Professor Jianhui Qiu, who works at Department of Machine Intelligence and Systems Engineering, Faculty of Systems Science and Technology of Akita Prefectural University. He imparted the knowledge of material science to me, and his elaborated guidance, considerable encouragement and invaluable discussion make my research of great achievement and my study life unforgettable. Thank you also for the financial support and the opportunities that were provided to me.

My deepest appreciation goes to the professors in Department of Machine Intelligence and Systems Engineering, Faculty of Systems Science and Technology at Akita Prefectural University, Dr. Teruo Bitoh, Dr. Nobuhiro Kanazawa and Professor in Department of Bioscience and Textile Technology, Faculty of Textile Science and Technology at Shinshu University, Dr. Qingqing Ni for the comments and suggestions, whose advices have inestimable value for my research.

I appreciate the technical support from Dr. Teruo Bitoh, Dr. Yongbo Wu, Dr. Ruilu Liang, Dr. Eiichi Sakai and Dr. Takao Komiyama in Akita Prefectural University, and Professor in Department of Engineering Mechanics, College of Aerospace Engineering at Chongqing University, Dr. Ning Hu. Thanks for Mrs. Qiu who has taken good care of me in three years. And thanks also go to my peer research group members including Lin Lei, Takuya Murata, Xueli Wu, Wenjuan Zhang, Lijun Wang, Bin Wang, Liqiang Gu, Baiyi Chen, Longxiang Zhu, Jiao Chen, Rie Nobe, Suguru Murakami, Yuki Iwase, Yuya Matsumura, for assisting with my research as well as providing friendship and support.

Gratitude is due to my Japanese teachers, Eiko Kamata, Minako Kudo and Chika Furukawa and for their support, patience and understanding throughout this endeavor.

A giant thank you also goes to my family for their support, encouragement and patience throughout the course of this PhD and indeed for my entire life.